PACIFIC EARTHQUAKE ENGINEERING RESEARCH CENTER

Rocking Response and Overturning of Equipment

Nicos Makris

Jian Zhang
University of California, Berkeley

A report to the PEER Program of Applied Earthquake Engineering Research on Lifeline Systems

The financial support of the sponsor organizations including the Pacific Gas & Electric Company (PG&E) and the California Energy Commission (CEC) is acknowledged.

PEER UTILITIES PROGRAM
REPORT NO. 2000/13

Rocking Response and Overturning of Anchored Equipment under Seismic Excitations

Final Report to PG&E

by

NICOS MAKRIS, PI
Associate Professor

JIAN ZHANG
Graduate Student Researcher

Department of Civil and Environmental Engineering,
University of California, Berkeley

September 1999

ABSTRACT

This report investigates the transient rocking response of anchored electrical equipment and other anchored structures that can be approximated as rigid blocks. Practical issues that control overturning, such as the effect of the vertical component of ground accelerations and the effect of the coefficient of restitution during impact, are also addressed.

The anchorages of equipment are assumed to have a pre-yielding linear behavior, a finite post-yielding strength, and some ductility. The nonlinear behavior of the restrainers in conjunction with the nonlinear dynamics of a rocking block yield a set of highly nonlinear equations which are solved numerically using a state-space formulation. The study uncovers that while for most of the frequency range, anchored blocks survive higher accelerations than free-standing blocks, there is a short frequency range where the opposite happens. This counterintuitive behavior is the result of the many ways that a block might overturn. It is shown that under a one-sine (Type-A) pulse or one-cosine (Type-B) pulse with frequency ω_p, a free-standing block with frequency parameter p has two modes of overturning; one with impact (mode 1), and one without impact (mode 2). The transition from mode 1 to mode 2 is sudden, and once ω_p/p is sufficiently large, then a substantial increase in the acceleration amplitude of the one-sine pulse is needed to achieve overturning. When a block is anchored the transition from mode 1 to mode 2 happens at slightly larger values of ω_p/p, and this results in a finite frequency range where a free-standing block survives acceleration levels that are capable of overturning the same block when it is anchored. The presence of restrainers is effective in preventing toppling of small, slender blocks. Prior to the transition from mode 1 to mode 2, the presence of restrainers has a destructive effect. When blocks overturn without impact (mode 2) the presence of restrainers has a marginal effect.

Furthermore, the investigation concludes that the effect of the vertical component of recorded ground motions is marginal and virtually does not affect the level of the horizontal acceleration needed to overturn an electrical equipment. An increasingly inelastic impact (smaller coefficient of restitution) results in smaller angles of rotation; however, the values of the impact velocities might be occasionally larger.

PROLOGUE

This report summarizes the work conducted during Phase II of the PEER-PG&E Program. The work is the continuation of a Phase I study during which the PI and a former graduate student examined the rocking response and overturning of free-standing equipment under pulse-type motions[1]. In that study it was indicated that the minimum overturning acceleration amplitude, a_{p0}, of a half-sine pulse as was computed by Housner[2] was incorrect. This result was corrected by showing that under the weaker half-sine pulse that accomplishes overturning, the block topples during its free-vibration regime — after a theoretically infinite long time — not at the instant that the pulse expires, as was assumed by Housner. Within the limits of the linear approximation the correct expression was derived, which yields the minimum overturning acceleration, a_{p0} (equation 3.8 of Reference 1):

$$\begin{aligned}&\cos\psi\cosh\left[\frac{p}{\omega_p}(\pi-\psi)\right]-\frac{\omega_p}{p}\sin\psi\sinh\left[\frac{p}{\omega_p}(\pi-\psi)\right]+1\\&+\cos\psi\sinh\left[\frac{p}{\omega_p}(\pi-\psi)\right]-\frac{\omega_p}{p}\sin\psi\cosh\left[\frac{p}{\omega_p}(\pi-\psi)\right]=0\end{aligned} \tag{1}$$

The solution of this transcendental equation gives the value of ψ for which the acceleration, $a_{p0} = \alpha g/\sin\psi$, is the minimum acceleration amplitude of the half-sine pulse with duration $T_p = 2\pi/\omega_p$ able to overturn a block with slenderness α and frequency parameter p.

Equation (1) can be further simplified by using the definition of the hyperbolic function, $\cosh x = (e^x + e^{-x})/2$ and $\sinh x = (e^x - e^{-x})/2$, and then factoring the terms $\cos\psi$ and $\sin\psi$. This gives

$$\frac{\omega_p}{p}\sin\psi-\cos\psi = e^{-\frac{p}{\omega_p}(\pi-\psi)} \tag{2}$$

Equation (2) was derived independently by Shi et al.[3] who stated correctly that under a half-sine pulse with the minimum acceleration that is needed to overturn a block, the kinetic energy of the block at the verge of overturning should be zero.

We take this opportunity to thank Professor James N. Brune (University of Nevada-Reno) for his interest to our work and for communicating to us reference 3. We are pleased to report that the energy approach followed by Shi et al.[3] and the kinematic approach followed by Makris and Roussos[1] are in agreement.

---

1. Makris, N., and Y. Roussos. 1998. *Rocking Response and Overturning of Equipment Under Horizontal Pulse-Type Motions*. PEER-98/05. Pacific Earthquake Engineering Research Center, University of California, Berkeley.
2. Housner, G. W. 1963. The behaviour of inverted pendulum structures during Earthquakes. *Bull. Seismological Soc.of America,* **53**: 404-17.
3. Shi, B., A. Anooshehpoor, Y. Zeng, and J. N. Brune. 1996. Rocking and overturning of precariously balanced rocks by earthquake. *Bull. Seismological Soc. of America* **86**(5): 1364-71.

CONTENTS

ABSTRACT iii
PROLOGUE v
TABLE OF CONTENTS vii
LIST OF FIGURES ix
LIST OF TABLES xv
ACKNOWLEDGMENTS xvii
CHAPTER 1: INTRODUCTION 1
CHAPTER 2: REVIEW OF THE ROCKING RESPONSE OF A FREE-STANDING BLOCK 5
2.1 Condition for Initiation of Rocking Motion 5
2.2 Governing Equations under Rocking Motion 10
2.3 Rocking Response to a One-Sine (Type-A) Pulse 12
2.3.1 Linear Formulation 12
2.3.2 Nonlinear Formulation 21
2.4 Rocking Response to a One-Cosine (Type-B) Pulse 24
CHAPTER 3: ROCKING RESPONSE OF A FREE-STANDING BLOCK UNDER HORIZONTAL AND VERTICAL EXCITATION 31
3.1 Numerical Formulation and Solution 31
3.2 Response Spectra and Effect of the Coefficient of Restitution 41
CHAPTER 4 ROCKING RESPONSE OF ANCHORED EQUIPMENT TO ONE-SINE (TYPE-A) PULSE 45
4.1 Elastic-Brittle Behavior 45
4.1.1 Nonlinear Formulation 45
4.1.2 Linear Formulation 54
4.2 Ductile Behavior 57
4.2.1 Elasto-Plastic Behavior 60
CHAPTER 5: ROCKING RESPONSE OF ANCHORED EQUIPMENT TO EARTHQUAKE EXCITATIONS 69
CHAPTER 6: CONCLUSIONS 79
REFERENCES 81

LIST OF FIGURES

Figure 1: Overturned electrical equipment at Sylmar Converter Station damaged after the 1971 San Fernando earthquake. Top: Front view. Bottom: Side view. — Steinbrugge Collection, PEER, University of California, Berkeley 2

Figure 2: Schematic of a free-standing block in rocking motion (top); and its moment rotation diagram (bottom) 6

Figure 3: Acceleration, velocity, and displacement histories of a one-sine pulse (left) and a one-cosine pulse (right) 7

Figure 4: Free-body diagram of a rigid block at the instant that it enters rocking 9

Figure 5: Overturning acceleration spectrum of a free-standing block with $\eta = 0.9$ subjected to a one-sine acceleration pulse with frequency ω_p. The analytical and numerical solutions shown are computed with the linear formulation. When ω_p/p is sufficiently large, a free-standing block overturns only without impact (mode 2) 17

Figure 6: Rotation and angular velocity time histories of a rigid block ($p = 2.14\ rad/sec$, $\alpha = 0.25\ rad$ and $\eta = 0.9$) subjected to a one-sine pulse with $\omega_p/p = 5$. Left: $a_p = 3.00\alpha g$, no overturning. Center: $a_p = 3.01\alpha g$, overturning with one impact (mode 1). Right: $a_p = 6.32\alpha g$, overturning with one impact (mode 1).....18

Figure 7: Rotation and angular velocity time histories of the same rigid block as in Figure 4 ($p = 2.14\ rad/sec$, $\alpha = 0.25\ rad$ and $\eta = 0.9$) subjected to a one-sine pulse with $\omega_p/p = 5$. Left: No overturning with $a_p = 6.33\alpha g$, that is slightly larger than the acceleration level, $a_p = 6.32\alpha g$, that created overturning. Center: The block does not overturn even for the acceleration amplitude $a_p = 7.17\alpha g$. Right: The block eventually overturns with $a_p = 7.18\alpha g$, without impact (mode 2) 19

Figure 8: Comparison of overturning acceleration spectra of a slender block ($p = 2.14\ rad/sec$, $\alpha = 0.25\ rad = 14.32°$, $\eta = 0.9$) under a one-sine pulse, computed with the linear and nonlinear formulations. When the frequency of the one-sine pulse is relatively low, both formulations yield comparable results. As the excitation frequency increases, the linear formulation yields minimum overturning acceleration amplitudes drastically larger than those obtained with the nonlinear formulation. This is because under the nonlinear formulation the overturning "bay" generated by mode 1 penetrates further into the safe area under the overturning spectrum due to mode 2. As the excitation frequency further increases the linear and nonlinear formulations again yield comparable results since under both formulations and a high-frequency pulse the block overturns with mode 2..... 22

Figure 9: Comparison of overturning acceleration spectra of a free-standing equipment with $\alpha = 0.349\ rad = 20°$, $p = 2\ rad/sec$ and $\eta = \sqrt{r_{max}} = 0.825$, under a one-sine pulse, computed with the linear and the nonlinear formulation 23

Figure 10: Normalized minimum coefficient of friction over the slenderness of a block that is needed to sustain pure rocking motion 25

Figure 11: Comparison of overturning acceleration spectra of a slender block ($p = 2.14\ rad/sec$, $\alpha = 0.25\ rad = 14.32°$, $\eta = 0.9$) under a one-cosine pulse, computed with the linear and the nonlinear formulation. In this case the difference between the results of the two formulations are less drastic than those observed under a one-sine pulse 26

Figure 12: Rotation and angular velocity time histories of a rigid block ($p = 2.14\ rad/sec$, $\alpha = 0.25\ rad$ and $\eta = 0.9$) subjected to a one-cosine pulse with $\omega_p/p = 3$. Left: $a_p = 1.91\alpha g$, no overturning. Center: $a_p = 1.92\alpha g$, overturning with one impact (mode 1). Right: $a_p = 6.54\alpha g$, overturning with one impact (mode 1).....28

Figure 13: Rotation and angular velocity time histories of the same rigid block as in Figure 9 ($p = 2.14\ rad/sec$, $\alpha = 0.25\ rad$ and $\eta = 0.9$) subjected to a one-cosine pulse with $\omega_p/p = 3$. Left: No overturning with $a_p = 6.55\alpha g$, that is slightly larger than the acceleration level, $a_p = 6.54\alpha g$, that created overturning. Center: The block does not overturn even for the acceleration amplitude $a_p = 11.18\alpha g$. Right: The block eventually overturns with $a_p = 11.19\alpha g$, without impact (mode 2).....29

Figure 14: Comparison of overturning acceleration spectra of a slender block ($\alpha = 0.349\ rad = 20°$, $p = 2.0\ rad/sec$, $\eta = 0.825$) under a one-cosine pulse, computed with the linear and the nonlinear formulation. In this case the difference between the results of the two formulations are less drastic than those observed under a one-sine pulse.....30

Figure 15: Rotation and angular velocity time histories of a rigid block ($b = 0.5\ m$, $h = 1.5\ m$) subjected to the fault-normal and vertical Rinaldi station records. Left: overturning under horizontal component alone (78% acceleration level). Center: overturning under horizontal and vertical components (74% acceleration level). Right: overturning under horizontal and vertical components with reversed polarity (83% acceleration level) 32

Figure 16: Rotation and angular velocity time histories of a rigid block ($b = 0.5\ m$, $h = 1.5\ m$) subjected to the fault-normal and vertical Sylmar station records. Left: overturning under horizontal component alone (118% acceleration level). Center: overturning under horizontal and vertical components (116% acceleration level). Right: overturning under horizontal and vertical components with reversed polarity (120% acceleration level).....33

Figure 17: Rotation and angular velocity time histories of a rigid block ($b = 0.5\ m$, $h = 1.5\ m$) subjected to the N-S and vertical Newhall station records. Left: overturning under horizontal component alone (183% acceleration level). Center: overturning under horizontal and vertical components (186% acceleration level). Right: overturning under horizontal and vertical components with reversed polarity (180% acceleration level).....35

Figure 18: Rotation and angular velocity time histories of a rigid block (*b = 0.5 m, h = 1.5 m*) subjected to the fault-normal and vertical El Centro Array #5 records. Left: overturning under horizontal component alone (129% acceleration level). Center: overturning under horizontal and vertical components (126% acceleration level). Right: overturning under horizontal and vertical components with reversed polarity (130% acceleration level) 36

Figure 19: Rotation and angular velocity time histories of a rigid block (*b = 0.5 m, h = 1.5 m*) subjected to the fault-normal and vertical El Centro Array #6 records. Left: overturning under horizontal component alone (149% acceleration level). Center: overturning under horizontal and vertical components (149% acceleration level). Right: overturning under horizontal and vertical components with reversed polarity (161% acceleration level) 37

Figure 20: Rotation and angular velocity time histories of a rigid block (*b = 0.5 m, h = 1.5 m*) subjected to the fault-normal and vertical El Centro Array #7 records. Left: overturning under horizontal component alone (152% acceleration level). Center: overturning under horizontal and vertical components (152% acceleration level). Right: overturning under horizontal and vertical components with reversed polarity (152% acceleration level) 38

Figure 21: Rotation and angular velocity time histories of a rigid block (*b = 0.5 m, h = 1.5 m*) subjected to the fault-parallel and vertical Los Gatos station records. Left: overturning under horizontal component alone (146% acceleration level). Center: overturning under horizontal and vertical components (145% acceleration level). Right: overturning under horizontal and vertical components with reversed polarity (151% acceleration level)....39

Figure 22: Rotation and angular velocity time histories of a rigid block (*b = 0.5 m, h = 1.5 m*) subjected to the fault-parallel and vertical Lucerne Valley records. Left: overturning under horizontal component alone (275% acceleration level). Center: overturning under horizontal and vertical components (285% acceleration level). Right: overturning under horizontal and vertical components with reversed polarity (295% acceleration level)....40

Figure 23: Rotation and angular velocity spectra due to the fault-normal motion recorded at the Rinaldi station for different values of the coefficient of restitution and various values of block slenderness....42

Figure 24: Rotation and angular velocity spectra due to the fault-normal motion recorded at the Sylmar station for different values of the coefficient of restitution and various values of block slenderness....43

Figure 25: Schematic of an anchored block in rocking motion 46

Figure 26: Moment-rotation curves of: (Top) Free-standing block; (Center) Elastic-brittle anchorage; (Bottom) Anchored block with elastic-brittle restrainers....47

Figure 27: Comparison of overturning acceleration spectra due to a one-sine pulse of an anchored equipment ($\alpha = 0.349\ rad = 20°$, $p = 2\ rad/sec$, $\eta = 0.825$, $q = 5.2\times10^{-4}$ and $\mu = 1$) computed with the nonlinear formulation for $F_u/W = 0$, 0.4 and 1.0 51

Figure 28: Normalized minimum overturning acceleration levels needed to overturn an anchored block (elastic-brittle behavior, $\mu = 1$) to the acceleration levels needed to overturn the same block when it is free standing 52

Figure 29: Comparison of overturning acceleration spectra due to a one-sine pulse of an anchored equipment ($\alpha = 0.349\ rad = 20°$, $p = 2\ rad/sec$, $\eta = 0.825$, $q = 5.2\times10^{-4}$ and $\mu = 1$) computed with the linear formulation for $F_u/W = 0$ and 0.6. Lines: analytical solution. Points: numerical solution 56

Figure 30: Comparison of the overturning acceleration spectra due to a one-sine pulse of an anchored equipment ($\alpha = 0.349\ rad = 20°$, $p = 2\ rad/sec$, $\eta = 0.825$, $q = 5.2\times10^{-4}$ and $\mu = 1$) computed with the linear and nonlinear formulations for $F_u/W = 0.4$ (top) and $F_u/W = 0.6$ (bottom) 58

Figure 31: Force-displacement curve of an element with bilinear behavior 59

Figure 32: Moment-rotation curves of: (Top) Free-standing block; (Center) Elastic-plastic anchorage; (Bottom) Anchored block with elastic-plastic restrainers 61

Figure 33: Overturning acceleration spectra due to a one-sine pulse of an anchored block ($\alpha = 0.349\ rad = 20°$, $p = 2\ rad/sec$, $\eta = 0.825$, $q = 5.2\times10^{-4}$ and $\mu = 5$) with restrainer strength $F_u/W = 0$, 0.4 and 1.0. The solution is computed with the nonlinear formulation 64

Figure 34: Normalized minimum overturning acceleration levels needed to overturn an anchored block (elastic-plastic behavior, $\mu = 5$) to the acceleration level needed to overturn the same block when it is free standing. When $\omega_p/p > 4$ blocks should not be anchored since the effect of the restrainers is destructive or virtually insignificant 66

Figure 35: Comparison of overturning acceleration spectra computed with the nonlinear formulation for an anchored block ($\alpha = 0.349\ rad = 20°$, $p = 2\ rad/sec$, $\eta = 0.825$ and $q = 5.2\times10^{-4}$) with two levels of ductility: $\mu = 1$ and $\mu = 5$. Top: $F_u/W = 0.4$; Bottom: $F_u/W = 1.0$ 67

Figure 36: Fault-normal components of the acceleration, velocity and displacement time histories recorded at the Rinaldi station during the January 17, 1994, Northridge, California earthquake (left), a cycloidal type-A pulse (center), and a cycloidal type-B pulse (right) 70

Figure 37: Rotation and angular velocity time histories of an anchored block ($b = 0.5\ m$, $h = 1.5\ m$, $F_u/W = 0.4$) subjected to the fault-normal Rinaldi station motion. An 88% acceleration level is capable of overturning the block with restrainers exhibiting ductility $\mu = 1$ 72

Figure 38: Rotation and angular velocity time histories of an anchored block ($b = 0.5\ m$, $h = 1.5\ m$, $F_u/W = 0.4$) subjected to the fault-normal Rinaldi station motion. A 93% acceleration level is capable of overturning the block with restrainers exhibiting ductility $\mu = 5$; whereas when $\mu = 10$ the block survives 73

Figure 39: Rotation and angular velocity time histories of an anchored block ($b = 0.5\ m$, $h = 1.5\ m$, $F_u/W = 0.4$, $\mu = 10$) subjected to the fault-normal Rinaldi station motion. Left: no overturning (98% acceleration level). Right: overturning (99% acceleration level) 74

Figure 40: Rotation and angular velocity time histories of the free-standing block ($b = 1.0\ m$, $h = 3.0\ m$) subjected to the fault-normal Rinaldi station motion. Left: no overturning (126% acceleration level). Right: overturning (127% acceleration level).....76

Figure 41: Rotation and angular velocity time histories of a larger anchored block ($b = 1.0\ m$, $h = 3.0\ m$, $F_u/W = 0.4$ and $\mu = 5$) subjected to the fault-normal Rinaldi station motion. Left: no overturning (118% acceleration level). Right: overturning (119% acceleration level). The free-standing block can survive a stronger acceleration level than the anchored block (see Figure 40) 77

LIST OF TABLES

Table 1: Minimum level of acceleration records needed to overturn a $0.5\ m \times 1.5\ m$ free-standing block ($\alpha = 18.43°$, $p = 2.157\ rad/sec$) 34

Table 2: Geometrical, physical and structural parameters of electrical equipment. 50

ACKNOWLEDGMENTS

The work described in this report was funded by the Pacific Earthquake Engineering Research (PEER) Center under the Pacific Gas & Electric Company Contract No. 09566. This financial support is gratefully acknowledged.

The valuable input and comments of Dr. Norman Abrahamson, Mr. Eric Fujisaki, and Mr. Henry Ho are greatly appreciated. Professor Gregory Fenves's efforts to coordinate this task are also acknowledged.

This work made use of Pacific Earthquake Engineering Research Center Shared Facilities supported by the Earthquake Engineering Research Center Program of the National Science Foundation under Award Number EEC-9701568.

CHAPTER 1
INTRODUCTION

The study of the rocking response and overturning of electrical equipment to near-source ground motions was motivated by the proximity of electric power substations in major urban areas to active faults. In the Bay Area the San Andreas fault runs 10 km west of San Francisco; the Hayward fault runs less than 10 km from most of Oakland; additionally, other smaller nearby faults such as the Rodgers Creek, Gregorio, Calaveras, Concord, and Green Valley faults have the potential to subject urban areas to strong ground motions. Similarly, a large part of metropolitan Los Angeles lies over buried thrust faults capable of generating strong motions like those recorded during the January 17, 1994, Northridge earthquake. The city of Kobe, Japan, was devastated by the January 17, 1995, Hyogoken-Nanbu earthquake, which generated unusually strong motions. Figure 1 shows electrical equipment at the Sylmar Converter Station that overturned during the 1971 San Fernando, California, earthquake.

In a recent study the transient response of a free-standing equipment subjected to horizontal pulse-type and near-source ground motions was investigated in depth (Makris and Roussos 1998). What makes these motions particularly destructive to a variety of structures is not only their occasionally high peak-ground acceleration, but also the area under the relatively long-duration acceleration pulse. This area represents the “incremental” ground velocity (Anderson and Bertero 1986), which is the net increment of the ground velocity along a monotonic segment of its time history. Such velocity increments are of the order of 0.5 m/sec or even higher. Although they do not happen very fast to generate an excessive ground acceleration, they happen at just the right pace to generate devastating shears at the base of flexible structures (Bertero et al. 1978; Anderson and Bertero 1986; Hall et al. 1995). The Makris and Roussos study showed that near-source ground motions do not bear any exceptional overturning potential for electrical equipment. This finding is because typical electrical equipments have dynamic properties that are too stiff to be resonated by the two- or three-second long coherent pulse of the near-source ground motion. In that study it was found that the toppling of smaller blocks is more sensitive to the peak ground acceleration; whereas, the toppling of larger blocks depends mostly on the incremental ground velocity. Accordingly, a smaller block will overturn due to the high-frequency fluctuations that override the long-duration pulse; whereas a larger block will overturn due to the long-duration pulse. In this light the overturning response of free-standing equipment was shown to be quite

Figure 1. Overturned electrical equipment at Sylmar Converter Station damaged after the 1971 San Fernando earthquake. Top: Front view. Bottom: Side view --- Steinbrugge collection, PEER, University of California, Berkeley

ordered and predictable despite the presence of the high-frequency content that overrides the coherent component of near-source ground motions.

After having established that peak ground acceleration controls the overturning of electrical equipment, in this study the rocking stability of electrical equipment is further investigated by looking into several practical issues such as (1) the effect of the vertical component of the ground motion; (2) the effect of an increasingly inelastic coefficient of restitution; and (3) the efficiency of typical anchorages used to prevent toppling.

In Chapter 2, the rocking response of a free-standing block subjected to a one-sine (Type-A) pulse and one-cosine (Type-B) pulses is revisited. The study reveals that blocks can overturn with two distinct modes: (a) by exhibiting one impact (mode 1) and (b) without impact (mode 2). The second mode (no impact) is responsible for the existence of a safe region that is located over the minimum overturning acceleration spectrum. The shape of this safe region depends on the coefficient of restitution and is sensitive to the nonlinear nature of the problem. The transition from mode 1 to mode 2 is sudden and results in a finite jump in the minimum overturning acceleration spectrum. In a recent study, Anooshehpoor et al. (1999) attempted to construct the minimum overturning acceleration spectra due to one-sine pulse. Their study failed to identify the second mode of overturning (without impact) and to indicate the presence of the aforementioned safe region. These conceptual oversights in the paper by Anooshehpoor et al. have been addressed in detail in the discussion by Zhang and Makris (1999). Chapter 3 concentrates on the effect of the vertical component of the ground motion, which is found to be negligible.

In Chapter 4 the rocking response and overturning of anchored blocks is investigated in depth. Restrainers with elastic-brittle and elastic-plastic behavior are considered. The elastic-plastic behavior is approximated with the Bouc-Wen hysteretic model. It is found that the restrainers are more efficient in preventing overturning of small slender blocks. Larger blocks overturn only without experiencing any impact, and in this case the effect of restrainers is marginal even when their strength equals the weight of the equipment. Easy-to-use graphs are offered to evaluate the effect of anchorages with various strength and ductility. Chapter 5 concentrates on the rocking response of anchored equipment subjected to selected recorded ground motions. Similar trends to those identified under a cycloidal pulse excitation are observed. Chapter 6 is devoted to a summary of the findings and conclusions.

CHAPTER 2
REVIEW OF THE ROCKING RESPONSE OF A FREE-STANDING BLOCK

2.1 Condition for Initiation of Rocking Motion

We consider the rigid block shown on Figure 2 (top) which can oscillate about the centers of rotation O and O' when it is set to rocking. Depending on the level and form of the ground acceleration, the block may translate with the ground, slide, rock or slide-rock. Prior to 1996, the mode of rigid-body motion that prevailed has been determined by comparing the available static friction to the width-to-height ratio of the block, irrespective of the magnitude of the horizontal ground acceleration. Shenton (1996) indicated that in addition to pure sliding and pure rocking, there is a slide-rock mode and its manifestation depends not only on the width-to-height ratio and the static friction coefficient, but also on the magnitude of the base acceleration.

Physically realizable cycloidal pulses have displacement histories which are continuous and differentiable signals that build up gradually from zero. Their corresponding acceleration histories might be zero at the time origin or exhibiting a finite value that can be as large as their maximum amplitude. Figure 3 plots the acceleration, velocity and displacement histories of a one-sine pulse (left) and one-cosine pulse (right). In the case of the one-sine pulse the ground acceleration is zero at the initiation of motion and builds up gradually. In contrast, in the case of a one-cosine pulse, the ground acceleration assumes its maximum value at the initiation of motion. Under other cycloidal pulses such as Type-C_n pulses (Makris and Chang 1998) the ground acceleration is finite at the initiation of motion but assumes a value that is smaller than its maximum amplitude a_p. With reference to Figure 2 and assuming that the coefficient of friction $\mu > \frac{b}{h} = \tan\alpha$, static equilibrium yields that the minimum horizontal acceleration that is needed to initiate rocking is $a_{p,\,min} = g\tan\alpha$. Consequently, pulses with amplitude $a_p > g\tan\alpha$ will induce rocking to a rectangular block with slenderness α.

Consider a cycloidal pulse with acceleration amplitude $a_p > g\tan\alpha$ and let, λa_p, to be the value of the ground acceleration when a block with slenderness α is about to enter rocking motion. Depending on the type of pulse, λ assumes different values; however it is bounded by

$$\frac{g\tan\alpha}{a_p} < \lambda \le 1 \tag{2-1}$$

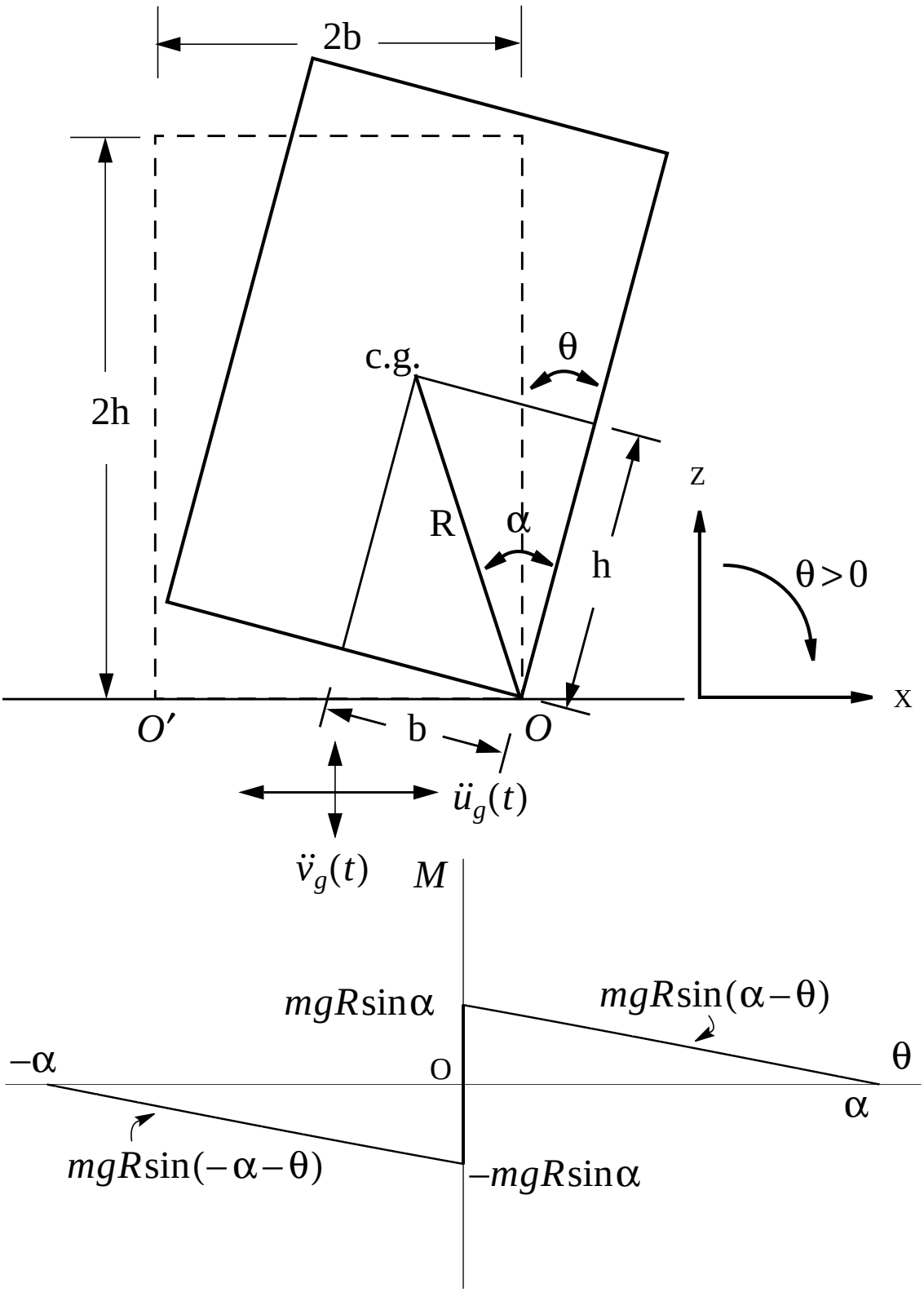

Figure 2. Schematic of a free-standing block in rocking motion (top); and its moment rotation diagram (bottom)

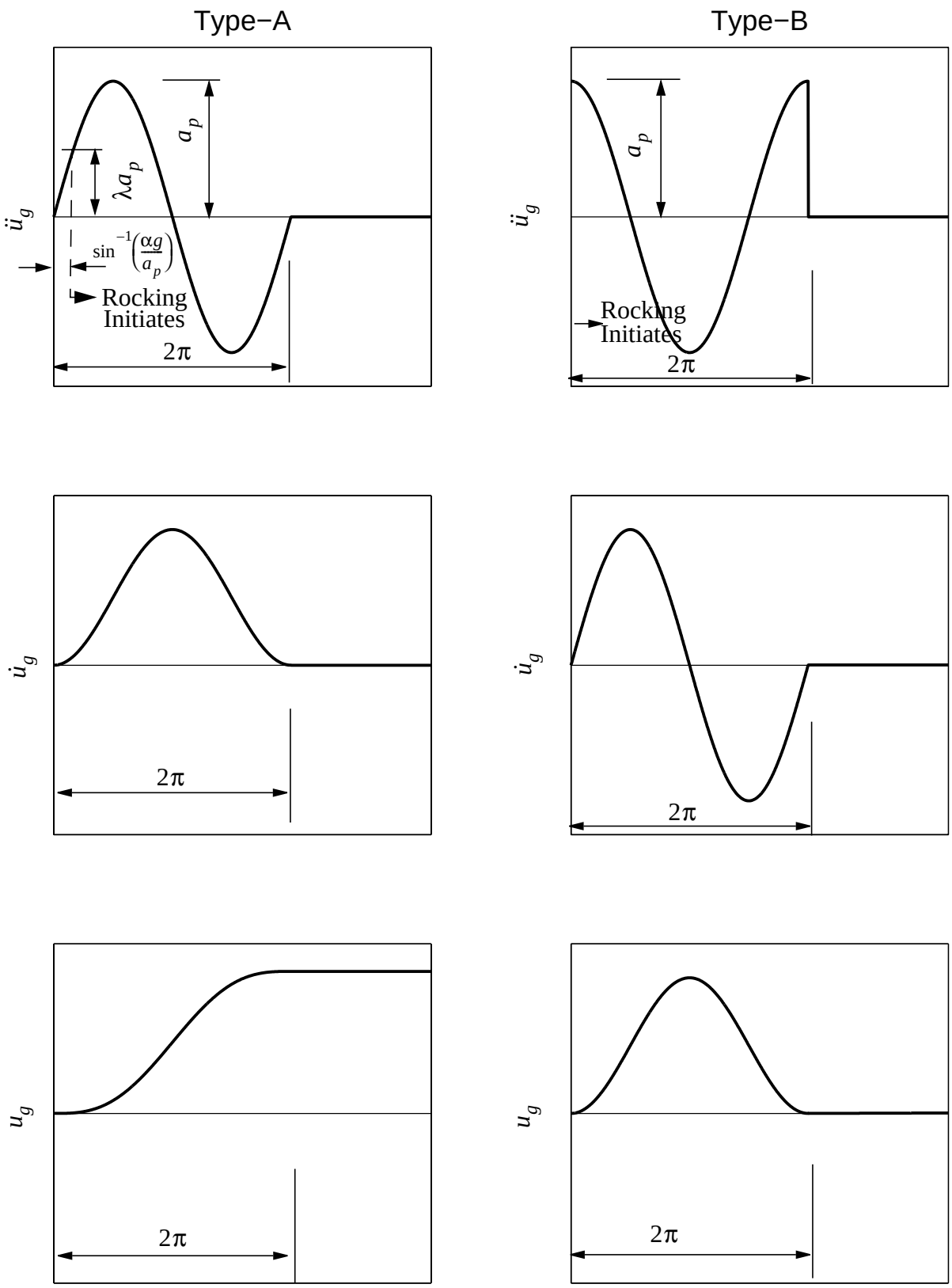

Figure 3. Acceleration, velocity, and displacement histories of a one-sine pulse (left) and a one-cosine pulse (right)

Figure 4 shows the free-body diagram of a free-standing block that is about to enter rocking motion due to a positive ground acceleration. With the system of axis shown, a positive acceleration will induce an initial negative rotation ($\theta < 0$). Adopting the notation introduced by Shenton (1996), let f_x and f_z be the horizontal and vertical reactions at the tip O' of the block. Dynamic equilibrium at this instant gives

$$f_x = m(\lambda a_p + h\ddot{\theta}) \tag{2-2}$$

$$f_z = m(g - b\ddot{\theta}) \tag{2-3}$$

$$I_{cg}\ddot{\theta} = -f_x h + f_z b \tag{2-4}$$

where I_{cg} is the moment of inertia of the block about its center of gravity (for rectangular blocks $I_{cg} = mR^2/3$). Substitution of (2-2) and (2-3) into (2-4) gives the value of the angular acceleration, $\ddot{\theta}_0$, at the instant when rocking initiates

$$\ddot{\theta}_0 = -p^2 \frac{h}{R} \tan\alpha \left(\frac{\lambda a_p}{g \tan\alpha} - 1 \right) \tag{2-5}$$

in which $p = \sqrt{3g/(4R)}$ is the frequency parameter of the block and is a quantity in rad/sec, whereas $R = \sqrt{b^2 + h^2}$ is the half diameter of the block — a measure of its size. In order to avoid sliding at this instant

$$\frac{f_x}{f_z} \le \mu \tag{2-6}$$

and substitution of the value computed by (2-5) into (2-2) and (2-3) gives the condition for a block to rock without sliding

$$\frac{\lambda a_p - \frac{3}{4} g \cos\alpha \sin\alpha \left(\lambda \frac{a_p}{g \tan\alpha} - 1 \right)}{g + \frac{3}{4} g \sin^2\alpha \left(\lambda \frac{a_p}{g \tan\alpha} - 1 \right)} \le \mu \tag{2-7}$$

Equation (2-7), initially presented by Shenton (1996), indicates that under some excitation pulses with amplitude a_p, the condition for a block to enter rocking motion without sliding depends on the value of a_p. However, this is true only for pulses that have a finite acceleration at the initiation of motion. For pulses that their acceleration history build up gradually (such as a one-sine pulse), the value of λa_p at the initiation of rocking is equal to $g \tan\alpha$ and equation (2-7) reduces to

$$\tan\alpha = \frac{b}{h} \le \mu \tag{2-8}$$

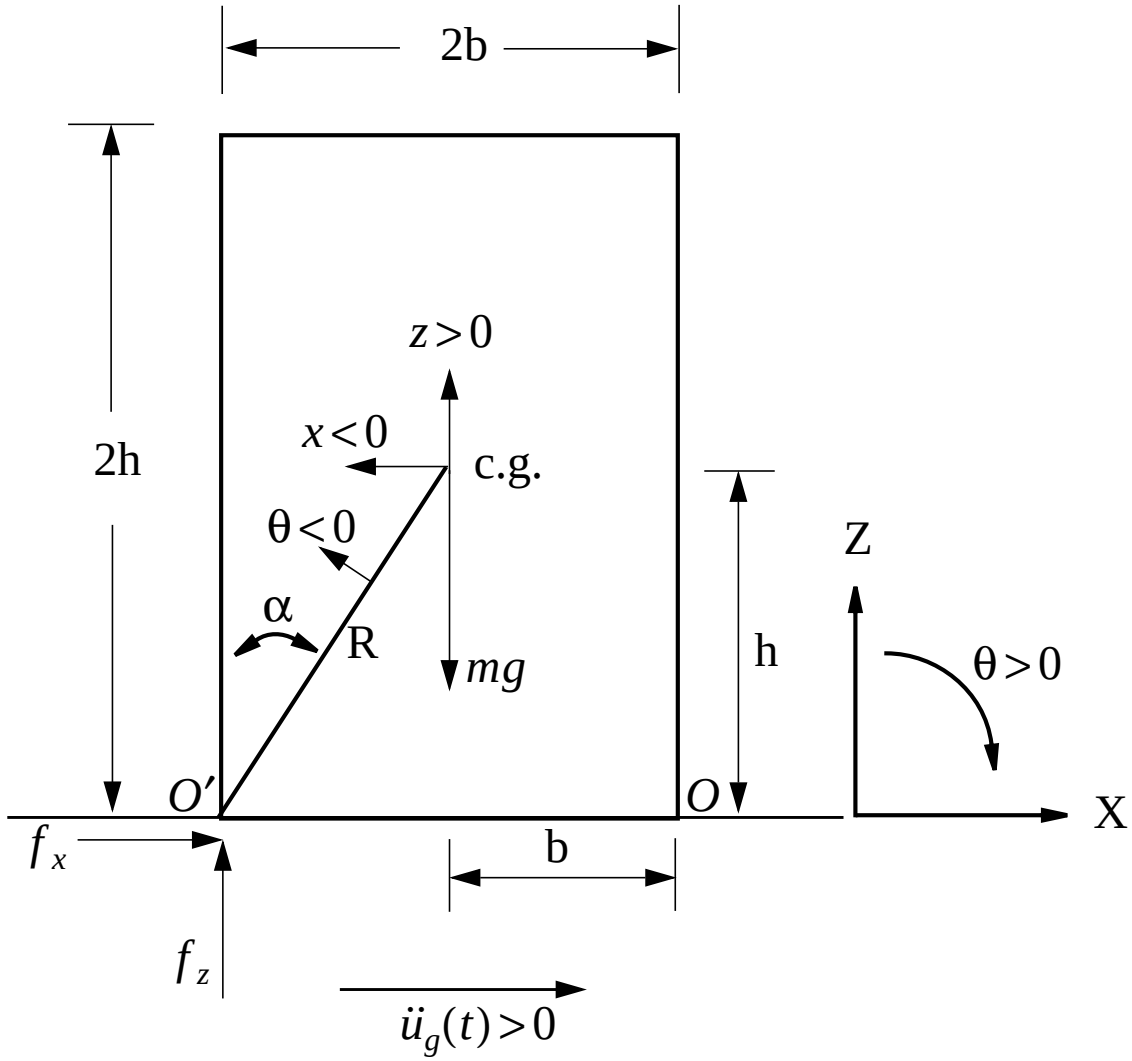

Figure 4. Free-body diagram of a rigid block at the instant that enters rocking

which is the traditional condition imposed in order for rocking to prevail. Consequently, the slide-rock mode introduced by Shenton (1996) will develop only under excitations with non-zero acceleration at the initiation of the motion.

2.2 Governing Equations Under Rocking Motion

Under a positive horizontal ground acceleration and assuming that the coefficient of friction is large enough so that there is no sliding, the block will initially rotate with a negative rotation, $\theta < 0$, and if it does not overturn, it will eventually assume a positive rotation, and so forth. The equations that govern the rocking motion under the simultaneous presence of horizontal, $\ddot{u}_g(t)$, and vertical, $\ddot{v}_g(t)$ ground acceleration are

$$I_0\ddot{\theta}(t) + mg\left(1 + \frac{\ddot{v}_g(t)}{g}\right)R\sin(-\alpha-\theta) = -m\ddot{u}_g(t)R\cos(-\alpha-\theta) \ , \ \theta < 0 \tag{2-9}$$

and

$$I_0\ddot{\theta}(t) + mg\left(1 + \frac{\ddot{v}_g(t)}{g}\right)R\sin(\alpha-\theta) = -m\ddot{u}_g(t)R\cos(\alpha-\theta) \ , \ \theta > 0 \tag{2-10}$$

Equation (2-9) and (2-10) are well known in the literature (Yim et al. 1980) and are valid for arbitrary values of the angle $\alpha = \operatorname{atan}(b/h)$. For rectangular blocks, $I_0 = \frac{4}{3}mR^2$, equation (2-9) and (2-10) can be expressed in the compact form

$$\ddot{\theta}(t) = -p^2\left\{\sin[\alpha\operatorname{sgn}[\theta(t)] - \theta(t)]\left(1 + \frac{\ddot{v}_g(t)}{g}\right) + \frac{\ddot{u}_g}{g}\cos[\alpha\operatorname{sgn}[\theta(t)] - \theta(t)]\right\} \tag{2-11}$$

where $p = \sqrt{\frac{3g}{4R}}$ is the frequency parameter of the block. The larger the block (larger *R*), the smaller *p*. The oscillation frequency of a rigid block under free vibration is not constant since it strongly depends on the vibration amplitude (Housner 1963). Nevertheless, the quantity *p* is a measure of the dynamic characteristics of the block. For an electrical transformer, $p \approx 2 \ rad/sec$, and for a household brick, $p \approx 8 \ rad/sec$.

Figure 2 (bottom) shows the moment-rotation relation during the rocking motion of a free-standing block. The system has infinite stiffness until the magnitude of the applied moment reaches $mgR\sin\alpha$, and once the block is rocking its stiffness decreases monotonically, reaching zero when $\theta = \alpha$. During the oscillatory rocking motion, the moment-rotation curve follows this curve without enclosing any area. Energy is lost only during impact when the angle of rotation reverses.

When the angle of rotation reverses, it is assumed that the rotation continues smoothly from point O to O'. Conservation of momentum about point O' just before the impact and right after the impact gives

$$I_0\dot{\theta}_1 - m\dot{\theta}_1 2bR\sin(\alpha) = I_0\dot{\theta}_2 \ , \tag{2-12}$$

where $\dot{\theta}_1$ is the angular velocity just prior to the impact, and $\dot{\theta}_2$ is the angular velocity right after the impact. The ratio of kinetic energy after and before the impact is

$$r = \frac{\dot{\theta}_2^2}{\dot{\theta}_1^2}, \tag{2-13}$$

which means that the angular velocity after the impact is only $\sqrt{r}$ times the velocity before the impact. Substitution of (2-13) into (2-12) gives

$$r = \left[1 - \frac{3}{2}sin^2\alpha\right]^2 . \tag{2-14}$$

The value of the coefficient of restitution given by (2-14) is the maximum value of *r* under which a block with slenderness, α, will undergo rocking motion. Consequently, in order to observe rocking motion the impact has to be inelastic. The less slender a block (larger α) the more plastic the impact, and for the value of $\alpha = \sin^{-1}\sqrt{2/3} = 54.73°$, the impact is perfectly plastic. During the rocking motion of slender blocks, if additional energy is lost due to interface mechanisms, the value of the true coefficient of restitution, *r*, will be less than the one computed from (2-14). The effect of the coefficient of restitution on the rocking response of free-standing blocks is shown later in this study.

In this chapter the rocking response of a free-standing block subjected to simple trigonometric pulses is revisited since new findings further elucidate the complex dynamic nature of the rocking problem.

The response of a free-standing block subjected to various horizontal cycloidal pulses, with frequency ω_p, such as one-sine pulse (Type-A pulse), a one-cosine pulse (Type-B pulse) and pulses with n-cycles in their displacement histories (Type-C_n pulses) was investigated in a recent study by Makris and Roussos (1998). That study was motivated by an increasing number of ground motions, recorded near the source of strong earthquakes, that contain one or more relatively long-duration coherent pulses. In view of the relatively long duration of the coherent pulses, the range of interest of the frequency ratio, ω_p/p, for electrical equipment with $p \approx 2\ rad/sec$ is $0 \le \omega_p/p \le 3$. Within this range of excitation frequencies ($0 \le \omega_p/p \le 3$), the minimum over-

turning acceleration spectrum of cycloidal pulses is nearly linear; Makris and Roussos (1998) proposed the approximate expression

$$\frac{a_{p0}}{\alpha g} \approx 1 + \beta \frac{\omega_p}{p} \tag{2-15}$$

where a_{p0} is the minimum overturning acceleration of the pulse and α is the angle of the block slenderness. The coefficient $\beta = 1/6$ for Type-A or -C_n pulses, and $\beta = 1/4$ for a Type-B pulse.

For values of $\omega_p/p \geq 3$ the minimum overturning acceleration spectra become increasingly nonlinear. Although the range of $\omega_p/p \geq 3$ is not of central interest in evaluating the overturning potential of near-source ground motions, it is of prime interest when the overturning of a block is the result of a high-frequency spike of short duration.

2.3 Rocking Response to a One-sine (Type-A) Pulse

The analysis presented in this section concentrates on the overturning potential of a one-sine pulse with ground acceleration

$$\ddot{u}_g(t) = \begin{cases} a_p \sin(\omega_p t + \psi) & -\psi/\omega_p \leq t \leq (2\pi - \psi)/\omega_p \\ 0 & otherwise \end{cases} \tag{2-16}$$

where $\psi = \sin^{-1}(\alpha g/a_p)$ is the phase angle when rocking initiates. At this instant $\ddot{u}_g(0) = \alpha g = \lambda a_p$ and according to equation (2-8) the condition for the block to enter pure rocking is $\tan\alpha = \frac{b}{h} < \mu$.

2.3.1 Linear Formulation

For tall, slender blocks, the angle $\alpha = \operatorname{atan}(b/h)$ is relatively small, and equations (2-9) and (2-10) can be linearized. Within the limits of the linear approximation and for a horizontal ground acceleration given by (2-16), equations (2-9) and (2-10) become

$$\ddot{\theta}(t) - p^2\theta(t) = -\frac{a_p}{g} p^2 \sin(\omega t + \psi) + p^2\alpha, \ \theta < 0 \tag{2-17}$$

and

$$\ddot{\theta}(t) - p^2\theta(t) = -\frac{a_p}{g} p^2 \sin(\omega t + \psi) - p^2\alpha, \ \theta > 0 \tag{2-18}$$

where $p = \sqrt{3g/(4R)}$ is the frequency parameter of a rectangular block with a half diagonal = R. The integration of (2-17) and (2-18) gives

$$\theta(t) = A_1 \sinh(pt) + A_2 \cosh(pt) - \alpha + \frac{1}{1+\frac{\omega_p^2}{p^2}} \frac{a_p}{g} \sin(\omega_p t + \psi)\,,\ \theta < 0 \tag{2-19}$$

and

$$\theta(t) = A_3 \sinh(pt) + A_4 \cosh(pt) + \alpha + \frac{1}{1+\frac{\omega_p^2}{p^2}} \frac{a_p}{g} \sin(\omega_p t + \psi)\,,\ \theta > 0 \tag{2-20}$$

where

$$A_1 = A_3 = \frac{\dot{\theta}_0}{p} - \frac{\omega_p/p}{1+\omega_p^2/p^2} \frac{a_p}{g} \cos(\psi) = \frac{\dot{\theta}_0}{p} - \alpha \frac{\omega_p/p}{1+\omega_p^2/p^2} \frac{\cos(\psi)}{\sin(\psi)}\,, \tag{2-21}$$

$$A_2 = \theta_0 + \alpha - \frac{1}{1+\omega_p^2/p^2} \frac{a_p}{g} \sin(\psi) = \theta_0 + \alpha - \frac{\alpha}{1+\omega_p^2/p^2}\,, \tag{2-22}$$

$$A_4 = \theta_0 - \alpha - \frac{1}{1+\omega_p^2/p^2} \frac{a_p}{g} \sin(\psi) = \theta_0 - \alpha - \frac{\alpha}{1+\omega_p^2/p^2}\,. \tag{2-23}$$

The time histories for the angular velocities are directly obtained from the time derivatives of (2-19) and (2-20)

$$\dot{\theta}(t) = pA_1 \cosh(pt) + pA_2 \sinh(pt) + \frac{\omega_p}{1+\frac{\omega_p^2}{p^2}} \frac{a_p}{g} \cos(\omega_p t + \psi)\,,\ \theta < 0 \tag{2-24}$$

and

$$\dot{\theta}(t) = pA_3 \cosh(pt) + pA_4 \sinh(pt) + \frac{\omega_p}{1+\frac{\omega_p^2}{p^2}} \frac{a_p}{g} \cos(\omega_p t + \psi)\,,\ \theta > 0 \tag{2-25}$$

The solutions given by equations (2-19) and (2-20) can be pieced together to construct the time history of the rocking response under a given acceleration amplitude, a_p. Furthermore, this solution can provide the minimum overturning acceleration amplitude, provided that a condition of overturning is available.

Under the minimum acceleration amplitude blocks overturn during their free-vibration regime at a theoretically infinite large time when the velocity tends to reach a local minimum (Makris and Roussos 1998). Accordingly the condition for overturning is that

$$\ddot{\theta}(t_\infty) = 0 \tag{2-26}$$

where t_∞ is a sufficiently large time where $\tanh(pt_\infty) = 1$.

Under a one-sine pulse, a free-standing block has two modes of overturning: (a) overturning with one impact (mode 1) and (b) overturning with no impact (mode 2). This result is true as long as ω_p/p is sufficiently small. As ω_p/p increases the first mode of impact vanishes, and the block overturns only without impact (mode 2). Accordingly, in order to back-figure the minimum overturning acceleration amplitude by imposing the condition of overturning given by (2-26) it is necessary to distinguish between mode 1 and mode 2.

Mode 1

Denoting by t_{fv}, the time when the block enters its free vibration regime, the condition for overturning after the block has experienced one impact (mode 1) is

$$\dot{\theta}(t_{fv}) + p[\theta(t_{fv}) - \alpha] = 0 \tag{2-27}$$

In the case where the impact happens before the excitation expires ($t_i < T_{ex}$), then $t_{fv} = T_{ex} = (2\pi - \psi)/\omega_p$ (CASE 1). In the case where the impact happens after the excitation expires ($t_i > T_{ex}$), then $t_{fv} = t_i$ (CASE 2).

CASE 1 ($t_i < T_{ex}$).

In this case the condition of overturning given by (2-26) yields:

$$\dot{\theta}(T_{ex}) + p[\theta(T_{ex}) - \alpha] = 0 \tag{2-28}$$

where

$$\theta(T_{ex}) = A_3 \sinh[p(T_{ex} - t_i)] + A_4 \cosh[p(T_{ex} - t_i)] + \alpha + \frac{a_p/g}{1 + \left(\frac{\omega_p}{p}\right)^2} \sin(\omega_p T_{ex} + \psi) \tag{2-29}$$

$$\dot{\theta}(T_{ex}) = pA_3 \cosh[p(T_{ex} - t_i)] + pA_4 \sinh[p(T_{ex} - t_i)] + \frac{\omega_p (a_p/g)}{1 + \left(\frac{\omega_p}{p}\right)^2} \cos(\omega_p T_{ex} + \psi) \tag{2-30}$$

where

$$A_3 = \frac{\eta \dot{\theta}^{before}(t_i)}{p} - \frac{\omega_p/p}{1 + \left(\frac{\omega_p}{p}\right)^2} \frac{a_p}{g} \cos(\omega_p t_i + \psi)\,, \tag{2-31}$$

$$A_4 = -\alpha - \frac{1}{1 + \left(\frac{\omega_p}{p}\right)^2} \frac{a_p}{g} \sin(\omega_p t_i + \psi)\,, \tag{2-32}$$

and η is the coefficient of restitution. The time of impact t_i is related to the acceleration amplitude, $a_p = \alpha g/\sin\psi$, with the expression

$$\tan\psi = \frac{\sin(\omega_p t_i) - \frac{\omega_p}{p}\sinh(p t_i)}{1 + \left(\frac{\omega_p}{p}\right)^2 - \left(\frac{\omega_p}{p}\right)^2 \cosh(p t_i) - \cos(\omega_p t_i)} \tag{2-33}$$

The condition of overturning given by (2-28) takes the form

$$(A_3 + A_4) e^{p(T_{ex} - t_i)} + \frac{\omega_p / p}{1 + \left(\frac{\omega_p}{p}\right)^2} \frac{a_p}{g} = 0 \tag{2-34}$$

where A_3 and A_4 are given by (2-31) and (2-32) and t_i is the solution of (2-33). The value of $a_p/(\alpha g)$ that satisfies (2-34) is the minimum overturning acceleration. Equation (2-34) is valid when $t_i \le T_{ex}$. Within the limits of the linear approximation (slender block) and assuming a value of $\eta = 0.9$, this happens when $0 \le \omega_p / p \le 4.8$.

CASE 2 ($t_i > T_{ex}$)

In this case the condition of overturning yields:

$$\dot{\theta}^{after}(t_i) - p\alpha = 0 \tag{2-35}$$

where $\dot{\theta}^{after}(t_i) = \eta \dot{\theta}^{before}(t_i)$, and

$$\begin{aligned} \dot{\theta}^{before}(t_i) = & \frac{\alpha\omega_p}{1 + \frac{\omega_p^2}{p^2}} \left[\frac{1}{\sin\psi} - \frac{\cosh(pT_{ex})}{\tan\psi} + \frac{\omega_p}{p}\sinh(pT_{ex}) \right] \cosh[p(t_i - T_{ex})] \\ & + \frac{\alpha\omega_p}{1 + \frac{\omega_p^2}{p^2}} \left[-\frac{\sinh(pT_{ex})}{\tan\psi} + \frac{\omega_p}{p}\cosh(pT_{ex}) \right] \sinh[p(t_i - T_{ex})] \end{aligned} . \tag{2-36}$$

In the above equations the impact time t_i is the solution of the transcendental equation

$$\begin{aligned} g(t_i, \psi) = & \frac{\alpha(\omega_p/p)}{1 + (\omega_p/p)^2} \Bigg(\left[\frac{1}{\sin\psi} - \frac{\cosh(pT_{ex})}{\tan\psi} + \frac{\omega_p}{p}\sinh(pT_{ex}) \right] \sinh[p(t_i - T_{ex})] + \\ & \left[-\frac{\sinh(pT_{ex})}{\tan\psi} + \frac{\omega_p}{p}\cosh(pT_{ex}) \right] \cosh[p(t_i - T_{ex})] - \alpha \Bigg) = 0 \end{aligned} \tag{2-37}$$

The solution of equations (2-35) and (2-37) gives the minimum overturning acceleration for the case $t_i > T_{ex}$.

Mode 2

Under this mode, the block does not experience any impact. The condition of overturning becomes

$$\frac{\dot{\theta}(T_{ex})}{p} + [\theta(T_{ex}) + \alpha] = 0 \tag{2-38}$$

where

$$\theta(T_{ex}) = \frac{\alpha(\omega_p/p)}{1+(\omega_p/p)^2}\left[-\frac{\sinh(pT_{ex})}{\tan\psi} + \frac{\omega_p}{p}\cosh(pT_{ex})\right] - \alpha \tag{2-39}$$

$$\dot{\theta}(T_{ex}) = \frac{\alpha\omega_p}{1+(\omega_p/p)^2}\left[-\frac{\cosh(pT_{ex})}{\tan\psi} + \frac{\omega_p}{p}\sinh(pT_{ex}) + \frac{1}{\sin\psi}\right] \tag{2-40}$$

The substitution of (2-39) and (2-40) into (2-38) leads to

$$\frac{\omega_p}{p}\sin\psi - \cos\psi = -e^{\frac{p}{\omega_p}(2\pi-\psi)} \tag{2-41}$$

The solution of (2-41) gives the minimum acceleration amplitude that is capable of overturning the block without any impact. Equation (2-41) is similar to equation (2) of the prologue; however, the duration of the forced vibration due to a one-sine pulse is $T_{ex} = (2\pi - \psi)/\omega_p$, rather than $T_{ex} = (\pi - \psi)/\omega_p$, which is the duration of the forced vibration under a half-sine pulse; and the sign in front of the exponential term in the right-hand side is negative rather than positive.

Figure 5 plots the solutions of the condition of overturning (for $\eta = 0.9$) after distinguishing carefully between mode 1 and mode 2 of overturning. Although the roots are computed numerically, this solution is referred to as an *analytical solution* since it is based on the analytical expressions of the response given by (2-19) and (2-20).

The distinction between mode 1 and mode 2 of overturning is of particular interest since the transition from overturning with one impact to overturning without impact is not immediate; and there is a finite margin of acceleration amplitudes with magnitudes larger than the minimum overturning acceleration (that corresponds to mode 1) that are unable to overturn the block. This interesting behavior is illustrated in Figures 6 and 7, where response time histories of a free-standing block with $p = 2.14$, $\alpha = 0.25$, $\eta = 0.9$ and $\omega/p = 5$ are shown for various levels of the amplitude, a_p, of the acceleration pulse.

The left and center plots in Figure 6 show normalized rotations and angular velocity histories at the verge of overturning due to the first (minimum) level of the acceleration amplitude. With $a_p = 3\alpha g$ the block does not overturn; whereas when $a_p = 3.01\alpha g$ the block overturns after experiencing one impact (mode 1). In this case the impact happens after the expiration of the pulse. A similar pattern of overturning prevails until the acceleration amplitude reaches,

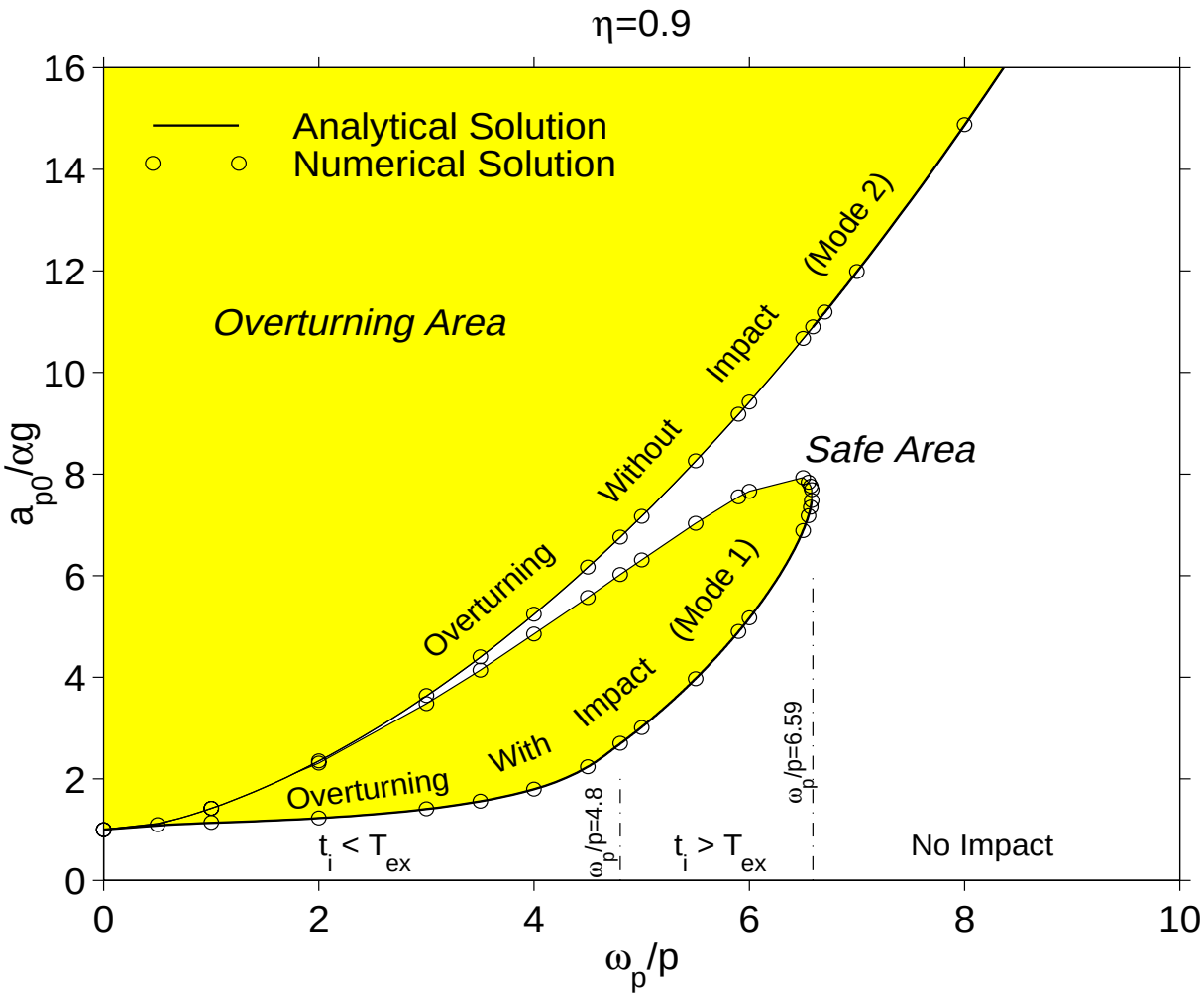

Figure 5. Overturning acceleration spectrum of a free-standing block with $\eta = 0.9$ subjected to a one-sine acceleration pulse with frequency ω_p. The analytical and numerical solutions shown are computed with the linear formulation. When ω_p / p is sufficiently large, a free-standing block overturns only without impact (mode 2).

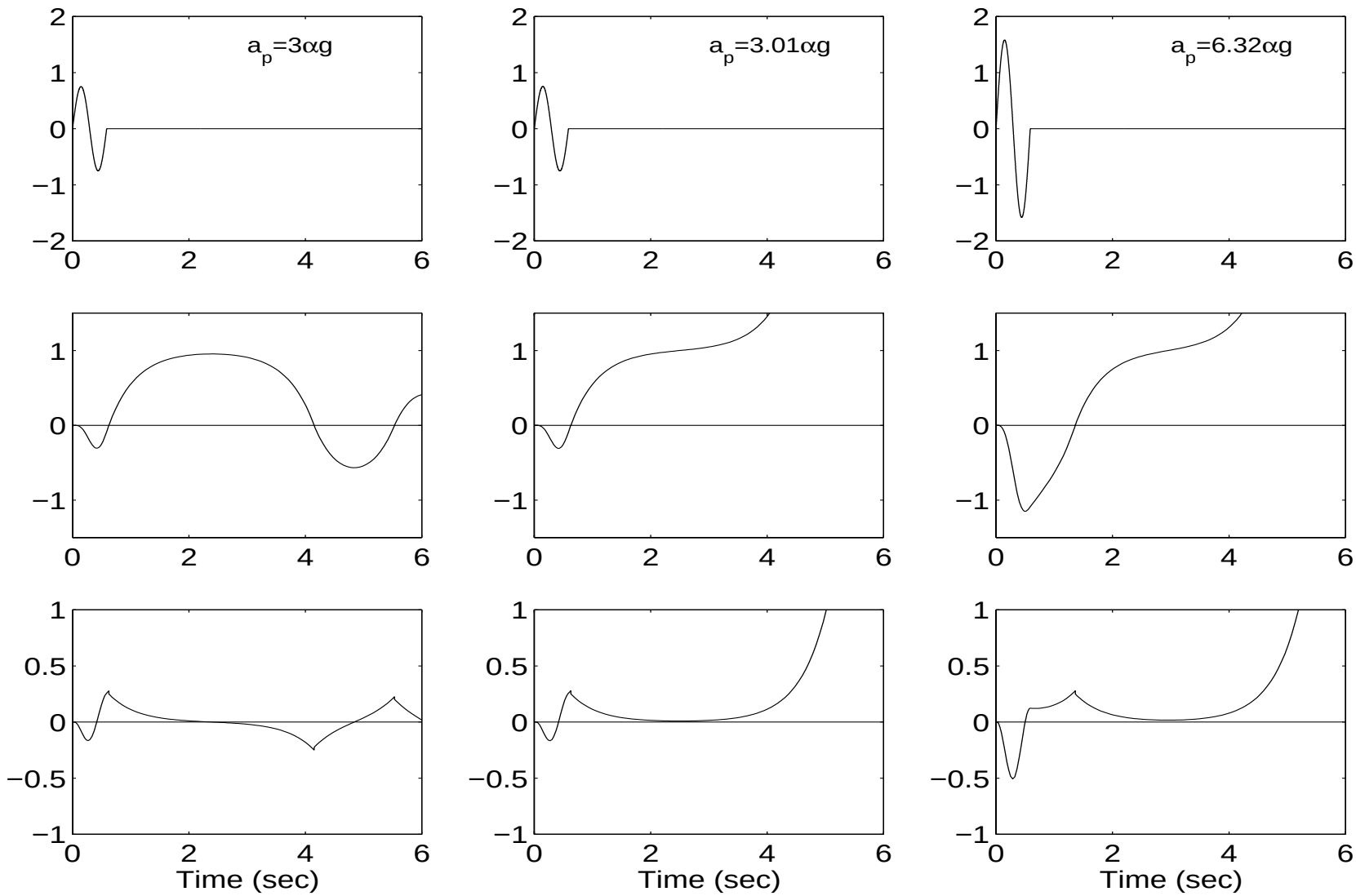

Figure 6. Rotation and angular velocity time histories of a rigid block ($p = 2.14\ rad/sec$, $\alpha = 0.25\ rad$ and $\eta = 0.9$) subjected to a one-sine pulse with $\omega_p/p = 5$. Left: $a_p = 3.00\alpha g$, no overturning. Center: $a_p = 3.01\alpha g$, overturning with one impact (mode 1). Right: $a_p = 6.32\alpha g$, overturning with one impact (mode 1).

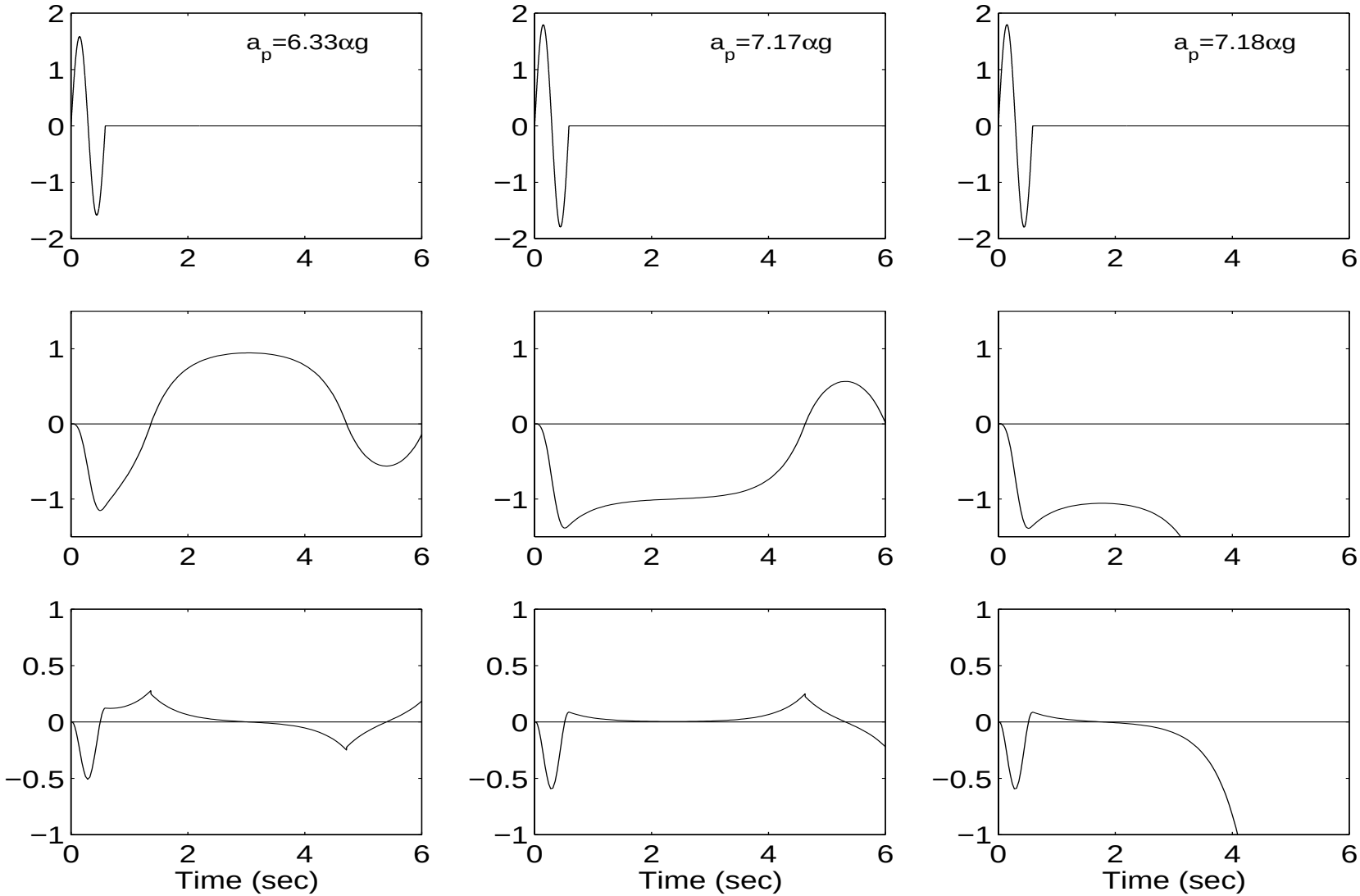

Figure 7. Rotation and angular velocity time histories of the same rigid block as in Figure 4 ($p = 2.14\ rad/sec$, $\alpha = 0.25\ rad$ and $\eta = 0.9$) subjected to a one-sine pulse with $\omega_p/p = 5$. Left: No overturning with $a_p = 6.33\alpha g$, that is slightly larger than the acceleration level, $a_p = 6.32\alpha g$, that created overturning. Center: The block does not overturn even for the acceleration amplitude $a_p = 7.17\alpha g$. Right: The block eventually overturns with $a_p = 7.18\alpha g$, without impact (mode 2).

$a_p = 6.32\alpha g$. A notable difference, shown in the right plots, is that although the first maximum positive rotation, θ, exceeds α, the deaccelerating motion of the ground is capable of recentering the block, which will experience an impact at a considerable later time and eventually overturn.

Figure 7 (left) shows the response of the same free-standing block when the acceleration amplitude of the one-sine pulse has been slightly increased, $a_p = 6.33\alpha g$. Interestingly, the block does not overturn. This is because the acceleration pulse is intense enough to induce such a large rotation that the block escapes most of the overturning effect of the deaccelerating portion of the excitation pulse. This beneficial arrangement of inertia and gravity forces holds until $a_p = 7.17\alpha g$, as shown in the center of Figure 7. Eventually, if the acceleration amplitude, a_p, is further increased the block will overturn without experiencing any impact (mode 2), as shown in Figure 7 (right). It should be noted that Yim et al. (1980) have reported the situation where a free-standing block topples under a certain level of a given ground motion, yet does not topple when the acceleration of the same ground motion is further increased. Figures 6 and 7 in association with the foregoing discussion elucidate this counterintuitive result.

Accordingly, in the frequency-acceleration plane there is a safe area that extends above the minimum overturning acceleration boundary due to mode 1 of overturning. When $0 < \omega_p / p \leq 6.59$, ($\eta = 0.9$), the minimum overturning acceleration is the result of mode 1 (one impact). With reference to Figure 5, when $\omega_p / p > 6.59$, blocks overturn only with mode 2 (no impact) and a substantial increase in the acceleration amplitude is needed to create overturning.

To further validate these results the various overturning boundaries were computed numerically via a state-space formulation that was developed to account for the nonlinear nature of the problem. With reference to equations (2-17) and (2-18), the state vector of the system is merely

$$\{y(t)\} = \begin{Bmatrix} \theta(t) \\ \dot{\theta}(t) \end{Bmatrix} \tag{2-42}$$

and the time-derivative vector $f(t)$ is

$$f(t) = \{\dot{y}(t)\} = \begin{Bmatrix} \dot{\theta}(t) \\ -p^2\left[\sin[\alpha \operatorname{sgn}[\theta(t)] - \theta(t)] + \dfrac{\ddot{u}_g}{g}\cos[\alpha \operatorname{sgn}[\theta(t)] - \theta(t)]\right] \end{Bmatrix} \tag{2-43}$$

For slender blocks, the linear approximation becomes dependable, and equation (2-43) reduces to

$$f(t) = \{\dot{y}(t)\} = \left\{ \begin{array}{c} \dot{\theta}(t) \\ p^2\left[-\alpha \mathrm{sgn}[\theta(t)] + \theta(t) - \dfrac{\ddot{u}_g(t)}{g}\right] \end{array} \right\} \tag{2-44}$$

The numerical integration of (2-43) or (2-44) is performed with standard ODE solvers available in MATLAB (1992). The results of the numerical solution of equation (2-44), shown on Figure 5 with circles, are in excellent agreement with the analytical solution.

2.3.2 Nonlinear Formulation

Figure 8 plots with crosses the overturning acceleration spectra of a rigid block with $\alpha = 0.25$ *rad*, $p = 2.14$ *rad/sec*, and $\eta = 0.9$, where the various overturning boundaries are computed numerically with the nonlinear formulation expressed with equation (2-43). The circles shown on Figure 8 are the results computed with the linear formulation expressed by equation (2-44). It is interesting to note that while for values of ω_p / p up to 6, the linear approximation gives equally good results as the nonlinear formulation, for $6 \le \omega_p / p \le 7.58$, the two formulations give drastically different results. As an example under a one-sine pulse with $\omega_p = 15.7$ rad/sec ($f = 2.5$ Hz), the linear formulation yields that the block with $\alpha = 0.25$ rad, $p = 2.14$ rad/sec, and $\eta = 0.9$ will overturn under a minimum acceleration amplitude, $a_{p0} = 3.24\ g$; whereas the nonlinear formulation yields $a_{p0} = 2.22\ g$. This drastic difference is because under the nonlinear formulation, the overturning "bay" penetrates further into the safe area. These drastic differences disappear for pulse frequencies beyond 2.58 Hz since, according to both formulations, the free-standing block overturns with mode 2 (no impact).

A recent study by Anooshehpoor et al. (1999) attempted to produce the minimum overturning acceleration spectra under one-sine pulses within the frequency range $0 \le \omega_p / p \le 10$. Unfortunately, the study by Anooshehpoor et al. failed to identify the existence of the second mode of overturning, the existence of the safe "cape" that embraces the overturning "bay", and the sensitivity of the response to the nonlinear nature of the problem even for blocks as slender as a train locomotive with $\alpha = 0.25\ rad = 14.32°$.

Figure 9 plots overturning acceleration spectra of a rigid equipment with $\alpha = 0.349\ rad = 20°$, $p = 2.0\ rad/sec$ and $\eta = \sqrt{r_{max}} \approx 0.825$. The crosses are the result of the nonlinear formulation, whereas the circles are the results computed with a linear formulation. Again within the low range of ω_p / p, the linear formulation gives equally good results as the non-

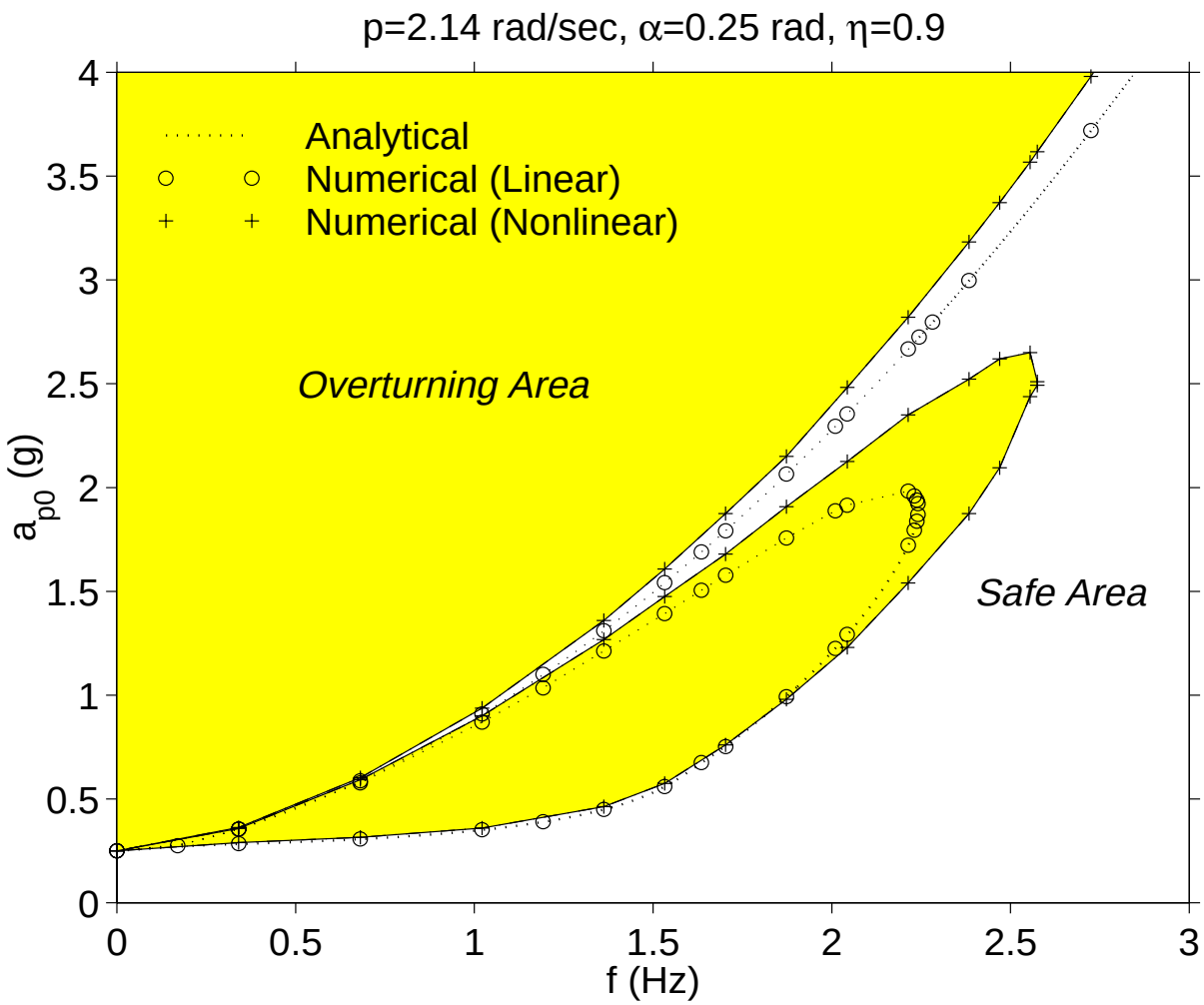

Figure 8. Comparison of overturning acceleration spectra of a slender block ($\alpha = 0.25\ rad = 14.32°$, $p = 2.14\ rad/sec$, $\eta = 0.9$) under a one-sine pulse, computed with linear and nonlinear formulations respectively. When the frequency of the one-sine pulse is relatively low, both formulations yield comparable results. As the excitation frequency increases, the linear formulation yields minimum overturning acceleration amplitudes drastically larger than those obtained with the nonlinear formulation. This is because under the nonlinear formulation the overturning "bay" generated by mode 1 penetrates further into the safe area under the overturning spectrum due to mode 2. As the excitation frequency further increases the linear and nonlinear formulations again yield comparable results since under both formulations and a high-frequency pulse the block overturns with mode 2.

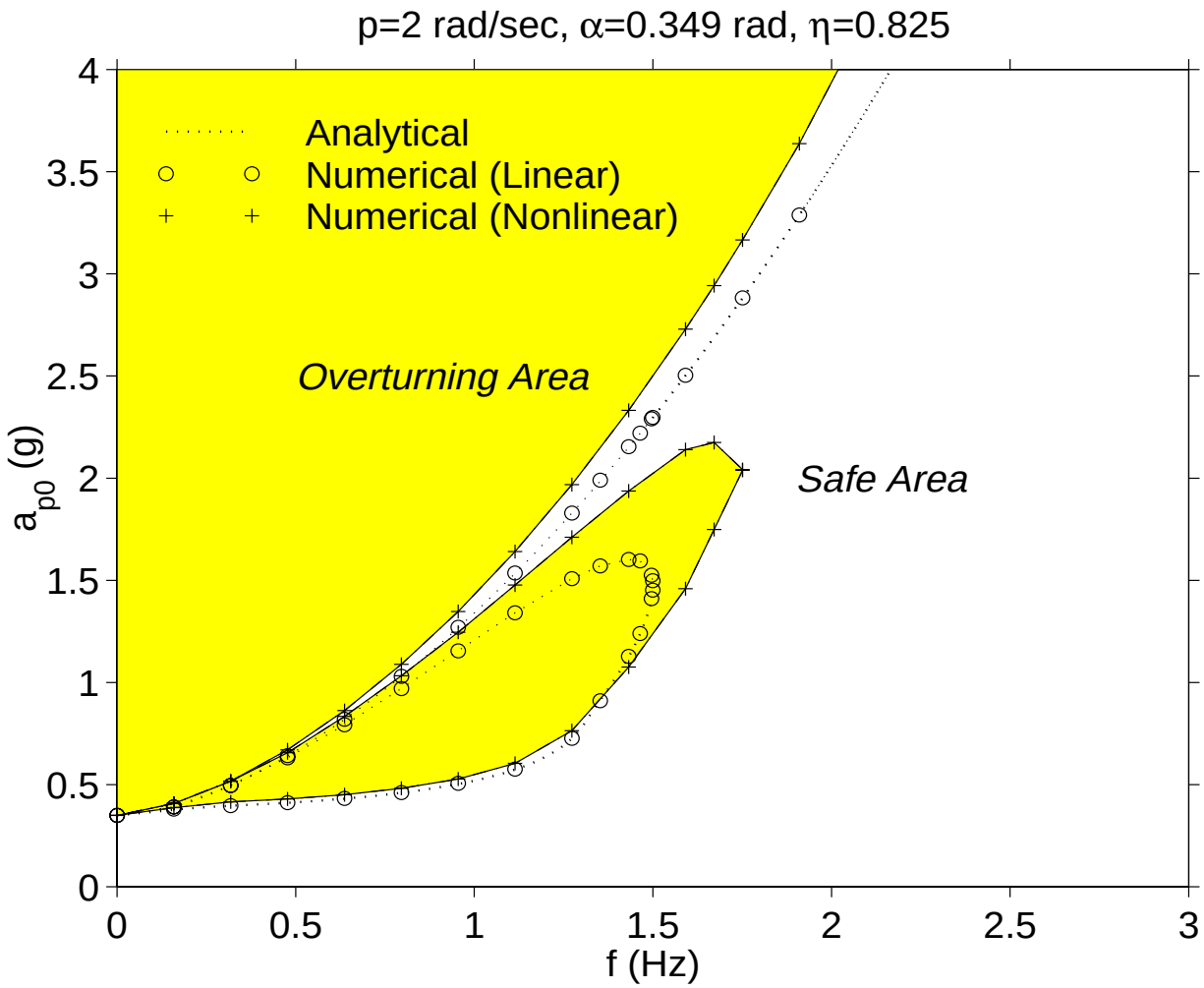

Figure 9. Comparison of overturning acceleration spectra of a free-standing equipment with $\alpha = 0.349\ rad = 20°$, $p = 2\ rad/sec$ and $\eta = \sqrt{r_{max}} = 0.825$, under a one-sine pulse, computed with the linear and the nonlinear formulation

linear formulation. However, within the range $5.8 \le \omega_p / p \le 7.35$, the two formulations gives drastically different results.

2.4 Rocking Response to a One-cosine (Type-B) Pulse

Whereas a one-sine acceleration pulse results to a forward ground displacement, a one-cosine acceleration pulse results to a forward-and-back ground displacement. With reference to Figure 3, under a one-cosine acceleration pulse the maximum ground acceleration is induced at the instant when rocking initiates ($\lambda = 1$) and the condition for pure rocking given by (2-7) becomes

$$\tan\alpha \cdot \frac{\dfrac{a_p}{g\sin\alpha} - \dfrac{3}{4}\cos\alpha\left(\dfrac{a_p}{g\tan\alpha} - 1\right)}{\dfrac{\tan\alpha}{\sin\alpha} + \dfrac{3}{4}\tan\alpha\sin\alpha\left(\dfrac{a_p}{g\tan\alpha} - 1\right)} < \mu \tag{2-45}$$

which for slender blocks ($\sin\alpha \approx \tan\alpha \approx \alpha$ and $\cos\alpha \approx 1$) simplifies to

$$\alpha \cdot \frac{\dfrac{3}{4} + \dfrac{1}{4}\dfrac{a_p}{\alpha g}}{1 + \dfrac{3}{4}\alpha^2\left(\dfrac{a_p}{\alpha g} - 1\right)} < \mu \tag{2-46}$$

Equation (2-45) or its slender block approximation given by (2-46) indicates that the stronger the acceleration pulse is, the larger needs to be the static coefficient of friction to sustain pure rocking. Figure 10 plots the magnification factor of the slenderness $\tan\alpha$, or α in equation (2-45) and (2-46) respectively as a function of $a_p/(\alpha g)$ for different values of the slenderness α. As an example, Figure 10 indicates that when a free-standing block with $\alpha = 0.25$ is subjected to a Type-B pulse with $a_p/(\alpha g) \approx 6$, the minimum coefficient of friction needed to sustain pure rocking is approximately two times the value of the block slenderness.

Figure 11 plots the overturning acceleration spectra due to a one-cosine acceleration pulse with time history

$$\ddot{u}_g(t) = \begin{cases} a_p \cos(\omega_p t) & 0 < t < 2\pi/\omega_p \\ 0 & otherwise \end{cases} \tag{2-47}$$

In this case the phase angle, ψ, when rocking initiates is zero since a one-cosine pulse yields its maximum acceleration at the instant when the pulse initiates. The same rigid block ($\alpha = 0.25$ *rad*, $p = 2.14$ *rad/sec*, and $\eta = 0.9$) is considered. The circles, shown on Figure 11, are the results computed with the linear formulation, whereas the crosses are the results obtained with the nonlinear formulation. In this case, the differences observed between the linear and the nonlinear

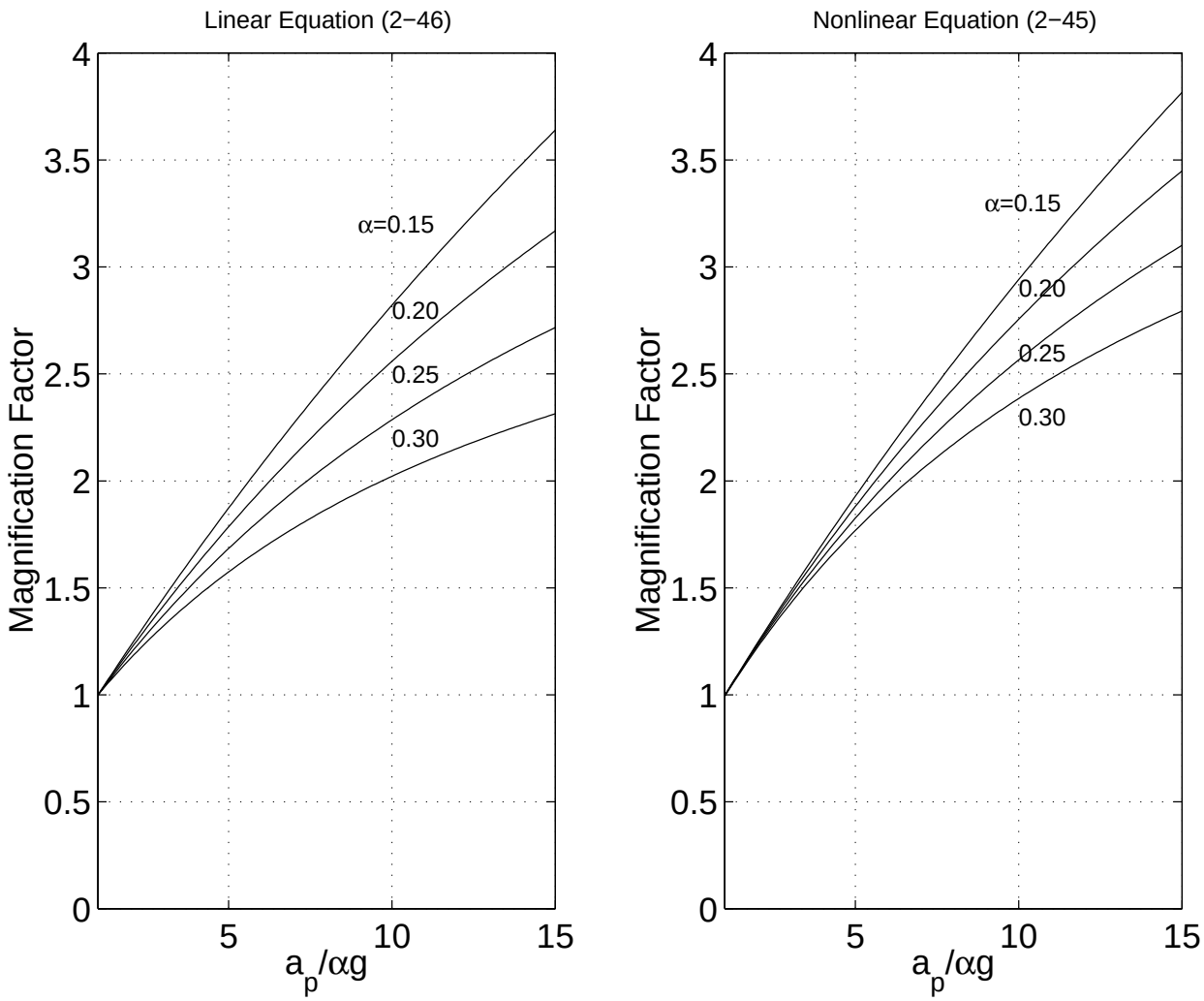

Figure 10. Normalized minimum coefficient of friction over the slenderness of a block that is needed to sustain pure rocking motion

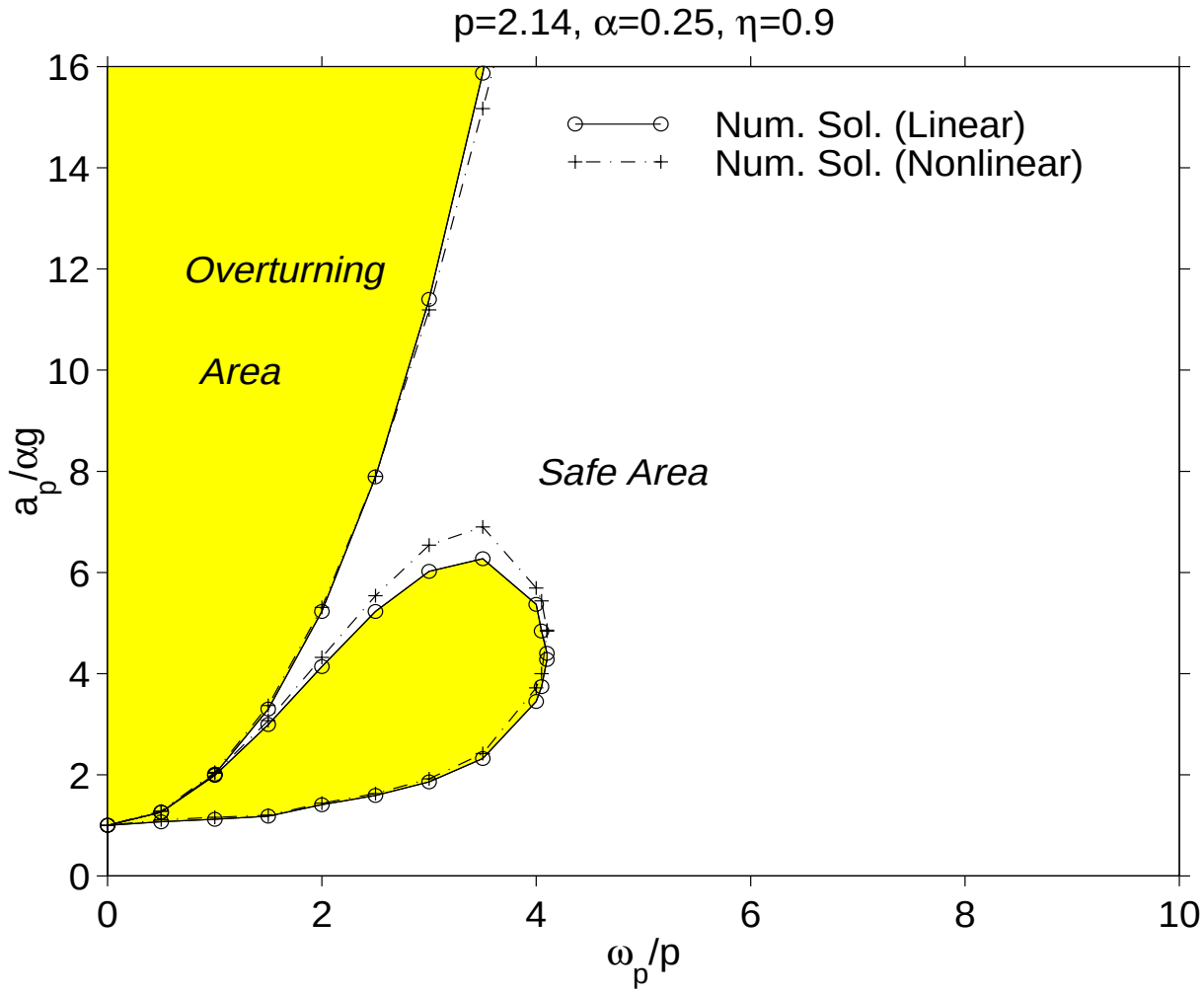

Figure 11. Comparison of overturning acceleration spectra of a slender block ($\alpha = 0.25\ rad = 14.32°$, $p = 2.14\ rad/sec$, $\eta = 0.9$) under a one-cosine pulse, computed with the linear and the nonlinear formulation. In this case the difference between the results of the two formulations are less drastic than those observed under a one-sine pulse.

formulation are less drastic. Figure 11 indicates that under a one-cosine pulse with frequency ω_p, blocks that are small enough so that $\omega_p / p \leq 4$, can experience two distinct modes of overturning. Again, the existence of these two modes are responsible for the generation of a safe region that embraces the minimum overturning acceleration spectrum. Consequently, similar to the case of a one-sine pulse, there is a finite margin of acceleration amplitudes with magnitudes larger than the minimum overturning acceleration (that corresponds to mode 1) that are unable to overturn the block. This interesting behavior is illustrated in Figures 12 and 13 where the response time histories of a free-standing block with α = 0.25 rad, p = 2.14 rad/sec η = 0.9 and ω_p / p = 3 are shown for various levels of the amplitude, a_p. Figure 14 plots overturning acceleration spectra under a one-cosine pulse of a rigid equipment with α = 0.349 rad = 20°, p = 2.0 rad$/sec$, and η = $\sqrt{r_{max}}$ = 0.825. The crosses are the result of the nonlinear formulation, whereas the circles are the results computed with the linear formulation. In comparing Figure 14 with 11 one concludes that the normalized overturning acceleration spectra have a mild dependence on the slenderness of the block, α.

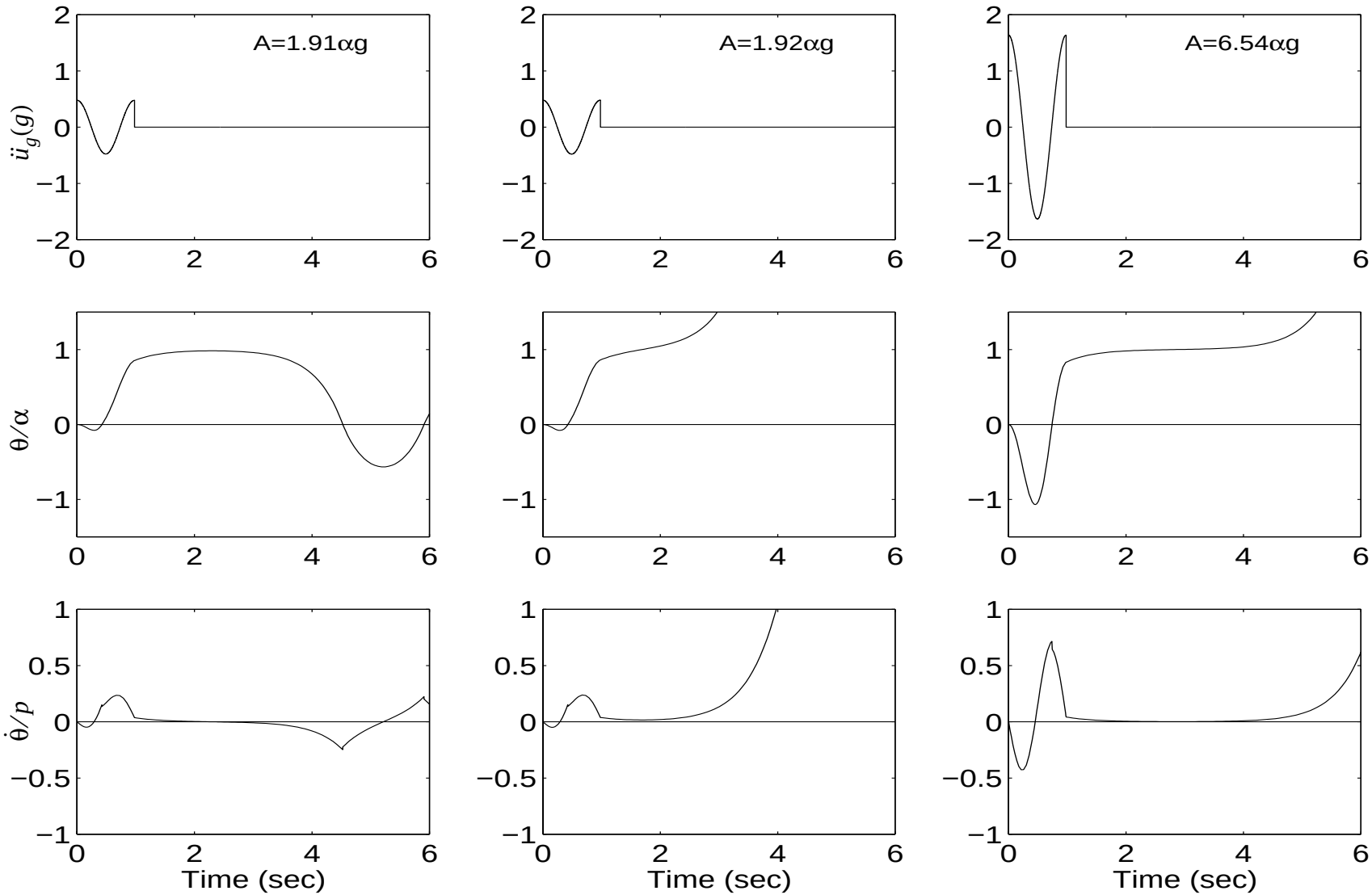

Figure 12. Rotation and angular velocity time histories of a rigid block ($p = 2.14\ rad/sec$, $\alpha = 0.25\ rad$ and $\eta = 0.9$) subjected to a one-cosine pulse with $\omega_p/p = 3$. Left: $a_p = 1.91\alpha g$, no overturning. Center: $a_p = 1.92\alpha g$, overturning with one impact (mode 1). Right: $a_p = 6.54\alpha g$, overturning with one impact (mode 1).

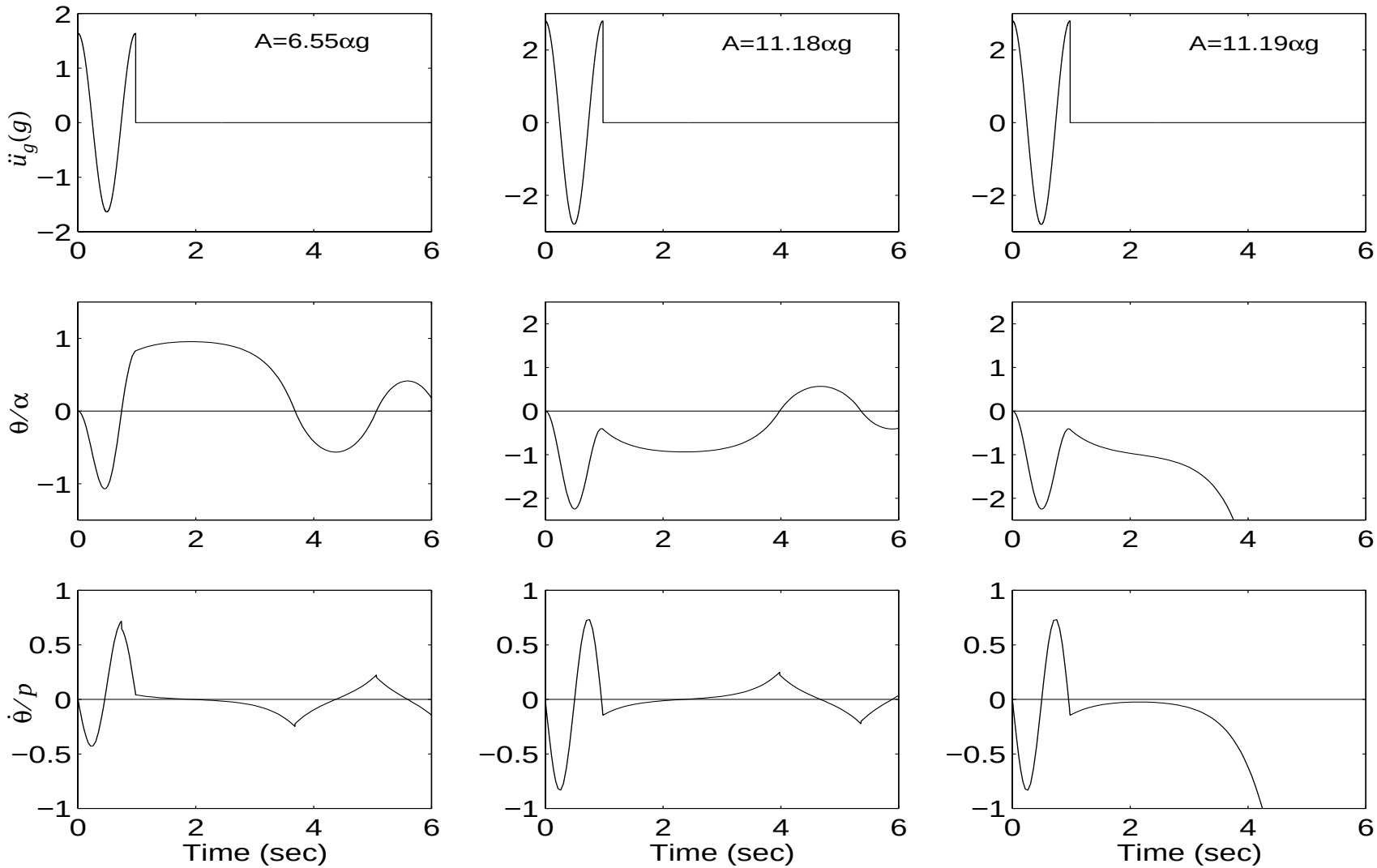

Figure 13. Rotation and angular velocity time histories of the same rigid block as in Figure 9 ($p = 2.14\ rad/sec$, $\alpha = 0.25\ rad$ and $\eta = 0.9$) subjected to a one-cosine pulse with $\omega_p/p = 3$. Left: No overturning with $a_p = 6.55\alpha g$, that is slightly larger than the acceleration level, $a_p = 6.54\alpha g$, that created overturning. Center: The block does not overturn even for the acceleration amplitude $a_p = 11.18\alpha g$. Right: The block eventually overturns with $a_p = 11.19\alpha g$, without impact (mode 2).

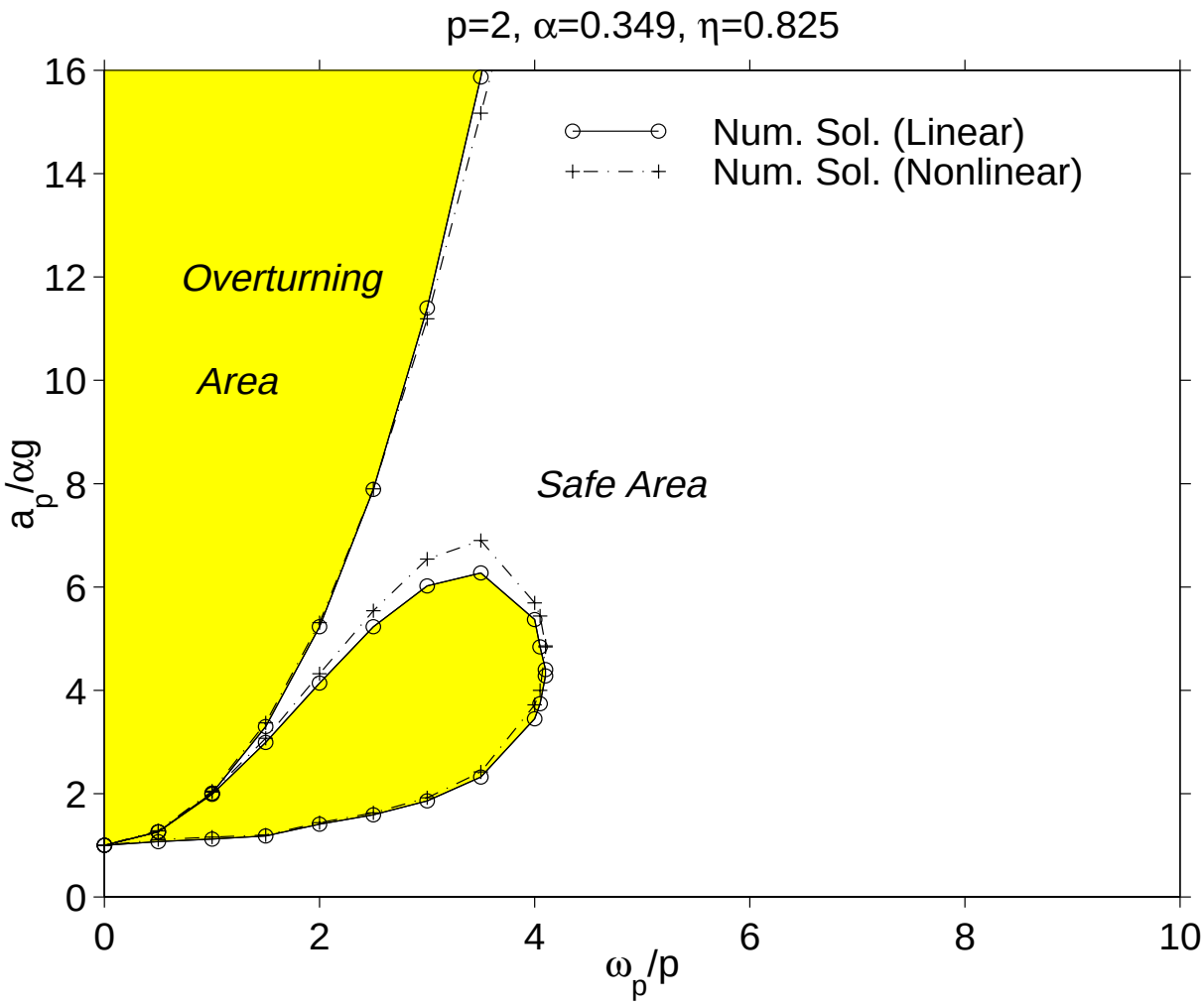

Figure 14. Comparison of overturning acceleration spectra of a slender block ($\alpha = 0.349\ rad = 20°$, $p = 2.0\ rad/sec$, $\eta = 0.825$) under a one-cosine pulse, computed with the linear and the nonlinear formulation. In this case the difference between the results of the two formulations are less drastic than those observed under a one-sine pulse.

CHAPTER 3
ROCKING RESPONSE OF A FREE-STANDING BLOCK UNDER HORIZONTAL AND VERTICAL EXCITATION

3.1 Numerical Formulation and Solution

The rocking response of a rigid block subjected to concurrent horizontal and vertical earthquake excitation is computed numerically via a state-space formulation that can accommodate the non-linear nature of the problem. Similar integration of the equation of motion has been carried out by Yim et al. (1980), Spanos and Koh (1984), Hogan (1989), and Shi et al. (1996) among others. The state vector of the system is merely

$$\{y(t)\} = \begin{Bmatrix} \theta(t) \\ \dot{\theta}(t) \end{Bmatrix} \tag{3-1}$$

and the time-derivative vector $f(t)$ is

$$f(t) = \{\dot{y}(t)\} = \begin{Bmatrix} \dot{\theta}(t) \\ -p^2\left[\sin[\alpha\,\mathrm{sgn}[\theta(t)] - \theta(t)]\left(1 + \frac{\ddot{v}_g}{g}\right) + \frac{\ddot{u}_g}{g}\cos[\alpha\,\mathrm{sgn}[\theta(t)] - \theta(t)]\right] \end{Bmatrix} \tag{3-2}$$

The numerical integration of (3-2) is performed with standard ODE solvers available in MATLAB (1992). Figure 15 plots the rotation and angular velocity of a $0.5\ m \times 1.5\ m$ free-standing block subjected to the minimum acceleration level of the Rinaldi station records (January 17, 1994, Northridge earthquake) that are needed to overturn it. In the first column of Figure 15 the vertical component of the acceleration is assumed to be zero and the horizontal component is 78% of the recorded motion. In the second column of Figure 15 the vertical component is considered and it is found that only 74% of the recorded time histories is needed to overturn the block. In this case the vertical acceleration contributes constructively to the overturning. However, as shown in the third column of Figure 15, when the polarity of the vertical motion is reversed, the vertical component contributes destructively, since 83% of the recorded time histories is now needed to overturn the block. Figure 15 also indicates that the rocking response of the block when the vertical acceleration is absent does not differ significantly from the case where the vertical excitation is included.

Similar trends are observed in Figure 16 that plots the rotation and angular velocity of the same $0.5\ m \times 1.5\ m$ block subjected to the minimum acceleration level of the Sylmar station records from the 1994 Northridge earthquake that are needed to overturn it. The second column of

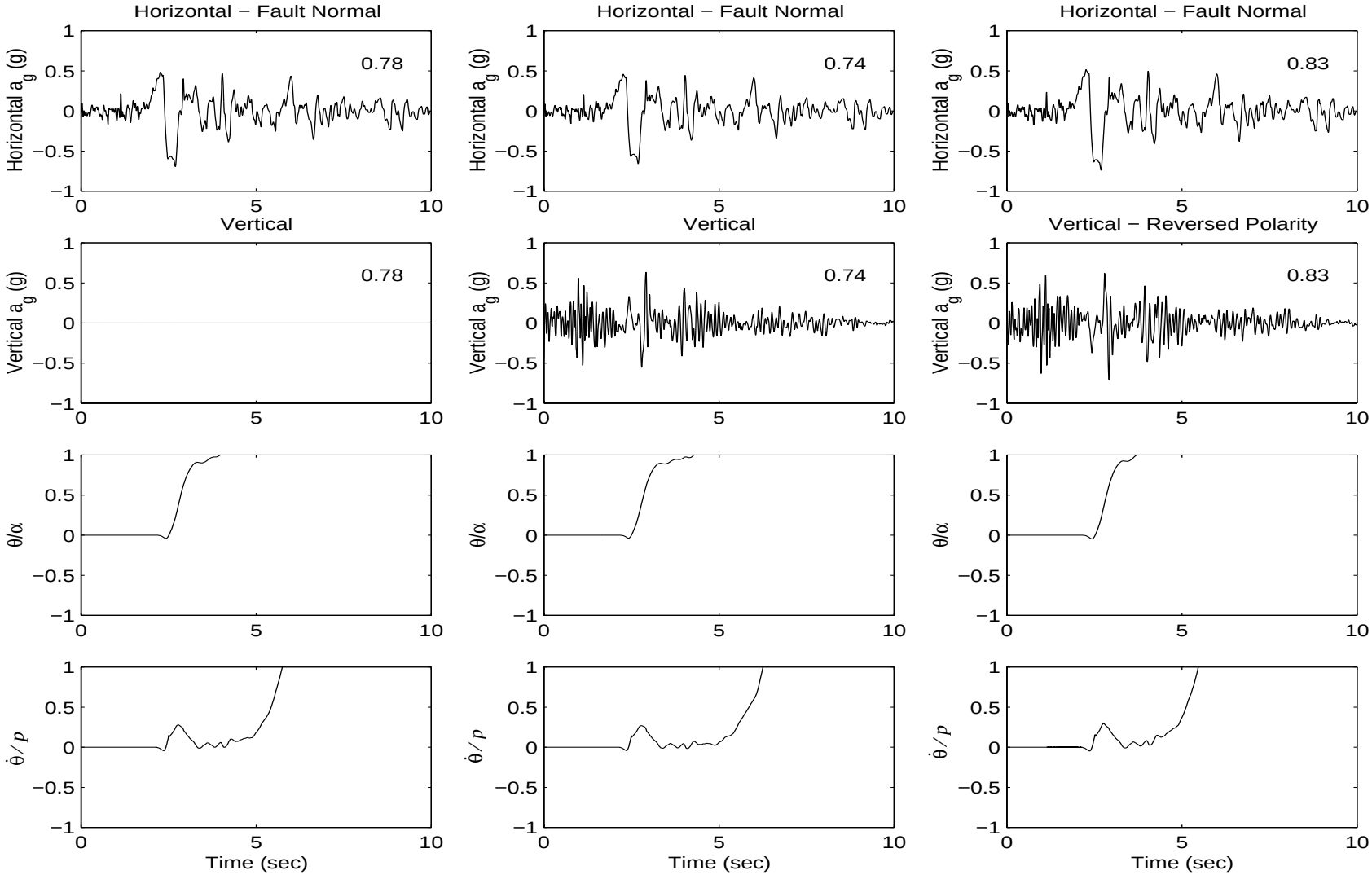

Figure 15. Rotation and angular velocity time histories of a rigid block (*b = 0.5 m*, *h = 1.5 m*) subjected to the fault-normal and vertical Rinaldi station records. Left: overturning under horizontal component alone (78% acceleration level). Center: overturning under horizontal and vertical components (74% acceleration level). Right: overturning under horizontal and vertical components with reversed polarity (83% acceleration level).

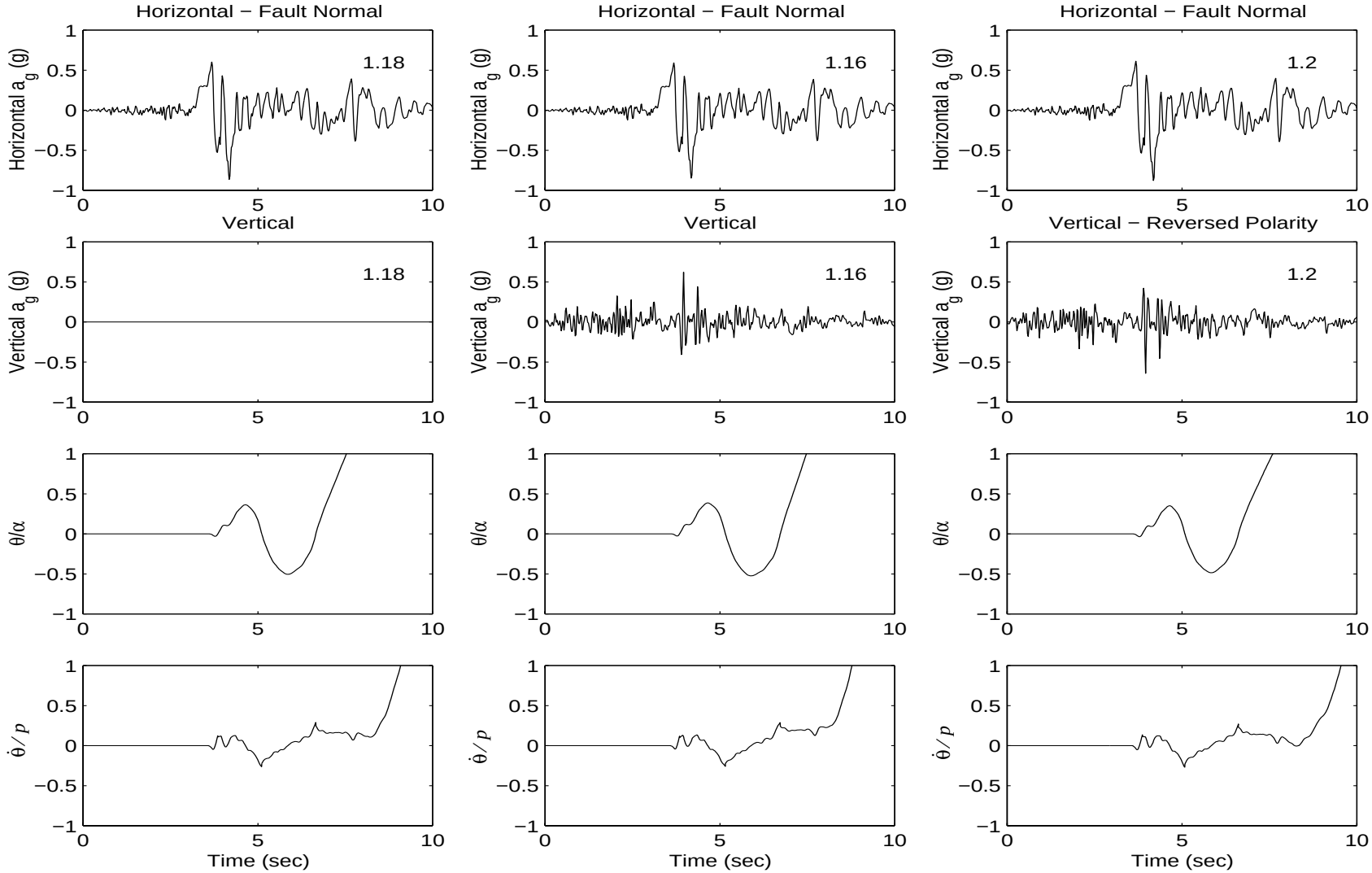

Figure 16. Rotation and angular velocity time histories of a rigid block (*b = 0.5 m, h = 1.5 m*) subjected to the fault-normal and vertical Sylmar station records. Left: overturning under horizontal component alone (118% acceleration level). Center: overturning under horizontal and vertical components (116% acceleration level). Right: overturning under horizontal and vertical components with reversed polarity (120% acceleration level).

Figure 16 shows that when the vertical component of the motion is considered, 116% of the recorded time histories is capable of overturning the block. This level of excitation is marginally lower than the 118% of the horizontal component alone that can overturn the block. Again, when the polarity of the vertical motion is reversed, the vertical component contributes destructively since now 120% of the recorded time histories is needed to overturn the block. It should be noted that the reversal of the polarity does not yield a destructive effect with all the records. Figure 17 plots the rotation and angular velocity of the $0.5\ m \times 1.5\ m$ block subjected to the minimum acceleration level of another Northridge record --- the Newhall record. In this case the right polarity of the vertical component has a destructive effect, whereas the reverse polarity has a constructive effect. Whatever the polarity, Figures 16 and 17 indicate that the simultaneous consideration of the vertical motion has a marginal effect on the acceleration level of the horizontal motion that is needed to overturn a given block. This finding is also shown in Figures 18 to 22 where the minimum overturning accelerations of other historic ground motions are shown. Table 1 summarizes the minimum levels of acceleration records, without and with the vertical component, that are needed to overturn a $0.5\ m \times 1.5\ m$ free-standing block.

TABLE 1. Minimum Level of Acceleration Records Needed to Overturn a $0.5\ m \times 1.5\ m$ Free-standing Block ($\alpha = 18.43°$, $p = 2.157\ rad/sec$).

Records	Levels of Acceleration Records		
	Horizontal	**Horizontal & Vertical**	**Horizontal & Vertical (reversed polarity)**
Rinaldi (FN), 1994 Northridge	0.78	0.74	0.83
Sylmar (FN), 1994 Northridge	1.18	1.16	1.20
Newhall (N-S), 1994 Northridge	1.83	1.86	1.80
El Centro #5 (FN), 1979 Imperial	1.29	1.26	1.30
El Centro #6 (FN), 1979 Imperial	1.49	1.49	1.61
El Centro #7 (FN), 1979 Imperial	1.52	1.52	1.52
Los Gatos (0), 1989 Loma Prieta	1.46	1.45	1.51
Lucerne Valley (FP), 1992 Landers	2.75	2.85	2.95

The marginal effect that the vertical acceleration has on the level of the horizontal acceleration that is needed to overturn a rigid block was also reported by Shi et al (1996).

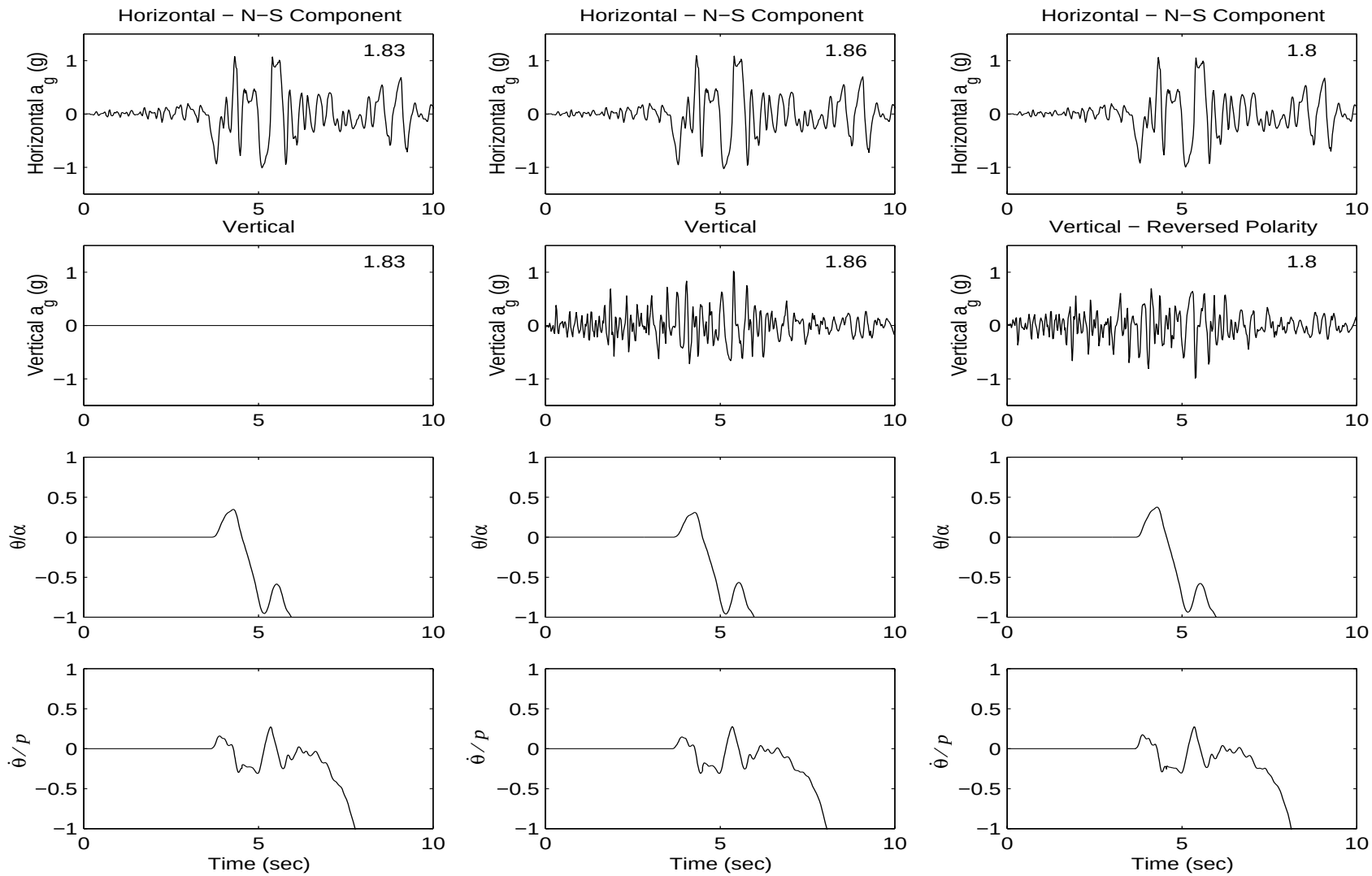

Figure 17. Rotation and angular velocity time histories of a rigid block (*b = 0.5 m, h = 1.5 m*) subjected to the N-S and vertical Newhall station records. Left: overturning under horizontal component alone (183% acceleration level). Center: overturning under horizontal and vertical components (186% acceleration level). Right: overturning under horizontal and vertical components with reversed polarity (180% acceleration level).

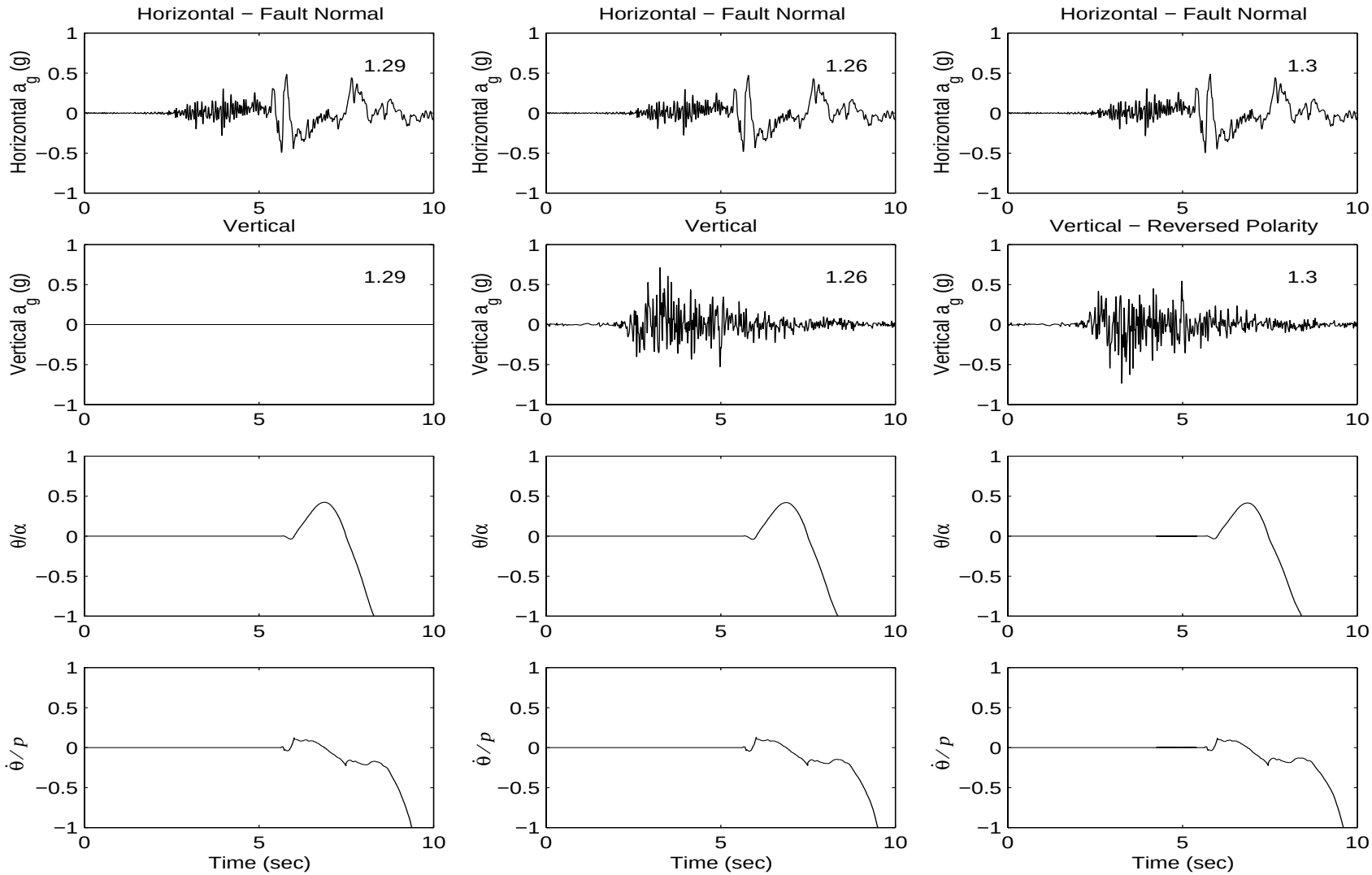

Figure 18. Rotation and angular velocity time histories of a rigid block (*b = 0.5 m*, *h = 1.5 m*) subjected to the fault-normal and vertical El Centro Array #5 records. Left: overturning under horizontal component alone (129% acceleration level). Center: overturning under horizontal and vertical components (126% acceleration level). Right: overturning under horizontal and vertical components with reversed polarity (130% acceleration level).

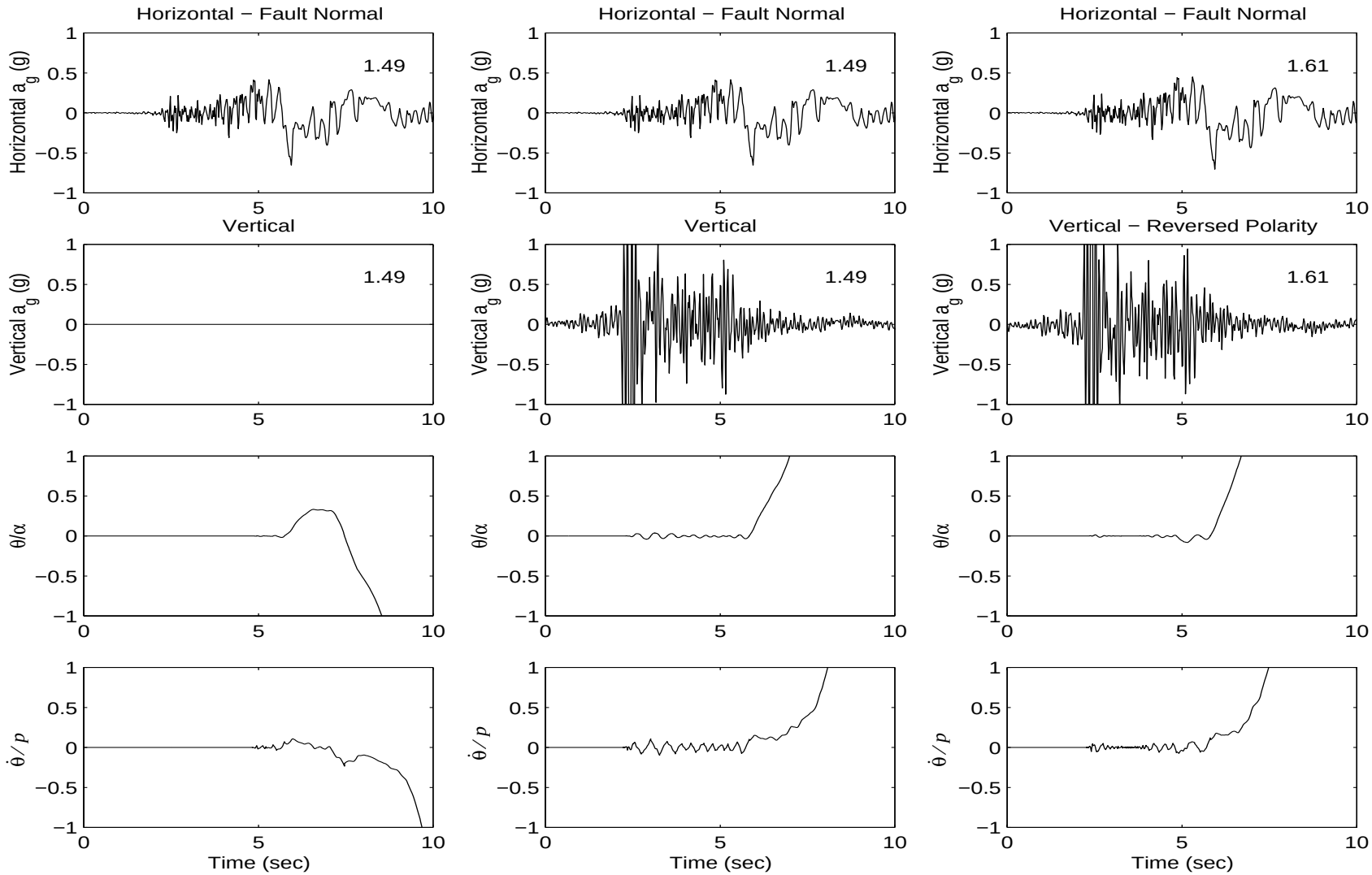

Figure 19. Rotation and angular velocity time histories of a rigid block (*b = 0.5 m, h = 1.5 m*) subjected to the fault-normal and vertical El Centro Array #6 records. Left: overturning under horizontal component alone (149% acceleration level). Center: overturning under horizontal and vertical components (149% acceleration level). Right: overturning under horizontal and vertical components with reversed polarity (161% acceleration level).

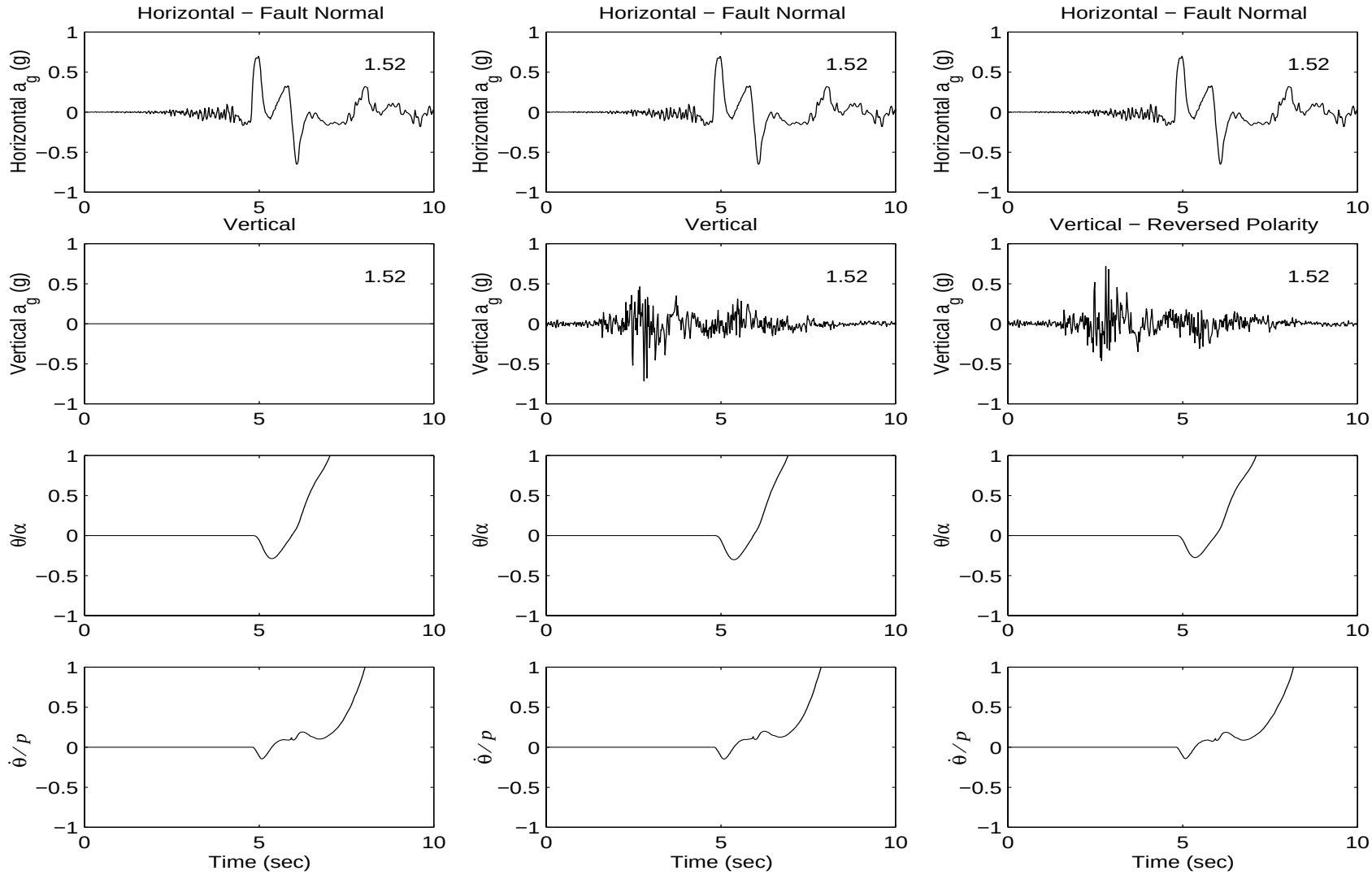

Figure 20. Rotation and angular velocity time histories of a rigid block (*b = 0.5 m, h = 1.5 m*) subjected to the fault-normal and vertical El Centro Array #7 records. Left: overturning under horizontal component alone (152% acceleration level). Center: overturning under horizontal and vertical components (152% acceleration level). Right: overturning under horizontal and vertical components with reversed polarity (152% acceleration level).

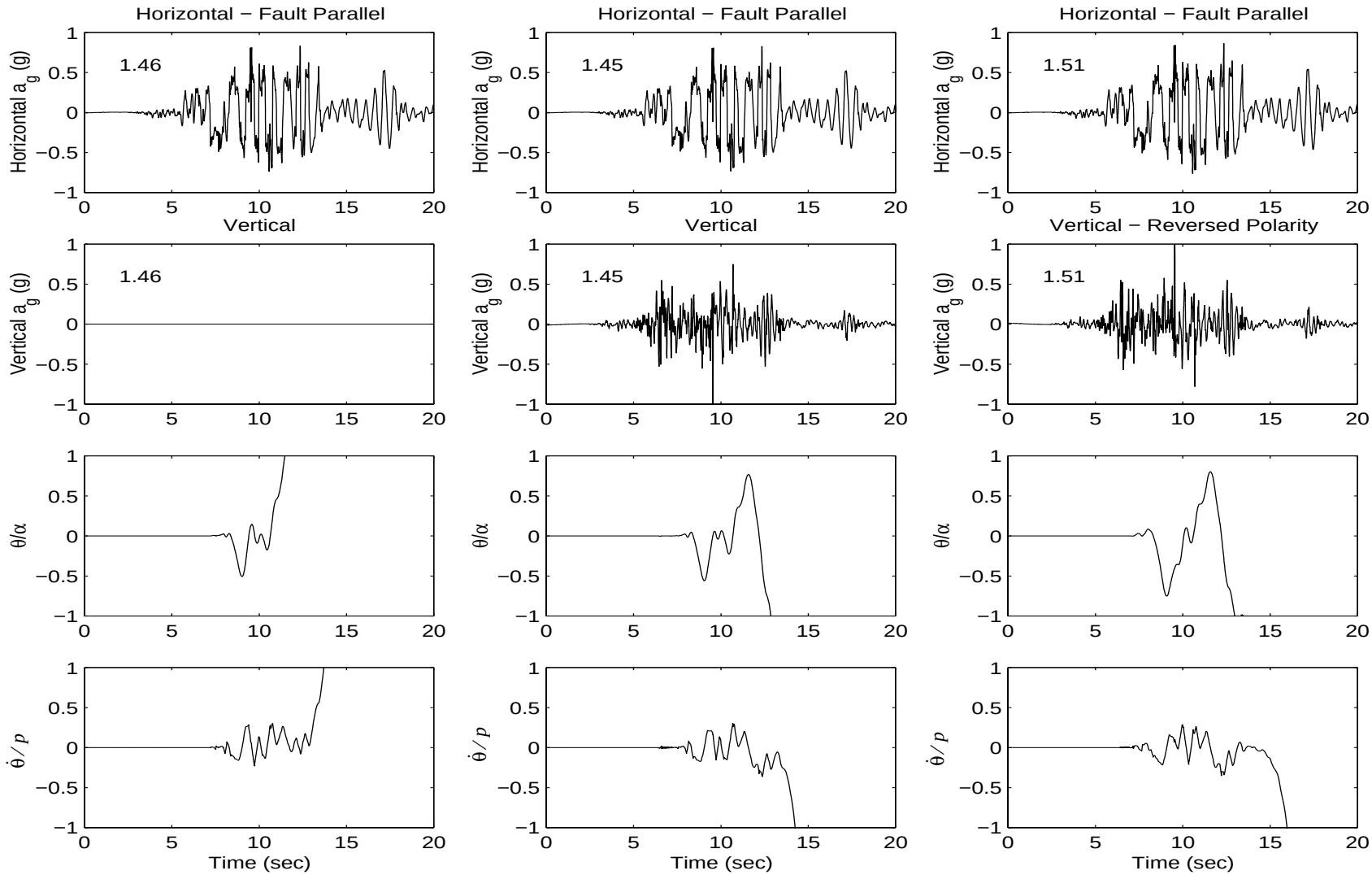

Figure 21. Rotation and angular velocity time histories of a rigid block (*b = 0.5 m, h = 1.5 m*) subjected to the fault-parallel and vertical Los Gatos station records. Left: overturning under horizontal component alone (146% acceleration level). Center: overturning under horizontal and vertical components (145% acceleration level). Right: overturning under horizontal and vertical components with reversed polarity (151% acceleration level).

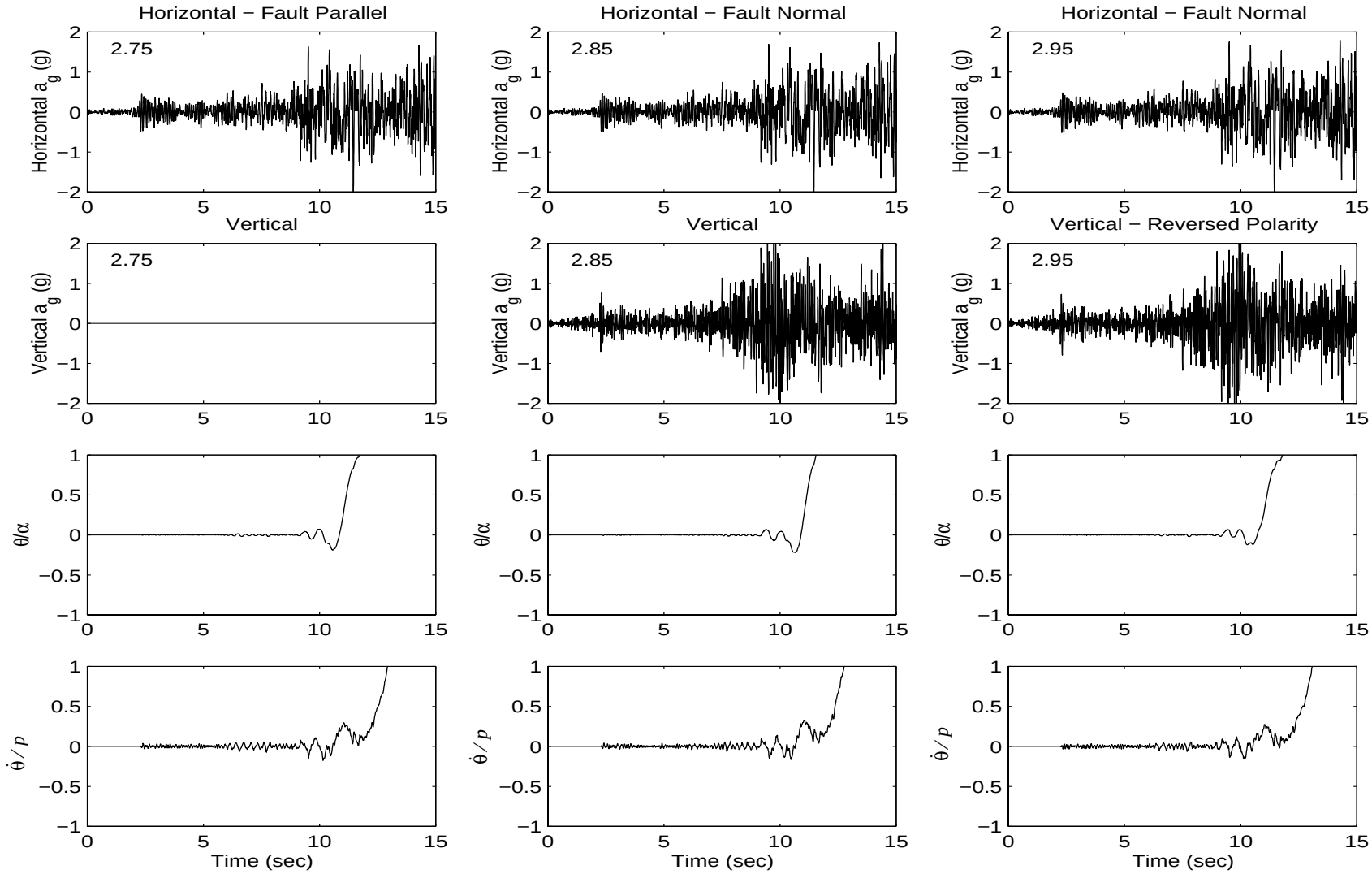

Figure 22. Rotation and angular velocity time histories of a rigid block (*b = 0.5 m*, *h = 1.5 m*) subjected to the fault-parallel and vertical Lucerne Valley records. Left: overturning under horizontal component alone (275% acceleration level). Center: overturning under horizontal and vertical components (285% acceleration level). Right: overturning under horizontal and vertical components with reversed polarity (295% acceleration level).

3.2 Response Spectra and Effect of the Coefficient of Restitution

In the foregoing analysis, Figures 15 to 22 show time histories of the response of a given block to the minimum acceleration level of a given ground motion that is needed to overturn it. In this section response maxima are computed of various blocks subjected to a given ground motion at its 100% level. Three different values of the block slenderness, $\alpha = 15°$, $20°$ and $25°$ have been selected while the frequency parameter, *p*, ranges from 1 rad/sec to 3 rad/sec. These values of slenderness and frequency parameter represent the geometric and dynamic characteristics of most electrical equipment of interest. Figure 23 plots response spectra for the maximum angle of rotation, θ_{max}/α, and the maximum angular velocity, $\dot{\theta}_{max}/p$, under the excitation recorded along the fault normal component at the Rinaldi station during the 1994 Northridge earthquake. The spectra shown in the left column of Figure 23 are computed by using the maximum value of the coefficient of restitution, $r = r_{max} = [1 - 1.5\sin^2\alpha]^2$, that allows for a rocking motion. For $\alpha = 15°$, $\sqrt{r_{max}} = 0.90$; whereas for $\alpha = 20°$ and $25°$, $\sqrt{r_{max}} = 0.825$ and 0.732 respectively. Figure 23 (center) shows the rotation and angular velocity spectra for $\sqrt{r} = 0.75$. In this case only the response of blocks with $\alpha = 15°$ and $\alpha = 20°$ are shown since for the case $\alpha = 25°$, $\sqrt{r_{max}} = 0.732 < 0.75$. Figure 23 (right) shows the rotation and angular velocity spectra for $\sqrt{r} = 0.5$.

The response spectra in Figure 23 show that a reduced coefficient of restitution (more energy lost during impact) results in smaller angles of rotation; however the values of the impact velocities might be larger. Similar trends are observed in Figure 24, where rocking response spectra are shown for the fault-normal motion recorded at the Sylmar station during the 1994 Northridge earthquake.

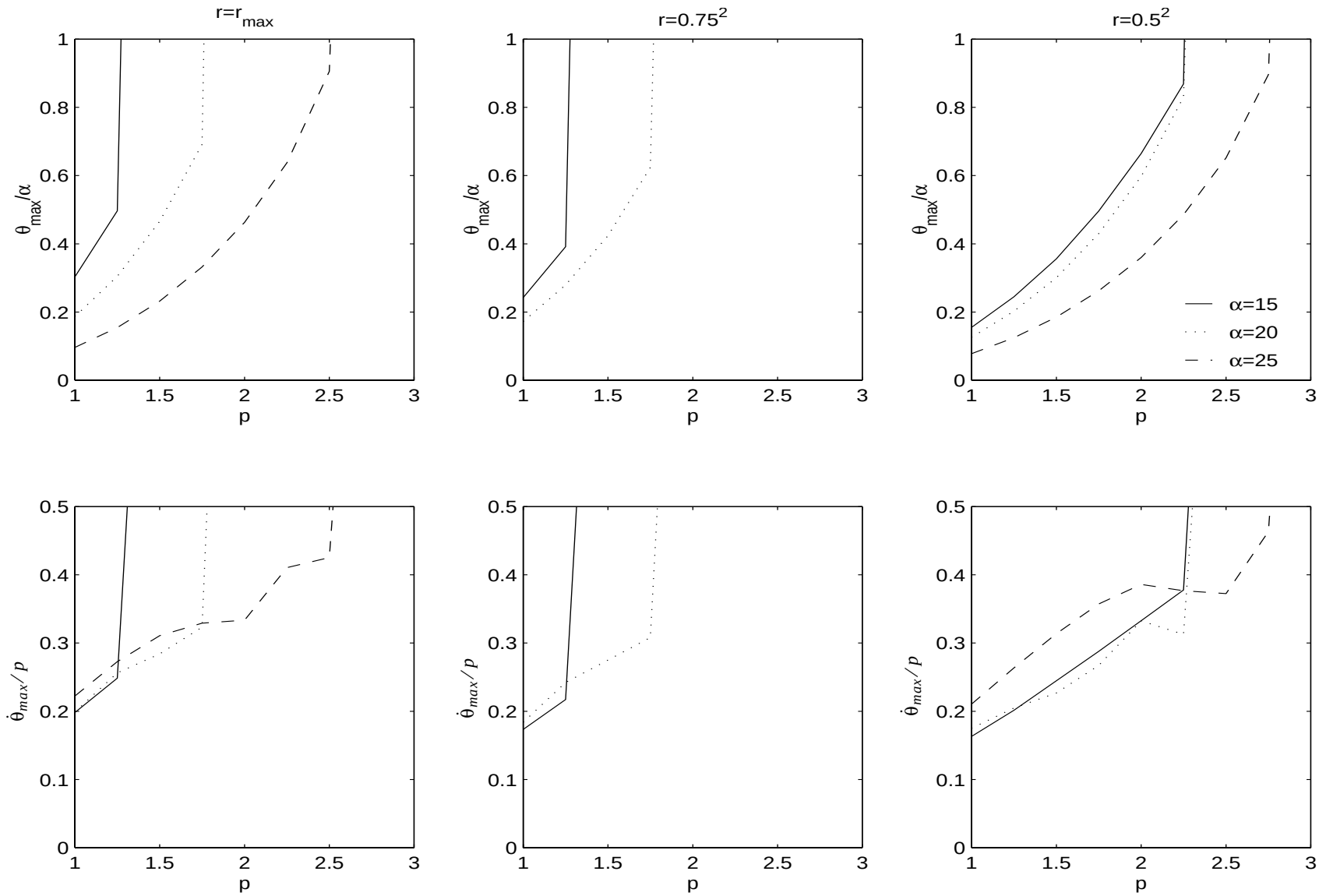

Figure 23. Rotation and angular velocity spectra due to the fault normal motion recorded at the Rinaldi station for different values of the coefficient of restitution and various values of block slenderness

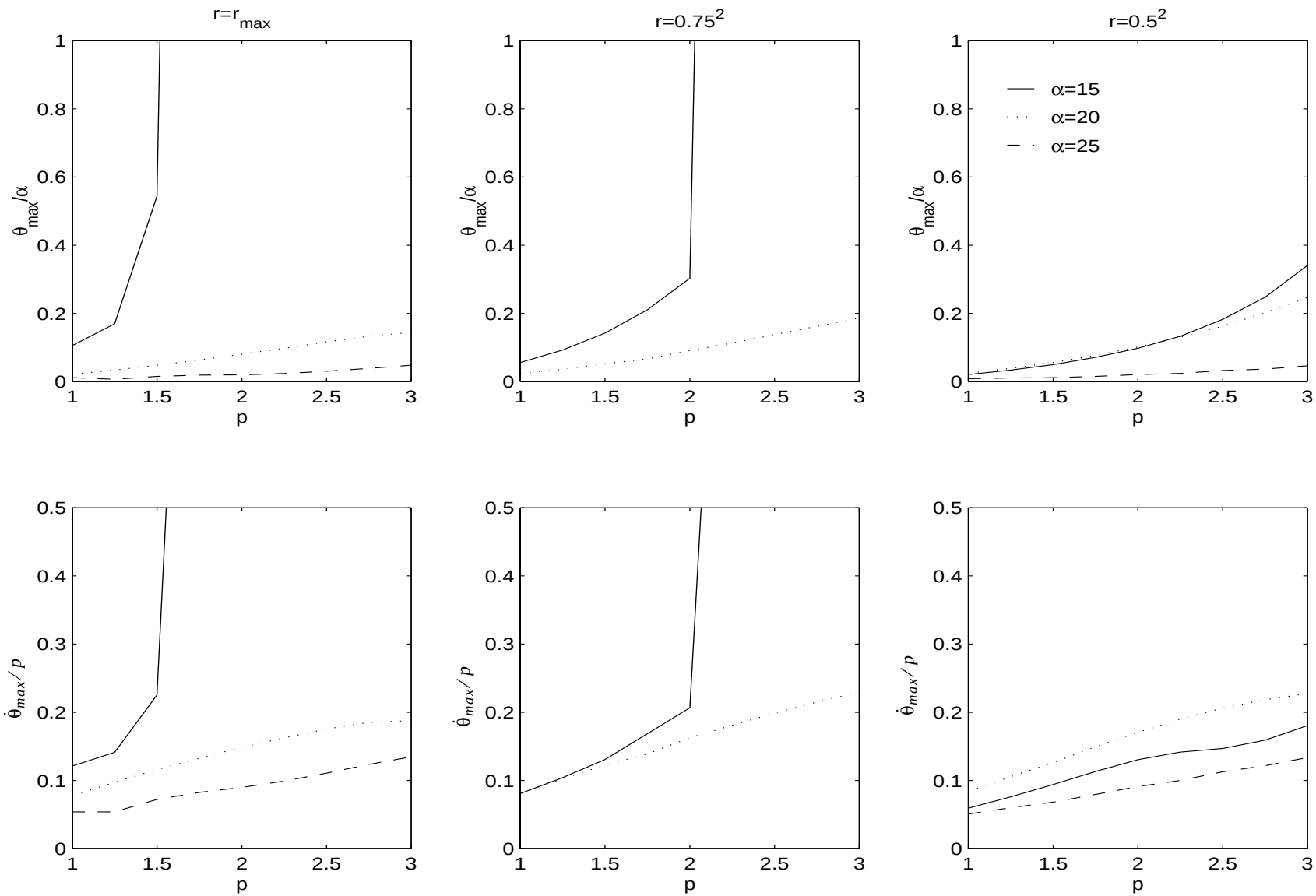

Figure 24. Rotation and angular velocity spectra due to the fault normal motion recorded at the Sylmar station for different values of the coefficient of restitution and various values of block slenderness

CHAPTER 4
ROCKING RESPONSE OF ANCHORED EQUIPMENT SUBJECTED TO A ONE-SINE (TYPE-A) PULSE

In order to prevent violent rocking of electrical equipment, restrainers (hold-downs) are placed at the base to anchor the equipment to its foundation. These restrainers have finite strength, F_u, that can be as low as 1 kip per anchorage up to 50 kips or even higher. Their stiffness also varies from a low value of $K = 10\ kips/in$ up to 500 $kips/in$. Considering that the weight, $W = mg$, of the electrical equipment of interest ranges from 40 kips up to 500 kips, the ratio between the restraining strength on each side of the equipment to the weight of the equipment is within $0.1 < F_u/W \leq 1.0$.

In this study two idealizations for the mechanical behavior of the restrainers are considered. The first simpler idealization is an elastic-brittle behavior. It assumes linear elastic behavior until the ultimate strength, F_u, is reached; and once the strength of the restrainer is exceeded it fractures and the block continues to rock without enjoining any restoring force. It is assumed that the stiffness of the restrainer maintains a constant value, K, until the restrainer fractures and subsequently its stiffness and strength are zero. The second more realistic idealization assumes an elastic-plastic behavior. The restrainer behaves linearly until the ultimate strength, F_u, is reached and subsequently deforms plastically until the fracture displacement, u_f, is reached. Beyond that point the restrainers fractures and the block continues to rock without enjoying any restoring or dissipative force.

In the entire analysis that follows, the base excitation is assumed to be along the horizontal direction only, since the findings of chapter 3 indicate that the vertical acceleration has a marginal constructive or destructive effect. Figure 25 shows a schematic of the problem at hand where the restoring elements on each side of the block represent the combined stiffnesses of all the restrainers that are present at the edge of the block that uplifts.

4.1 Elastic-Brittle Behavior

4.1.1 Nonlinear Formulation

Figure 26 (center) illustrates the moment-rotation relation that results from the presence of restrainers with elastic-brittle behavior; while Figure 26 (top) illustrates the moment-rotation relation of a free-standing block. Under these two restoring mechanisms and assuming horizontal

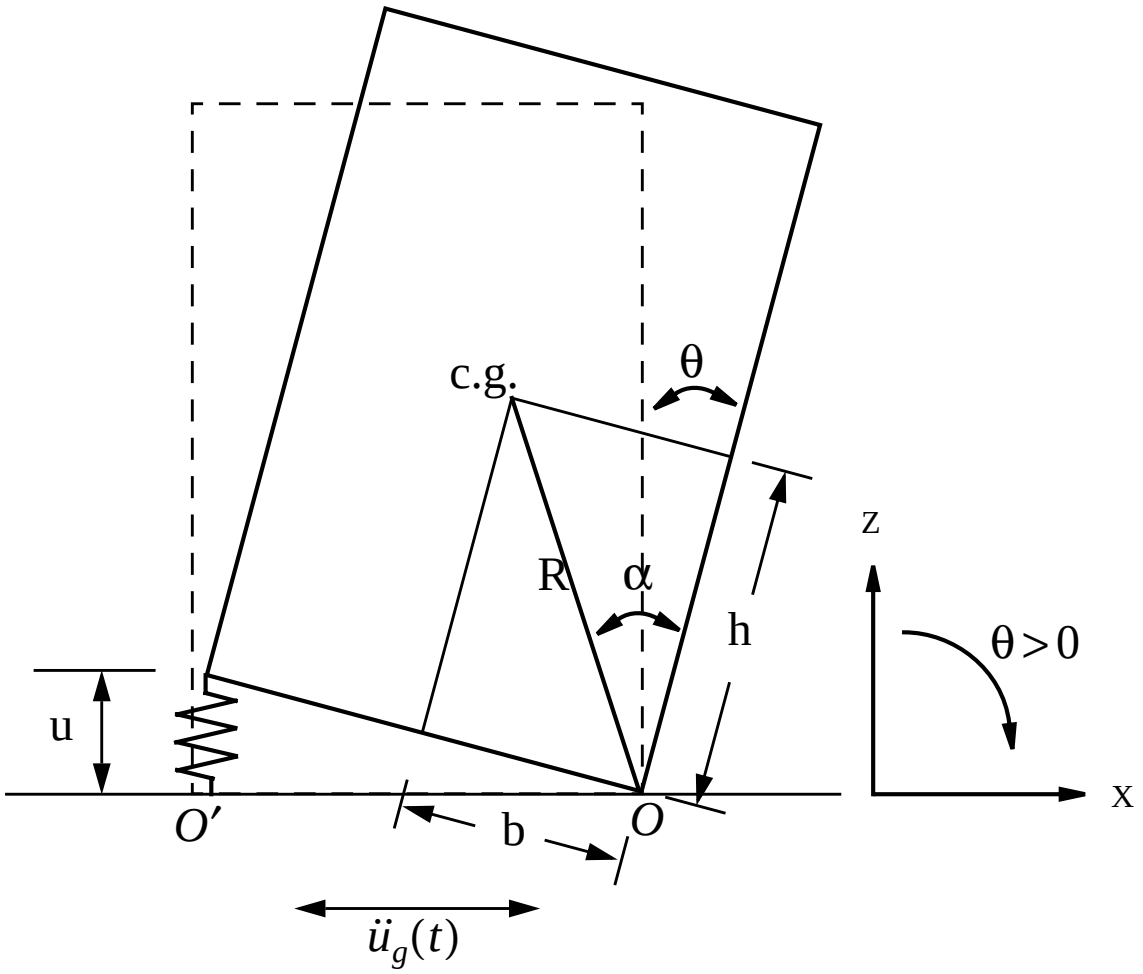

Figure 25. Schematic of an anchored block in rocking motion

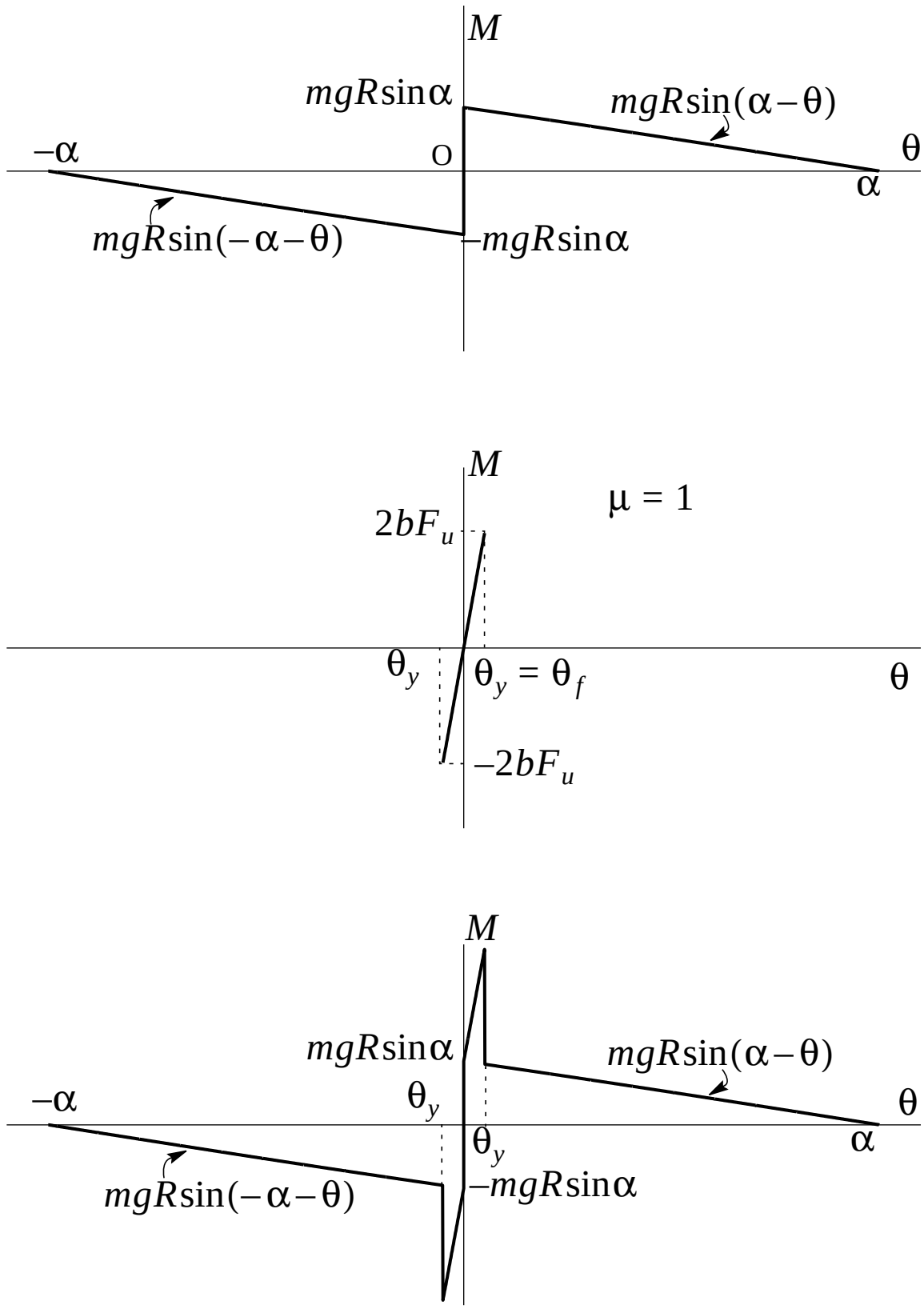

Figure 26. Moment-rotation curves of: (Top) Free-standing block; (Center) Elastic-brittle anchorage; (Bottom) Anchored block with elastic-brittle restrainers

excitation only, the equations that govern the rocking motion of an anchored block with mass m are

$$I_0\ddot{\theta}(t) + mgR\sin[-\alpha-\theta(t)] + 4Kb^2\sin\theta(t) = -m\ddot{u}_g(t)R\cos[-\alpha-\theta(t)]\,,\ \theta<0 \tag{4-1}$$

$$I_0\ddot{\theta}(t) + mgR\sin[\alpha-\theta(t)] + 4Kb^2\sin\theta(t) = -m\ddot{u}_g(t)R\cos[\alpha-\theta(t)]\,,\ \theta>0 \tag{4-2}$$

For a rectangular block, $I_0 = \frac{4}{3}mR^2$, equations (4-1) and (4-2) can be expressed in the compact form:

$$\ddot{\theta}(t) = -p^2\left\{\sin(\alpha\,\mathrm{sgn}[\theta(t)]-\theta(t)) + \frac{3K\sin^2\alpha}{mp^2}\sin\theta(t) + \frac{\ddot{u}_g}{g}\cos[\alpha\,\mathrm{sgn}\theta(t)-\theta(t)]\right\} \tag{4-3}$$

in which $p = \sqrt{3g/(4R)}$.

Equation (4-3) is valid as long as the restrainers hold. Once they fail it reduces to

$$\ddot{\theta}(t) = -p^2\left\{\sin(\alpha\,\mathrm{sgn}[\theta(t)]-\theta(t)) + \frac{\ddot{u}_g}{g}\cos(\alpha\,\mathrm{sgn}\theta(t)-\theta(t))\right\} \tag{4-4}$$

which is the equation of motion of the free-standing block under horizontal excitation only.

Figure 26 (bottom) shows the moment-rotation relation during the rocking motion of an anchored block. For rotation angles, $|\theta(t)| \le \theta_y$, energy is lost only during impact. Once θ_y is exceeded, the restrainer from the uplifted side fractures and additional energy is dissipated equal to the area of the small triangle that is superimposed to the moment-rotation graph of the free-standing block. This energy is dissipated once, since in subsequent post-fracture oscillations the moment-rotation relation reduces to that of the free-standing block.

The transition from equation (4-3) to (4-4) is conducted by following a fracture function $f(\theta)$. The finite ultimate strength of the restrainer, F_u, in conjunction with the linear pre-fracture behavior defines the angle of rotation θ_y that the restrainers yield and also, in this case, fracture

$$F_u = Ku_y = 2Kb\theta_y\,; \tag{4-5}$$

from which

$$\theta_y = \frac{F_u}{2Kb}\,. \tag{4-6}$$

The fracture function $f(\theta)$ is defined as

$$f(\theta) = 1 \text{ when } |\theta(t)| \le \theta_y \tag{4-7}$$

and

$$f(\theta) = 0 \text{ when } |\theta(t)| \ge \theta_y \tag{4-8}$$

With the help of the fracture function, after replacing K/m with $(F_u/u_y)(g/W)$, the pre-fracture and post-fracture equation of motion of the rigid block can be expressed in a compact form

$$\ddot{\theta}(t) = -p^2\left\{\sin[\alpha\,\mathrm{sgn}\theta - \theta(t)] + \frac{3F_u g\sin^2\alpha}{Wu_y p^2}\sin\theta(t)\,f(\theta) + \frac{\ddot{u}_g}{g}\cos[\alpha\,\mathrm{sgn}\theta - \theta(t)]\right\}. \qquad (4\text{-}9)$$

With this formulation the rocking response of anchored blocks is described by four parameters: the slenderness, α, the frequency parameter, p (that includes the size effect), the strength parameter, $\sigma = F_u/W$, and the influence factor, $q = u_y p^2/g$. Table 2 summarizes the physical and mechanical parameters of selected electrical equipment utilized by PG&E (Fujisaki 1999).

The solution of (4-9) is computed numerically via the same state-space formulation introduced in chapter 3. The state vector of the system is the one given by (3-1). The time-derivative vector, $f(t)$, is the one given by (3-2) in which its second component is replaced with the right-hand side of (4-9).

Figure 27 plots overturning acceleration spectra of a rigid equipment with $\alpha = 0.349\ rad\ (20°)$, $p = 2.0\ rad/sec$ and $\eta = \sqrt{r_{max}} = 0.825$. The results are computed with the nonlinear formulation given by (4-9) for the case where $F_u/W = 0$ (free-standing), $F_u/W = 0.4$ and $F_u/W = 1.0$. For small values ω_p/p (approximately $\omega_p/p < 4$) anchored equipment survive higher accelerations; however for values of $4 < \omega_p/p < 6$, anchored equipment topple under a lower acceleration than the acceleration needed to overturn the same equipment when it is free standing. This counterintuitive behavior happens in the neighborhood of the transition from mode 1 to mode 2. Anchored equipment enter this transition at a slightly larger value of ω_p/p. Furthermore, when a free-standing equipment has just entered mode 2 of overturning, the anchored equipment still overturns due to mode 1 (overturning with impact) under a smaller acceleration amplitude. As ω_p/p increases, the anchored equipment will also overturn due to mode 2, and now a higher acceleration is needed to topple it in comparison to the acceleration needed to topple the free-standing block. However, the additional acceleration amplitude that an anchored block can withstand, even with $F_u/W = 1.0$, is negligible compared to the acceleration amplitude needed to overturn the free-standing block. Figure 27 indicates that anchorages are effective at the low range of ω_p/p (low frequency pulses and/or small blocks).

Figure 28 plots the ratio of the minimum acceleration needed to overturn an anchored block, a_{p0}^{AN}, to the minimum acceleration needed to overturn a free-standing block, a_{p0}^{FS}, for vari-

Table 2: Geometrical, Physical and Structural Parameters of Electrical Equipment

Equip Weight (kips)	b (in)	h (in)	K (kips/in)	F_u (kips)	$\sigma = \frac{F_u}{W}$	α (degree)	p (rad/sec)	$q = \frac{u_y p^2}{g}$	θ_y	b/B
40	36	84	175	4	0.100	23.20	1.7803	1.8×10^{-4}	5.56×10^{-4}	N/A
40	20	59	300	16	0.400	18.43	2.157	6.4×10^{-4}	1.33×10^{-3}	N/A
550	69	100	1500	79	0.144	34.61	1.5441	3.2×10^{-4}	3.82×10^{-4}	0.7188
193	38	89	1000	53	0.275	23.12	1.7301	4.1×10^{-4}	6.97×10^{-4}	0.6667
150	44	68	1000	53	0.353	32.91	1.8911	4.9×10^{-4}	6.02×10^{-4}	0.5641
230	38	90	1500	79	0.343	22.89	1.7219	4.0×10^{-4}	6.93×10^{-4}	0.5067
175	38	74	1500	79	0.451	27.18	1.8660	4.7×10^{-4}	6.93×10^{-4}	0.5758
60	35	90	500	26	0.433	21.25	1.7320	4.0×10^{-4}	7.43×10^{-4}	0.6140
44	34	68	500	26	0.591	26.57	1.9519	5.7×10^{-4}	7.65×10^{-4}	0.5965

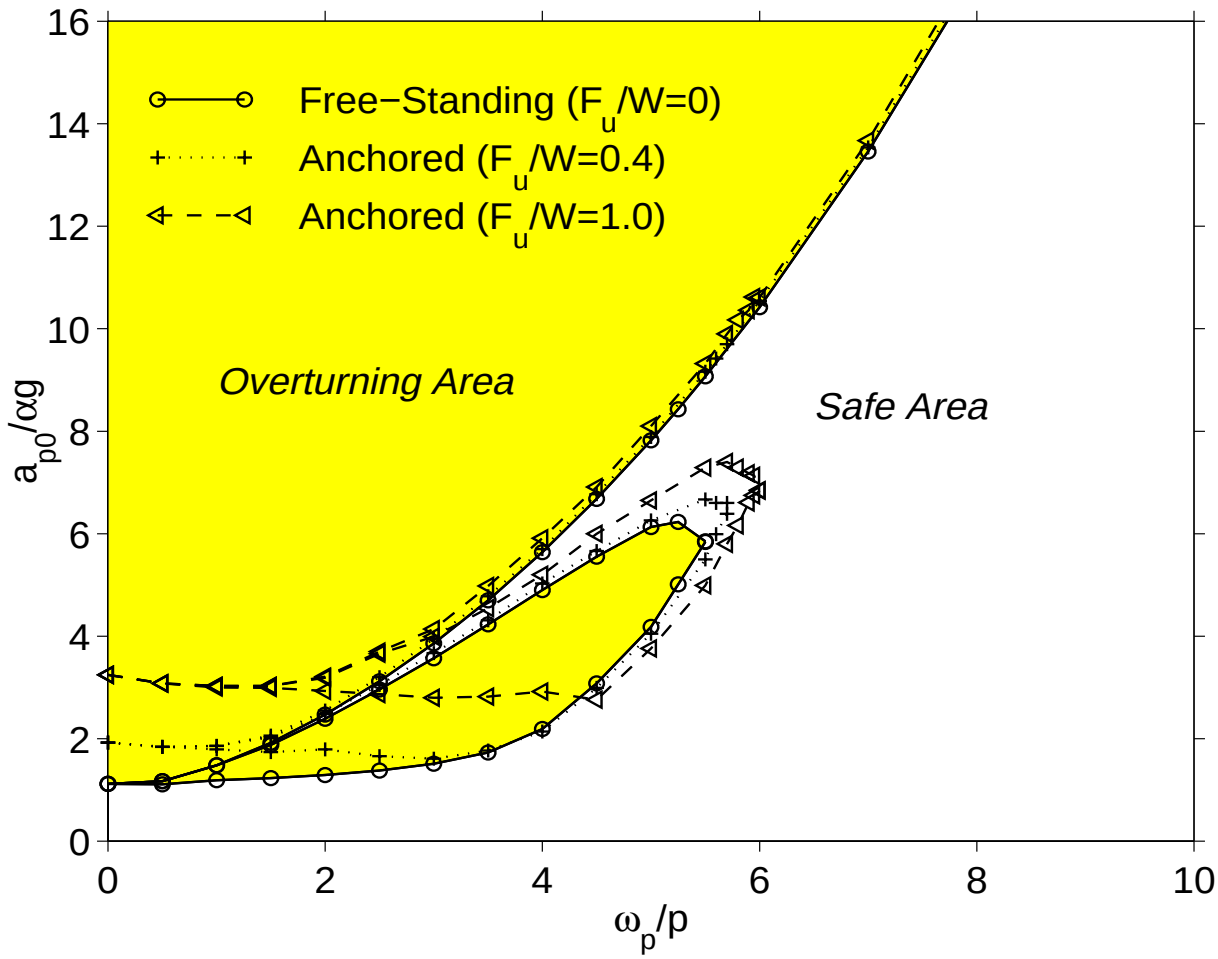

Figure 27. Comparison of overturning acceleration spectra due to a one-sine pulse of an anchored equipment ($\alpha = 0.349\ rad = 20°$, $p = 2\ rad/sec$, $\eta = 0.825$, $q = 5.2\times10^{-4}$ and $\mu = 1$) computed with the nonlinear formulation for $F_u/W = 0$, *0.4* and *1.0*

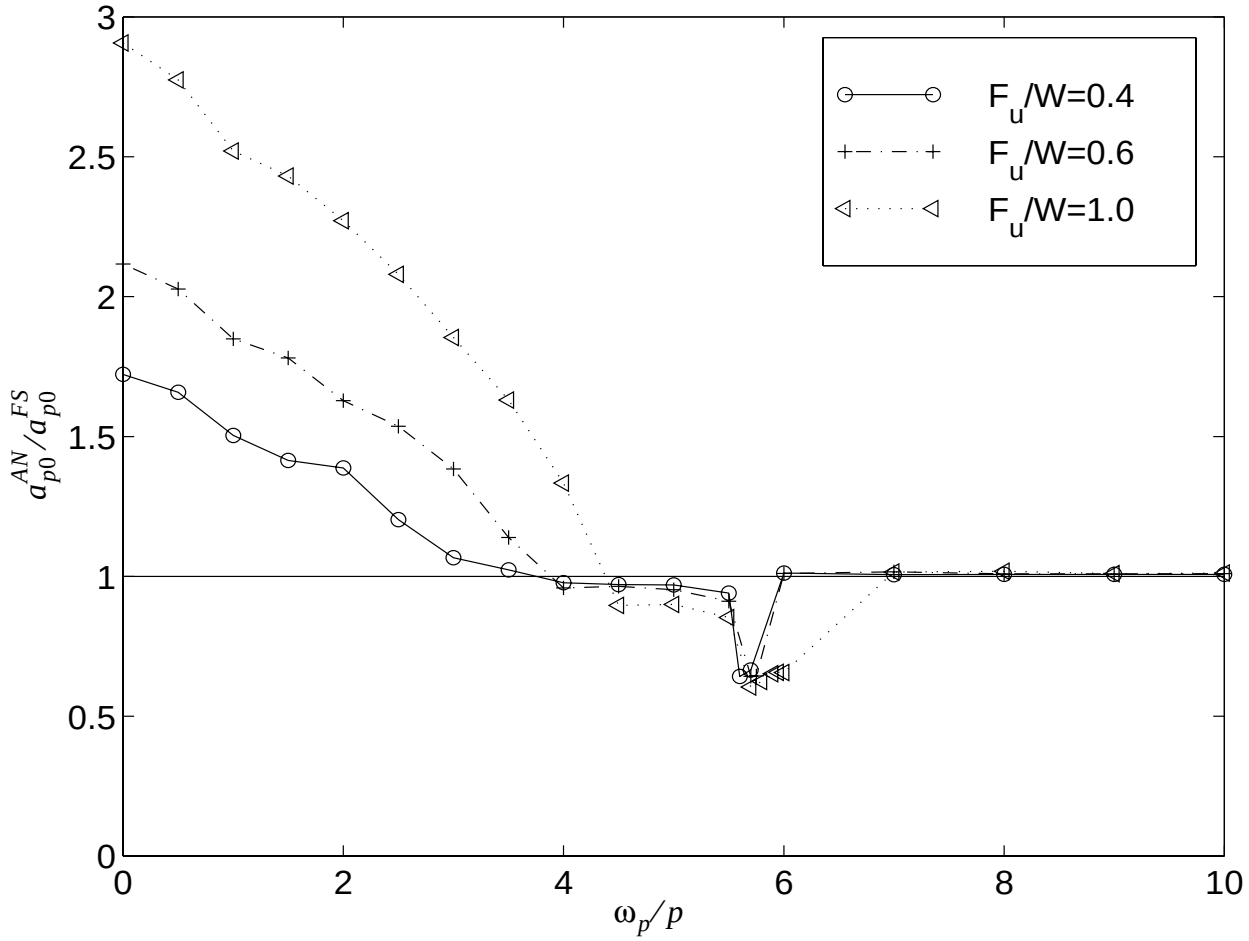

Figure 28. Normalized minimum overturning acceleration levels needed to overturn an anchored block (elastic-brittle behavior, $\mu = 1$) to the acceleration levels needed to overturn the same block when it is free-standing

ous values of the strength parameter $\sigma = F_u/W$. The results shown on Figure 28 indicate that for pulses with $\omega_p/p > 4$, blocks should not be anchored since the effect of restrainers is either destructive or virtually insignificant.

The limit capacity of the restrainers to prevent the toppling of a larger block is illustrated by comparing the potential energy of the block at the verge of overturning with the strain energy dissipated by the restrainers.

Assuming an elastic-brittle behavior, Figure 26 (center) indicates that the strain energy dissipated by the restrainers before they fracture is

$$SE = \frac{1}{2}F_u u_y \tag{4-10}$$

At the verge of overturning ($\theta = \alpha$), the kinetic energy of the block is zero since the one-sine pulse has expired and its potential energy is

$$PE = mgR(1-\cos\alpha) \tag{4-11}$$

The substitution of $\cos\alpha$ in (4-11) with its series expansion $1-\frac{\alpha^2}{2}+\ldots$ gives

$$PE \approx mgR\frac{\alpha^2}{2} \tag{4-12}$$

and the ratio of the dissipated strain energy to the total energy of the block at the verge of overturning is

$$\frac{SE}{PE} \approx \frac{F_u u_f}{mgR\alpha^2} = \frac{1}{\alpha^2}\frac{F_u}{W}\frac{u_y}{R} \tag{4-13}$$

where, $u_y = F_u/K$, is the yield displacement.

For a block with $\alpha = 0.349\ rad\ (20°)$, $p = 2.0\ rad/sec$, $R = 1.839\ m$, $u_y = 1.25\times10^{-3}\ m$ and $F_u = W$, the strain energy lost from the failure of each restrainer is approximately 0.6% of the energy that is needed to topple the free-standing block.

Equation (4-13) reveals some interesting geometrical and scale effects:

(i) The $1/\alpha^2$ term indicates that restrainers are much more effective in preventing toppling the slender of two blocks of the same size (same *R*).

(ii) The $1/R$ term indicates that restrainers are more effective in preventing toppling the smaller of two geometrically similar blocks that have the same F_u/W.

4.1.2 Linear Formulation

Equations (4-1) and (4-2) and their compact form given by (4-9) are valid for arbitrary values of the block angle, α. For slender blocks, the angle $\alpha = \tan^{-1}(b/h)$ is relatively small and equations (4-1) and (4-2) can be linearized. This linearization allows for the derivation of closed-form solutions when the excitation is expressed in a functional form. Herein, the solution of the linearized equations is derived for a sinusoidal ground motion for both positive and negative rotations in order to validate the fidelity of the numerical solution presented in the foregoing subsection. Within the limits of the linear approximation and for a ground acceleration

$$\ddot{u}_g(t) = a_p \sin(\omega_p t + \psi) \tag{4-14}$$

equations (4-1) and (4-2) become

$$\ddot{\theta}(t) + \lambda^2 p^2 \theta(t) = -p^2 \frac{a_p}{g} \sin(\omega_p t + \psi) + \alpha p^2 \,,\ \theta < 0 \tag{4-15}$$

and

$$\ddot{\theta}(t) + \lambda^2 p^2 \theta(t) = -p^2 \frac{a_p}{g} \sin(\omega_p t + \psi) - \alpha p^2 \,,\ \theta > 0 \tag{4-16}$$

where $\psi = \sin^{-1}(\alpha g / a_p)$ is the phase when rocking initiates and $\lambda^2 = 3(F_u/W)(g/u_y p^2)\sin^2\alpha - 1 = 3(\sigma/q)\sin^2\alpha - 1$. For typical anchorages of electrical equipment $\lambda^2 > 0$. Once the restrainers fail, $\lambda^2 = -1$. Accordingly, the solution of (4-15) and (4-16) is presented for the four segment $-\theta_y \le \theta(t) \le 0$, $\theta(t) < -\theta_y \le 0$, $0 < \theta(t) < \theta_y$ and $0 < \theta_y < \theta(t)$:

$$\theta(t) = A_1 \sin(\lambda p t) + A_2 \cos(\lambda p t) + \frac{\alpha}{\lambda^2} - \frac{1}{\lambda^2 - \frac{\omega_p^2}{p^2}} \frac{a_p}{g} \sin(\omega_p t + \psi_1) \,,\ -\theta_y \le \theta(t) \le 0 \tag{4-17}$$

$$\theta(t) = A_3 \sinh(pt) + A_4 \cosh(pt) - \alpha + \frac{1}{1 + \frac{\omega_p^2}{p^2}} \frac{a_p}{g} \sin(\omega_p t + \psi_2) \,,\ \theta(t) < -\theta_y \le 0 \tag{4-18}$$

$$\theta(t) = A_5 \sin(\lambda p t) + A_6 \cos(\lambda p t) - \frac{\alpha}{\lambda^2} - \frac{1}{\lambda^2 - \frac{\omega_p^2}{p^2}} \frac{a_p}{g} \sin(\omega_p t + \psi_3) \,,\ 0 < \theta(t) < \theta_y \tag{4-19}$$

$$\theta(t) = A_7 \sinh(pt) + A_8 \cosh(pt) + \alpha + \frac{1}{1+\frac{\omega_p^2}{p^2}} \frac{a_p}{g} \sin(\omega_p t + \psi_4),\ 0 < \theta_y < \theta(t) \tag{4-20}$$

where

$$A_1 = \frac{\dot{\theta}_0}{\lambda p} + \frac{1}{\lambda} \frac{\omega_p / p}{\lambda^2 - \omega_p^2 / p^2} \frac{a_p}{g} \cos\psi_1 \tag{4-21}$$

$$A_2 = -\frac{\alpha}{\lambda^2} + \frac{1}{\lambda^2 - \omega_p^2 / p^2} \frac{a_p}{g} \sin\psi_1 \tag{4-22}$$

$$A_3 = \frac{\dot{\theta}_y^-}{p} - \frac{\omega_p / p}{1 + \omega_p^2 / p^2} \frac{a_p}{g} \cos\psi_2 \tag{4-23}$$

$$A_4 = -\theta_y + \alpha - \frac{1}{1 + \omega_p^2 / p^2} \frac{a_p}{g} \sin\psi_2 \tag{4-24}$$

$$A_5 = \frac{\dot{\theta}_0}{\lambda p} + \frac{1}{\lambda} \frac{\omega_p / p}{\lambda^2 - \omega_p^2 / p^2} \frac{a_p}{g} \cos\psi_3 \tag{4-25}$$

$$A_6 = \frac{\alpha}{\lambda^2} + \frac{1}{\lambda^2 - \omega_p^2 / p^2} \frac{a_p}{g} \sin\psi_3 \tag{4-26}$$

$$A_7 = \frac{\dot{\theta}_y^+}{p} - \frac{\omega_p / p}{1 + \omega_p^2 / p^2} \frac{a_p}{g} \cos\psi_4 \tag{4-27}$$

$$A_8 = \theta_y - \alpha - \frac{1}{1 + \omega_p^2 / p^2} \frac{a_p}{g} \sin\psi_4 \tag{4-28}$$

In (4-21) and (4-22) $\psi_1 = \psi = \sin^{-1}(\alpha g / a_p)$ is the phase when rocking initiates. In (4-23) and (4-24) $\psi_2 = \omega_p t_y^- + \psi$, where t_y^- is the time that $-\theta_y$ is reached. In (4-25) and (4-26), $\psi_3 = \omega_p t_i + \psi$, where t_i is the time that $\theta = 0$ and the block experiences its first impact. In (4-27) and (4-28), $\psi_4 = \omega_p t_y^+ + \psi$, where t_y^+ is the time that θ_y is reached. Stepping through time the values of t_y^-, t_i and t_y^+ are detected by monitoring the value of the rotation angle θ. The solution obtained with the linear formulation is used to validate the fidelity of the numerical solution of (4-9) that is achieved with a state-space formulation.

Figure 29 plots the minimum overturning acceleration spectra computed with the linear formulation. A behavior similar to that computed with the nonlinear formulation is observed. For small values ω_p / p (approximately $\omega_p / p < 4$) anchored equipment survive higher accelerations;

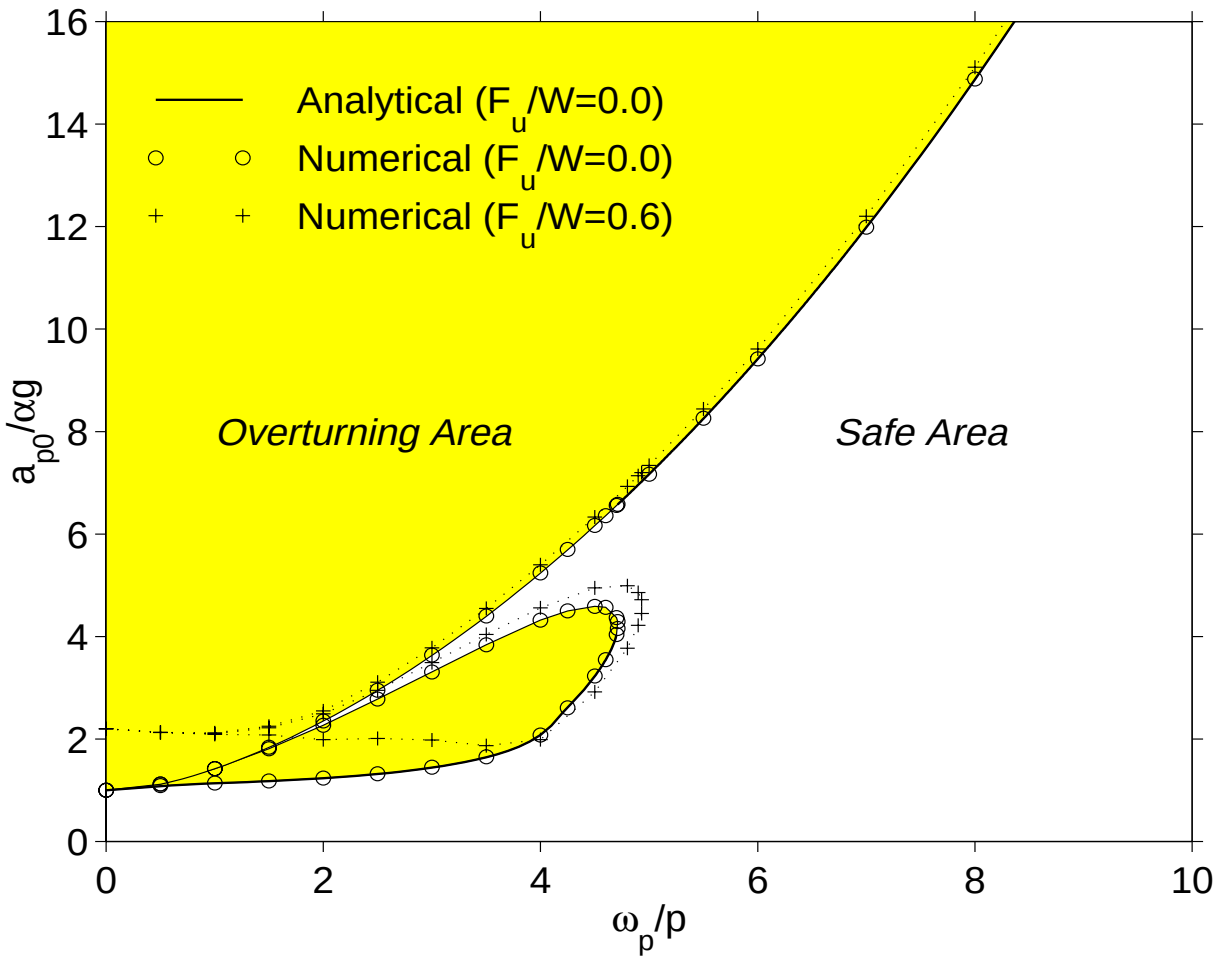

Figure 29. Comparison of overturning acceleration spectra due to a one-sine pulse of an anchored equipment ($\alpha = 0.349\ rad = 20°$, $p = 2\ rad/sec$, $\eta = 0.825$, $q = 5.2\times10^{-4}$, and $\mu = 1$) computed with the linear formulation for $F_u/W = 0$ and *0.6*. Lines: analytical solution. Points: numerical solution.

however for values of $\omega_p/p > 4$, anchored equipment topple under a lower acceleration than that needed to overturn the same equipment that is free standing. The results are computed with the analytical solution presented herein and the numerical integration that is achieved with a state-space formulation. The agreement of the two solutions is excellent.

The elastic-brittle behavior in conjunction with the linear formulation allows for an analytical solution that was used to validate the fidelity of the numerical integration. It was found that even at the limit of the linear approximation, there is a neighborhood of ω_p/p values where a free-standing block can survive a stronger acceleration than anchored blocks. Figure 30 compares the overturning spectra of an anchored block with $F_u/W = 0.4$ (top) and $F_u/W = 0.6$ (bottom) computed with the linear and nonlinear formulation. When the frequency of the one-sine pulse is relatively low, both formulations yield comparable results. As the excitation frequency increases, the linear formulation yields minimum overturning acceleration amplitudes drastically larger than those obtained with the nonlinear formulation. This result is because under the nonlinear formulation, the overturning "bay" generated by mode 1 of overturning penetrates further into the safe area under the overturning spectrum due to mode 2. As the excitation frequency further increases, the linear and nonlinear formulations again yield comparable results. This finding indicates that when $4 < \omega_p/p < 6$, the linear formulation should be avoided since it gives erroneous results even for slender blocks.

4.2 Ductile Behavior

Figure 31 illustrates the force-displacement relation of restrainers with ductile behavior. In general the restrainers can exhibit a post-yielding stiffness and maintain their strength until they reach a fracture displacement, u_f. A measure of their ductile behavior is the ductility coefficient, $\mu = u_f/u_y$. A suitable model to approximate such nonlinear hysteretic behavior is given by

$$P(t) = \varepsilon K u(t) + (1-\varepsilon) K u_y Z(t) \tag{4-29}$$

where $u(t)$ is the extension of the restrainer, K is the pre-yielding stiffness, ε is the ratio of the post- to pre-yielding stiffness, u_y is the yield displacement, and $Z(t)$ is a hysteretic dimensionless quantity that is governed by

$$u_y \dot{Z}(t) + \gamma |\dot{u}(t)| Z(t) |Z(t)|^{n-1} + \beta \dot{Z}(t) |Z(t)|^n - \dot{u}(t) = 0 \tag{4-30}$$

In the above equation β, γ and n are dimensionless quantities that control the shape of the hysteretic loop. The hysteretic model, expressed by (4-29) and (4-30), was originally proposed by

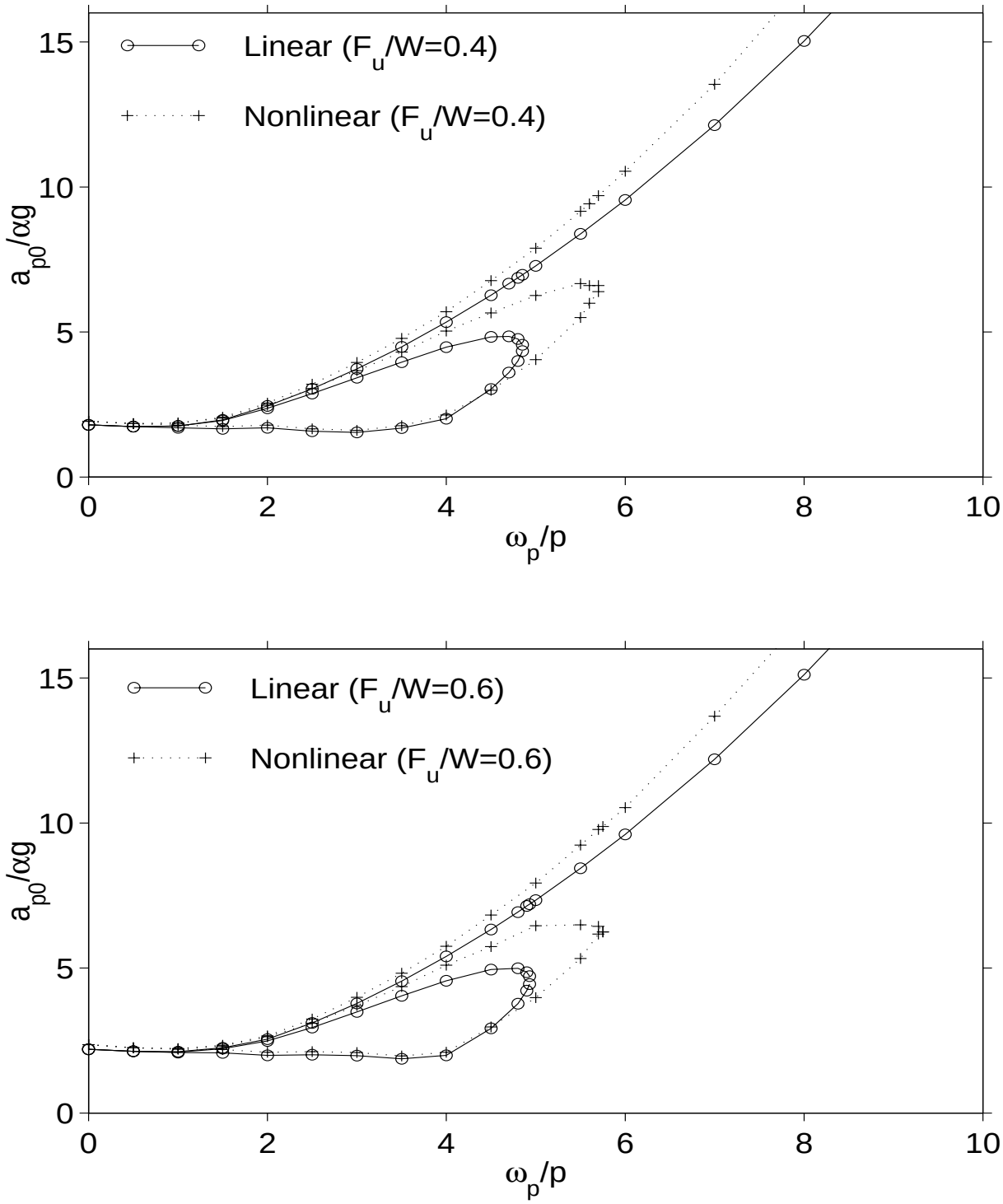

Figure 30. Comparison of the overturning acceleration spectra due to a one-sine pulse of an anchored equipment ($\alpha = 0.349\ rad = 20°$, $p = 2\ rad/sec$, $\eta = 0.825$, $q = 5.2\times10^{-4}$ and $\mu = 1$) computed with the linear and nonlinear formulation for $F_u/W = 0.4$ (top) and $F_u/W = 0.6$ (bottom)

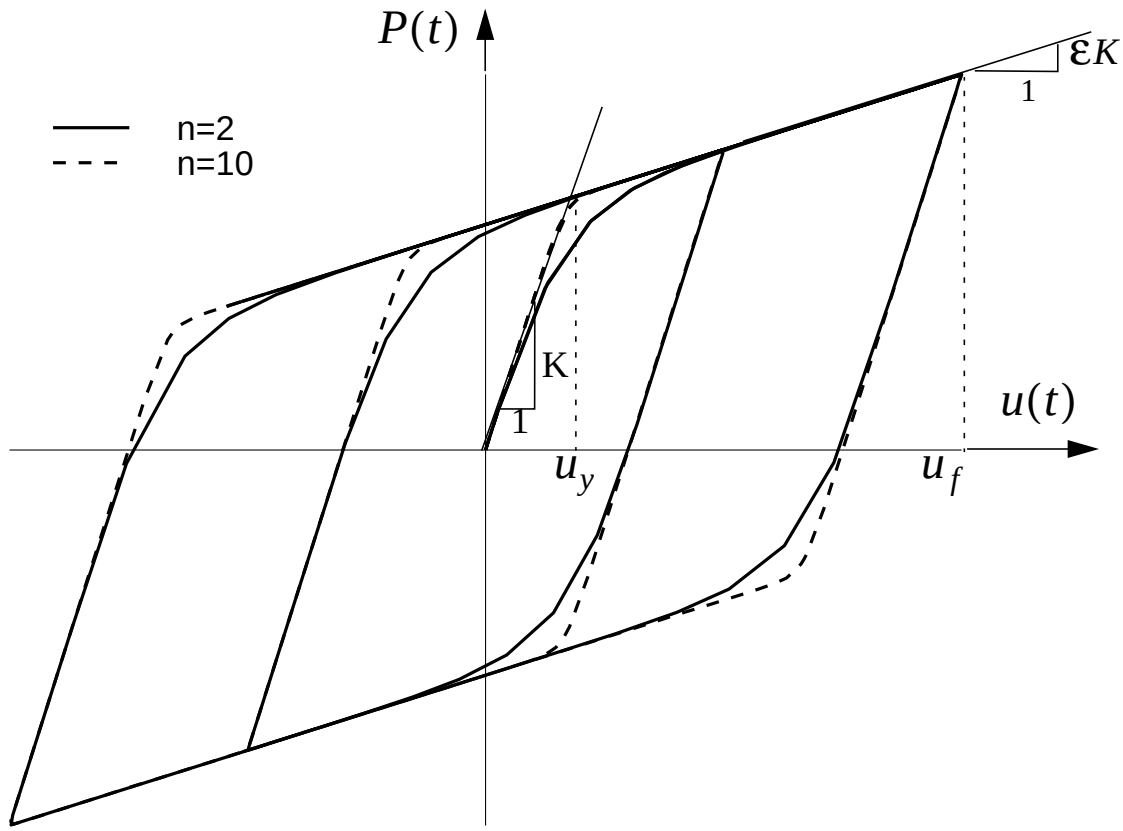

Figure 31. Force-displacement curve of an element with bilinear behavior

Bouc (1971) for n = 1, subsequently extended by Wen (1975, 1976), and used in random vibration studies of inelastic systems.

In this study the special case of elasto-plastic behavior is considered by setting the post-yielding stiffness equal to zero ($\varepsilon = 0$). However, the developed formulation can easily be extended to account for situations with $\varepsilon \neq 0$.

4.2.1 Elasto-Plastic Behavior

Figure 32 (center) illustrates the moment-rotation relation that results from the presence of restrainers with elasto-plastic behavior; while Figure 32 (top) illustrates again the moment-rotation relation of a free-standing block. Under these two restoring mechanisms, the equations that govern the rocking motion of an anchored block with mass m and moment of inertia I_0 (about pivot point O or O') is

$$I_0\ddot{\theta}(t) + m\ddot{u}_g R\cos(-\alpha-\theta) = -mgR\sin(-\alpha-\theta) - P(t)2b\cos\left(\frac{\theta}{2}\right),\ \theta<0 \tag{4-31}$$

and

$$I_0\ddot{\theta}(t) + m\ddot{u}_g R\cos(\alpha-\theta) = -mgR\sin(\alpha-\theta) - P(t)2b\cos\left(\frac{\theta}{2}\right),\ \theta>0 \tag{4-32}$$

where $P(t)$ is the force originating from the restrainers that for the general case is give by (4-29) and the special elasto-plastic case ($\varepsilon = 0$) reduces to

$$P(t) = Ku_yZ(t) \tag{4-33}$$

With reference to Figure 32, $u_y = 2b\theta_y$, and equation (4-33) gives

$$P(t) = 2Kb\theta_yZ(t) \tag{4-34}$$

Substitution of (4-34) into (4-31) and (4-32)gives

$$I_0\ddot{\theta}(t) + mgR\sin(-\alpha-\theta) + 4Kb^2\theta_yZ(t)\cos\left(\frac{\theta}{2}\right) = -m\ddot{u}_g(t)R\cos(-\alpha-\theta),\ \theta<0 \tag{4-35}$$

and

$$I_0\ddot{\theta}(t) + mgR\sin(\alpha-\theta) + 4Kb^2\theta_yZ(t)\cos\left(\frac{\theta}{2}\right) = -m\ddot{u}_g(t)R\cos(\alpha-\theta),\ \theta>0 \tag{4-36}$$

Using that for a rectangular block, $I_0 = \frac{4}{3}mR^2$, equation (4-35) and (4-36) can be expressed in the compact form:

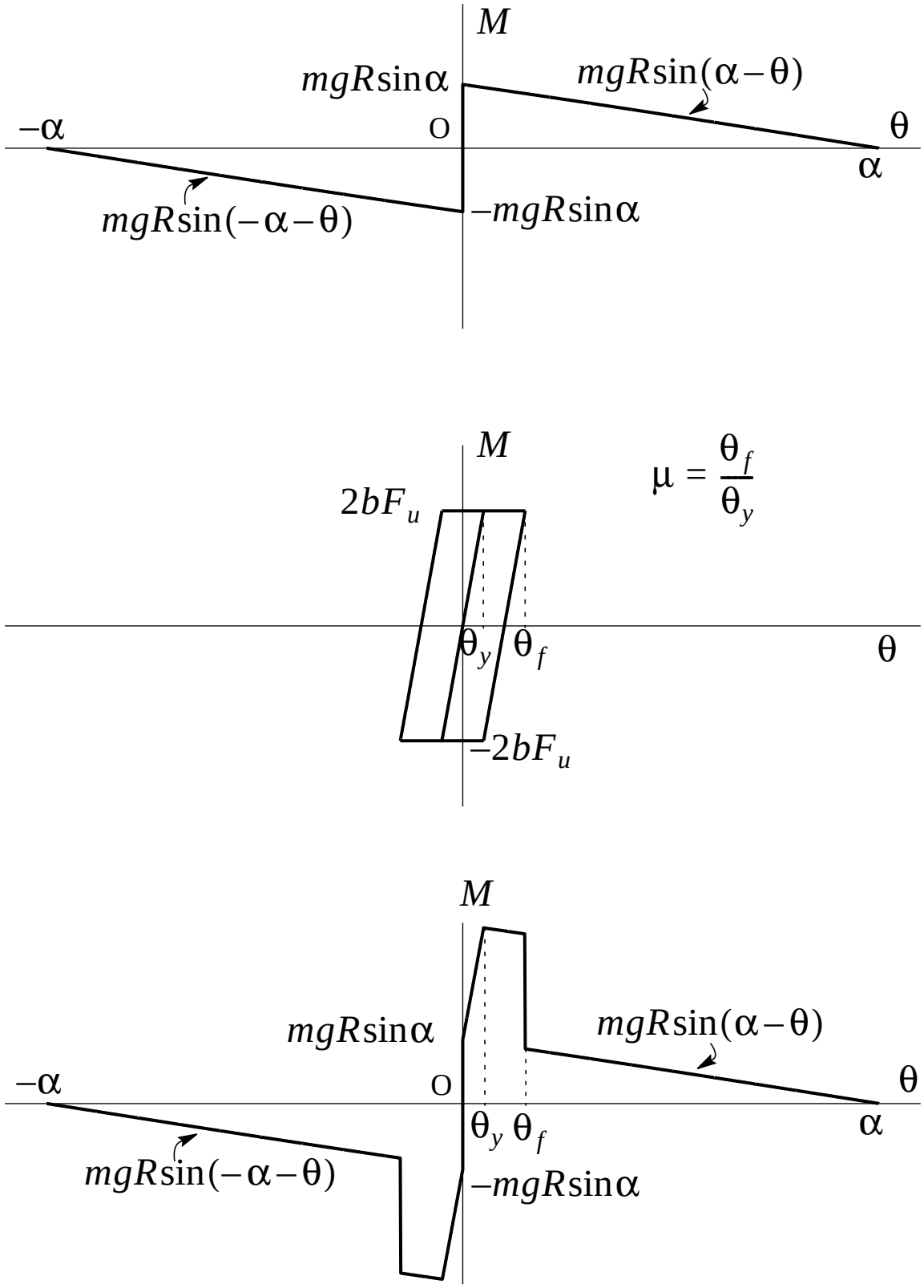

Figure 32. Moment-rotation curves of (Top) Free-standing block; (Center) Elastic-plastic anchorage; (Bottom) Anchored block with elastic-plastic restrainers

$$\ddot{\theta}(t) = -p^2\left\{\sin[\alpha\,\mathrm{sgn}\,\theta(t)-\theta(t)] + \frac{\ddot{u}_g(t)}{g}\cos[\alpha\,\mathrm{sgn}\,\theta(t)-\theta(t)] + \frac{3\sigma\sin^2\alpha}{q}\theta_y Z(t)\cos\left(\frac{\theta}{2}\right)\right\} \tag{4-37}$$

where $p = \sqrt{3g/(4R)}$, $\sigma = F_u/W$, $q = u_y p^2/g$, and $Z(t)$ is the solution of (4-30) which in terms of rotations takes the form

$$\theta_y\dot{Z}(t) + \gamma|\dot{\theta}(t)|Z(t)|Z(t)|^{n-1} + \beta\dot{\theta}(t)|Z(t)|^n - \dot{\theta}(t) = 0 \tag{4-38}$$

Equation (4-37) is valid as long as the restrainers hold. Once their fracture displacement, $u_f = 2b\sin\theta_f$, is reached they do not provide any resistance, and equation (4-37) reduces to the equation of motion of the free-standing block given by (4-4).

Figure 32 (bottom) shows the moment-rotation relation during the rocking motion of an anchored block that its restrainers exhibit elasto-plastic behavior. For rotation angles $|\theta(t)| \le \theta_y$, energy is lost only during the reversal of motion due to impact. Once θ_y is exceeded, the restrainers along the uplifted side yield. In the case that the motion reverses before the rotation reaches θ_f, additional energy is dissipated equal to the area of the flag-shape shaded regions. This dissipation mechanism will be repeated as long as the maximum rotation does not reach the fracture rotation, θ_f. If θ_f is exceeded, the restrainers fracture and the moment curvature curve reduces to that of the free-standing block.

The transition from equation (4-37) to (4-4) is conducted with the fracture function $f(\theta)$ defined as

$$f(\theta) = 1 \text{ when } |\theta(t)| \le \theta_f \tag{4-39}$$

and

$$f(\theta) = 0 \text{ when } |\theta(t)| \ge \theta_f \tag{4-40}$$

where $\theta_f = \mu\theta_y$ and θ_y is given by (4-6). With the help of the fracture function, the pre-fracture and post-fracture equation of rocking motion can be expressed as

$$\ddot{\theta}(t) = -p^2\left\{\sin[\alpha\,\mathrm{sgn}\,\theta-\theta(t)] + \frac{\ddot{u}_g(t)}{g}\cos[\alpha\,\mathrm{sgn}\,\theta-\theta(t)] + \frac{3\sigma\sin^2\alpha}{q}\theta_y Z(t)\cos\left(\frac{\theta(t)}{2}\right)f(\theta)\right\} \tag{4-41}$$

The integration of (4-41) requires the simultaneous integration of (4-38). In this case the state vector of the system is

$$\{y(t)\} = \begin{Bmatrix} \theta(t) \\ \dot{\theta}(t) \\ Z(t) \end{Bmatrix} \tag{4-42}$$

and the time derivative vector $f(t)$ is

$$f(t) = \begin{Bmatrix} \dot{\theta}(t) \\ -p^2\Big(\sin[\alpha \operatorname{sgn}\theta(t) - \theta(t)] + \dfrac{\ddot{u}_g}{g}\cos[\alpha \operatorname{sgn}\theta(t) - \theta(t)] \\ + \dfrac{3\sigma \sin^2\alpha}{q}\theta_y Z(t)\cos\Big(\dfrac{\theta(t)}{2}\Big) f(\theta)\Big) \\ \dfrac{1}{\theta_y}[\dot{\theta}(t) - \gamma|\dot{\theta}(t)|Z(t)|Z(t)|^{n-1} - \beta\dot{\theta}(t)|Z(t)|^n] \end{Bmatrix} \tag{4-43}$$

Figure 33 plots the normalized minimum acceleration amplitude, $a_{p0}/\alpha g$, of a one-sine pulse needed to overturn an anchored block. The results are computed with the nonlinear formulation for an influence factor $q = 5.2\times10^{-4}$, ductility $\mu = 5$, and various values of the restrainer strength F_u/W.

At the zero-limit of ω_p/p a block with finite size is subjected to a very long duration pulse. When this pulse is near its peak, the block is subjected to a nearly constant acceleration a_{p0}. When the restrainers yield elastic-plastic behavior (see Figure 32) the balance of moment when the restrainers reach their ultimate strength is

$$ma_{p0}R\cos(\alpha-\theta_y) = mg\sin(\alpha-\theta_y) + F_u 2b\cos\Big(\frac{\theta_y}{2}\Big) \tag{4-44}$$

in which θ_y is given by (4-6). After dividing both sides of (4-44) with $mR\cos(\alpha-\theta_y)$ one obtains

$$a_{p0} = g\frac{\sin(\alpha-\theta_y)}{\cos(\alpha-\theta_y)} + 2\frac{F_u}{W}g\tan\alpha\frac{\cos(\theta_y/2)}{\cos(\alpha-\theta_y)} \tag{4-45}$$

Equation (4-45) is the equivalent West's formula (Milne 1885) for an anchored block with elasto-plastic restrainers that exhibit ultimate strength F_u. The parameters F_u, K, and b, related to electrical equipment, yield a value of θ_y much smaller than α, while $\cos\frac{\theta_y}{2} \approx 1$. Under these conditions equation (4-45) simplifies to

$$a_{p0} = g\tan\alpha + 2\frac{F_u}{W}g\tan\alpha\frac{1}{\cos\alpha}, \tag{4-46}$$

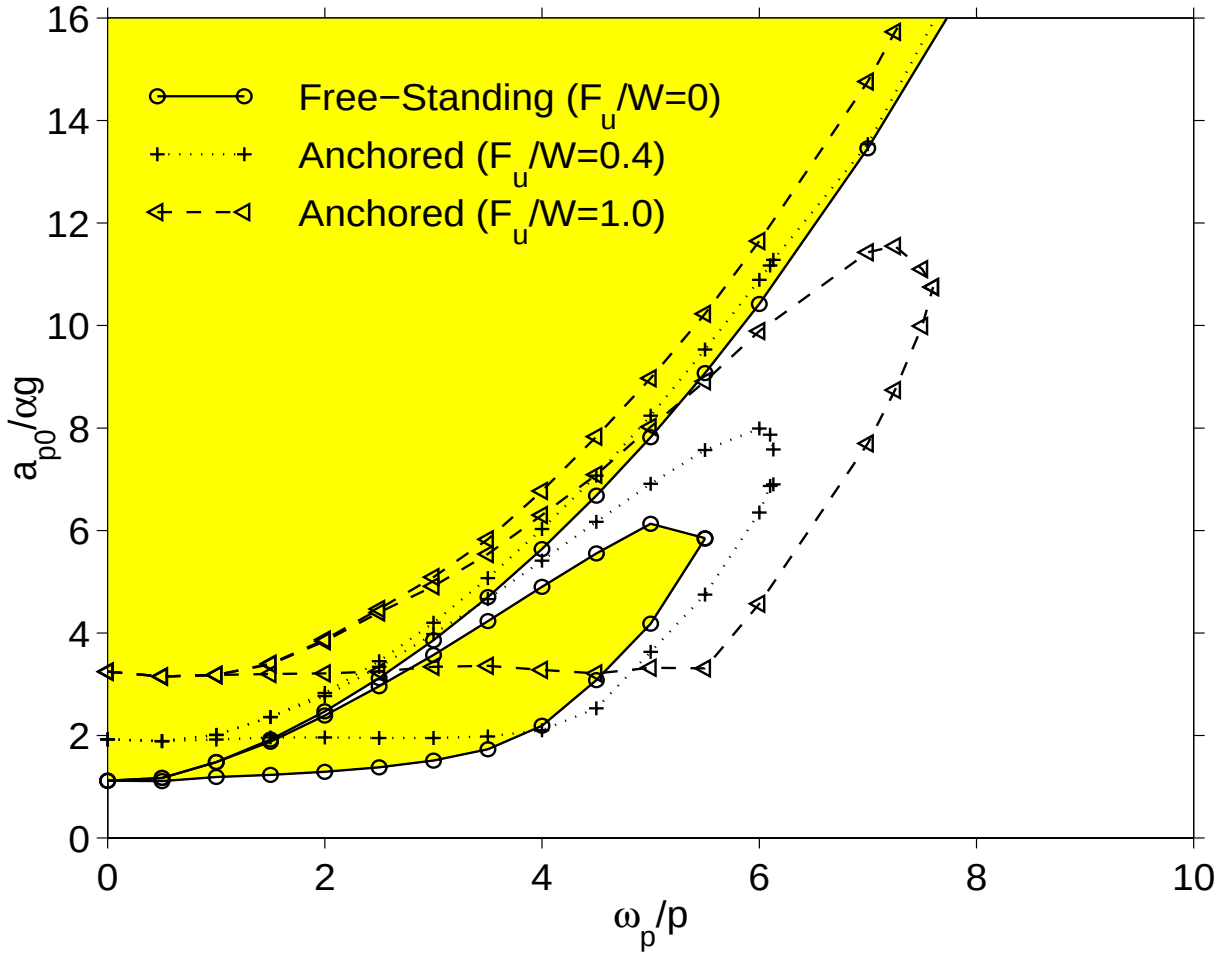

Figure 33. Overturning acceleration spectra due to a one-sine pulse of an anchored block ($\alpha = 0.349\ rad = 20°$, $p = 2\ rad/sec$, $\eta = 0.825$, $q = 5.2\times10^{-4}$ and $\mu = 5$) with restrainer strength $F_u/W = 0$, *0.4*, and *1.0*. The solution is computed with the nonlinear formulation.

and for slender blocks, $\tan\alpha \approx \alpha + \alpha^3/3$, $\cos\alpha \approx 1 - \alpha^2/2$; therefore, equation (4-46) further simplifies to

$$\frac{a_{p0}}{\alpha g} \approx \left[1 + 2\frac{F_u}{W} + \alpha^2\left(\frac{1}{3} + \frac{5}{3}\frac{F_u}{W}\right)\right] \tag{4-47}$$

when terms are retained up to α^2.

At the zero-frequency limit the numerical solution for a_{p0} approaches the static limit computed with (4-46) or with its slender-block approximation given by (4-47). As the ratio ω_p/p increases, the acceleration needed to overturn an anchored block with ductility $\mu = 5$ maintains a nearly constant value and then increases drastically. The larger the strength ratio, $\sigma = F_u/W$, the larger is the frequency range that the minimum overturning acceleration is constant. This finding leads to the counterintuitive situation where within the range $4 < \omega_p/p < 7.5$, the stronger the restrainers, the smaller the acceleration needed to overturn the block; whereas, free-standing blocks are the most stable. When ω_p/p is sufficiently large so that an anchored block overturns with mode 2, then an anchored block can sustain a slightly larger acceleration than free-standing blocks.

Figure 34 plots the ratio between the minimum overturning acceleration of an anchored block, a_{p0}^{AN}, to the minimum overturning acceleration, a_{p0}^{FS}, of a free-standing block. In the frequency range, $4 < \omega_p/p < 7.5$, the ratio a_{p0}^{AN}/a_{p0}^{FS} is less than one; therefore, the effect of anchorage is destructive. For an electrical equipment with frequency parameter $p \approx 2\ rad/sec$, this range corresponds to frequencies $1.27\ Hz < f_p < 2.28\ Hz$; or in terms of predominant pulse periods $0.4\ sec < T_p < 0.8\ sec$. For this period range that is of central interest to earthquake engineering, a free-standing block can withstand a larger acceleration amplitude than an anchored block.

Figure 35 compares the overturning acceleration spectra of anchored blocks that have restrainers with the same strength but different ductility. Again there is a frequency range where the block equipped with the less ductile restrainers will survive stronger accelerations than the block with more ductile restrainers.

The limited capacity of the restrainers with finite ductility to prevent the toppling of large blocks can be illustrated again by comparing the potential energy of the block at the verge of overturning with the strain energy dissipated by the ductile restrainers. Assuming an elasto-plastic behavior ($\varepsilon = 0$), Figure 32 (center) indicates that the strain energy dissipated by the restrainers before they fracture is

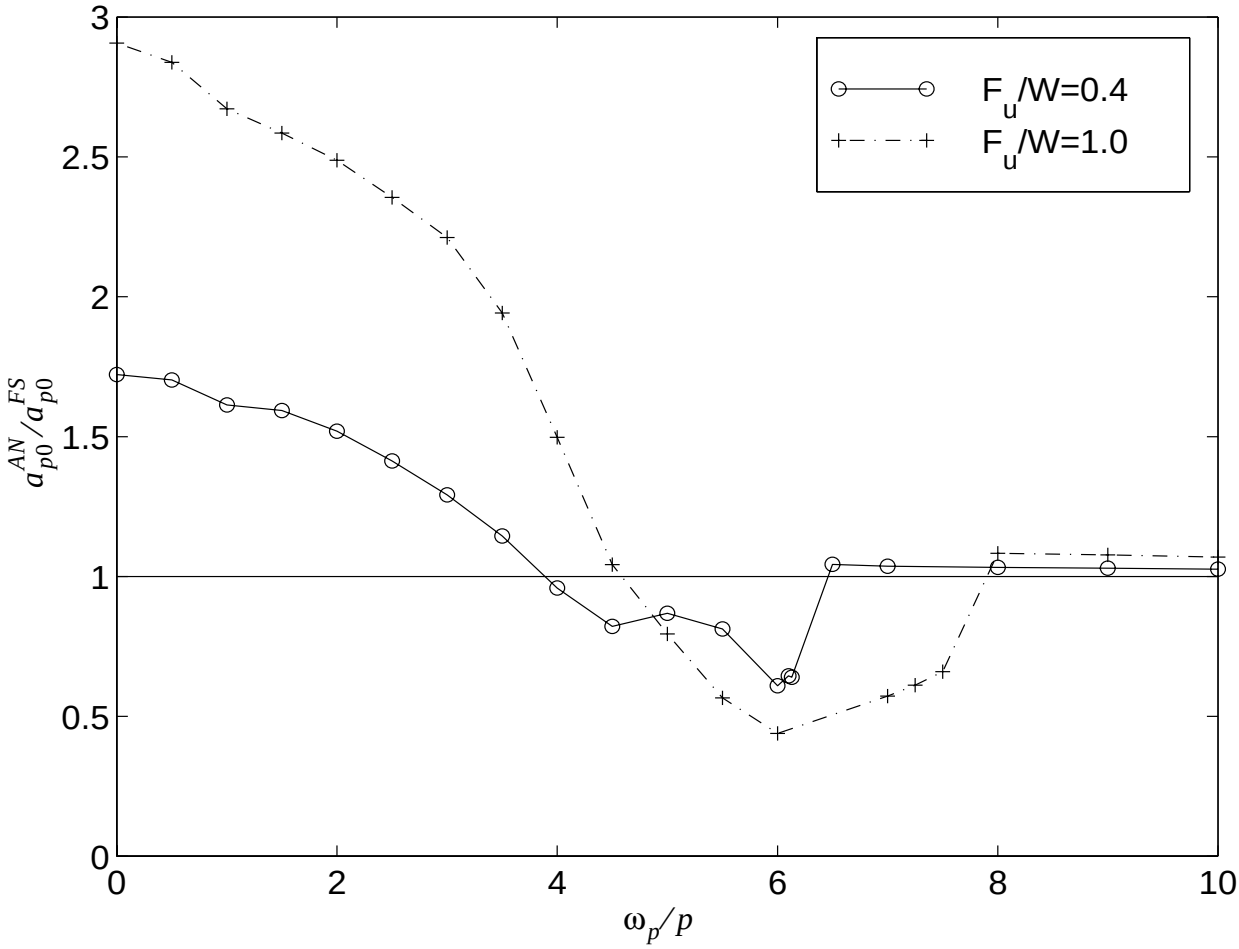

Figure 34. Normalized minimum overturning acceleration levels needed to overturn an anchored block (elastic-plastic behavior, $\mu = 5$) to the acceleration level needed to overturn the same block when it is free standing. When $\omega_p/p > 4$, blocks should not be anchored since the effect of the restrainers is destructive or virtually insignificant.

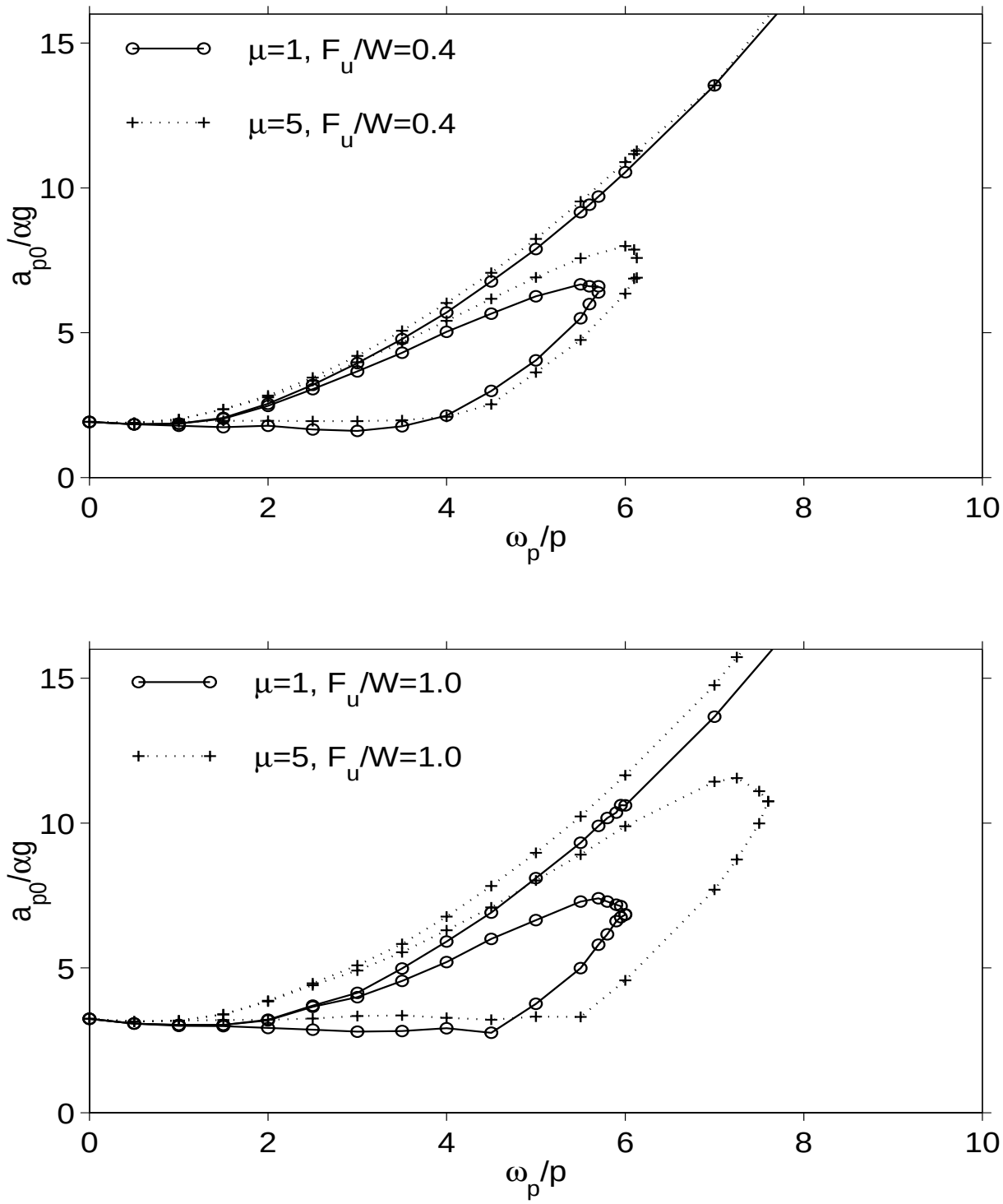

Figure 35. Comparison of overturning acceleration spectra computed with the nonlinear formulation for an anchored block ($\alpha = 0.349\ rad = 20°$, $p = 2\ rad/sec$, $\eta = 0.825$ and $q = 5.2\times10^{-4}$) with two levels of ductility: $\mu = 1$ and $\mu = 5$. Top: $F_u/W = 0.4$; Bottom: $F_u/W = 1.0$.

$$SE \approx F_u u_f \tag{4-48}$$

At the verge of overturning ($\theta = \alpha$) the kinetic energy of the block is zero since the one-sine pulse has expired and its potential energy is given by (4-12). Therefore, the ratio of the dissipated strain energy to the total energy of the block at the verge of overturning is

$$\frac{SE}{PE} \approx \frac{2F_u u_f}{mgR\alpha^2} = \frac{2}{\alpha^2}\frac{F_u}{W}\mu\frac{u_y}{R} \tag{4-49}$$

where, $u_y = F_u/K$, is the yield displacement.

For a value of $F_u/W = 0.1$ and ductility $\mu = 5$, the ratio SE/PE for the $0.5\ m \times 1.5\ m$ block ($\alpha = 0.3217$, $u_y = 1.30\times10^{-3}\ m$ and $R = 1.581\ m$) is equal to 0.83%, which is a very small fraction. Even if the restrainers had strength $F_u = W$, the strain energy lost due to ductile behavior is 8.3% of the energy needed to topple the free-standing block.

Equation (4-49) reveals the same geometrical and scale effects:

(i) The $1/\alpha^2$ term indicates that restrainers are much more effective in preventing toppling the slender of two blocks of the same size (same *R*).

(ii) The $1/R$ term indicates that restrainers are more effective in preventing toppling the smaller of two geometrically similar blocks that have the same F_u/W.

Equation (4-49) can be expressed alternatively in terms of the length, L_B, of the bolts used to anchored the equipment. Using that the yield strain of the bolt $\varepsilon_y = u_y/L_B$, equation (4-49) gives

$$\frac{SE}{PE} \approx \frac{2}{\alpha^2}\frac{F_u}{W}\mu\varepsilon_y\frac{L_B}{R} \tag{4-50}$$

in which $10^{-3} \le \varepsilon_y \le 5\times10^{-3}$ depending on the bolt steel.

Equation (4-49) or (4-50) is the result of an ultimate strength approach that is independent of the dynamic effect. Consequently the ratio $(PE + SE)/PE$, which is the ratio of the total energy that the anchored block has adopted at the verge of overturning, to the corresponding energy that the free-standing block has adopted does not relate directly to the ratio between the minimum overturning acceleration of the anchored block, a_{p0}^{AN}, and the minimum overturning acceleration, a_{p0}^{FS}, of the free-standing block.

CHAPTER 5
ROCKING RESPONSE OF ANCHORED EQUIPMENT TO EARTHQUAKE EXCITATIONS

In chapter 4 an in-depth analysis of the rocking response of anchored equipment subjected to a Type-A trigonometric pulse was presented. The analysis revealed that under a one-sine (Type-A) pulse there are two modes of overturning. The presence of restrainers is more effective for low-frequency pulses or small blocks. As the size of the block or the frequency of the pulse increases, the presence of restrainers is destructive, since anchored blocks overturn under acceleration amplitudes smaller than those needed to overturn free-standing blocks. For large values of ω_p / p, blocks overturn only along mode 2 (no impact) and the effect of the restrainers is marginal.

In this chapter the seismic response of anchored blocks subjected to selected strong ground motions is presented. Figure 36 (left) portrays the fault-normal component of the acceleration, velocity, and displacement histories of the January 17, 1994, Northridge California, earthquake recorded at the Rinaldi station. This motion resulted in a forward ground displacement that recovered partially. The velocity history has a large positive pulse and a smaller negative pulse that is responsible for the partial recovery of the ground displacement. Had the negative velocity pulse generated the same area as the positive velocity pulse, the ground displacement would have fully recovered. Accordingly, the fault-normal component of the Rinaldi station record is in between a forward and a forward-and-back pulse. Figure 36 (center) plots the acceleration, velocity and displacement histories of a Type-A cycloidal pulse given by (Jacobsen and Ayre 1958; Makris 1997)

$$\ddot{u}_g(\tau) = \omega_p \frac{v_p}{2} \sin(\omega_p \tau) \ , \ 0 \le \tau \le T_p \ , \tag{5-1}$$

$$\dot{u}_g(\tau) = \frac{v_p}{2} - \frac{v_p}{2} \cos(\omega_p \tau) \ , \ 0 \le \tau \le T_p \ , \tag{5-2}$$

$$u_g(\tau) = \frac{v_p}{2} \tau - \frac{v_p}{2\omega_p} \sin(\omega_p \tau) \ , \ 0 \le \tau \le T_p \ . \tag{5-3}$$

by assuming a pulse duration $T_p = 0.8 \ sec$ and a velocity amplitude $v_p = 1.75 \ m/sec$ which are approximations of the duration and velocity amplitude of the first main pulse shown in the record. This comparison indicates that the simple one-sine pulse that was used in this study to uncover the many complexities of the rocking response of a rigid block can approximate the kine-

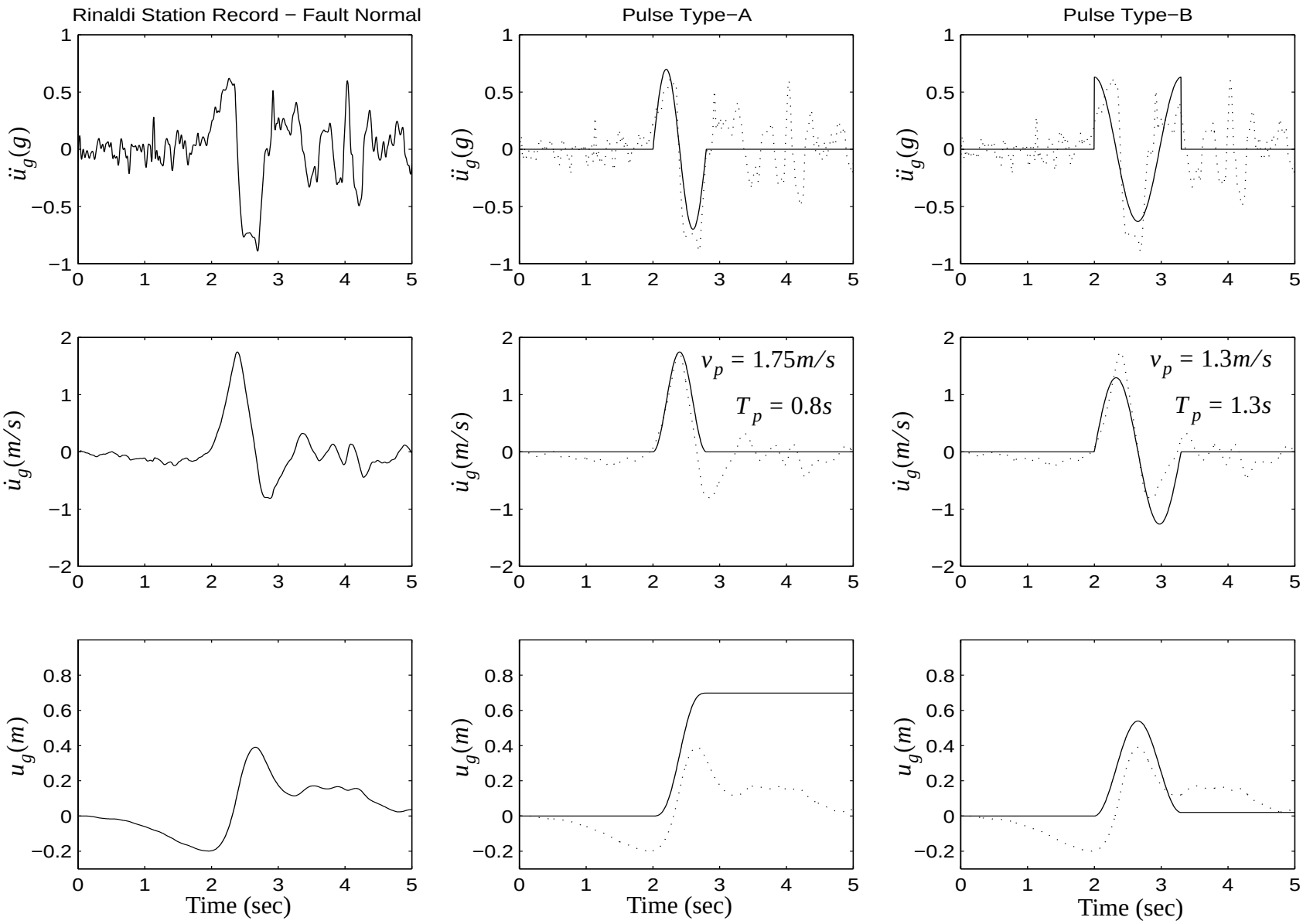

Figure 36. Fault normal components of the acceleration, velocity, and displacement time histories recorded at the Rinaldi station during the January 17, 1994, Northridge, California, earthquake (left); a cycloidal type-A pulse (center); and a cycloidal type-B pulse (right)

matic characteristics of some recorded ground motions. Figure 36 (right) plots the acceleration, velocity and displacement histories of a Type-B cycloidal pulse given by (Makris 1997)

$$\ddot{u}_g(\tau) = \omega_p v_p \cos(\omega_p \tau) \ , \ 0 \le \tau \le T_p \ , \tag{5-4}$$

$$\dot{u}_g(\tau) = v_p \sin(\omega_p \tau) \ , \ 0 \le \tau \le T_p \ , \tag{5-5}$$

$$u_g(\tau) = \frac{v_p}{\omega_p} - \frac{v_p}{\omega_p} \cos(\omega_p \tau) \ , \ 0 \le \tau \le T_p \ . \tag{5-6}$$

by considering a pulse duration $T_p = 1.3\ sec$ and a velocity amplitude $v_p = 1.3\ m/sec$.

We commence our analysis by computing rocking time histories of a $0.5\ m \times 1.5\ m$ $(19.7\ in \times 59.0\ in)$ block with frequency parameter, $p = 2.157$, and slenderness, $\alpha = 18.43°$. Consider that this block is the idealization of an electrical equipment with weight, $W = mg = 40\ kips$ that is anchored with restrainers that exhibit an ultimate strength from each side of $F_u = 0.4W = 16\ kips$ and a yield displacement $u_y = 0.05\ in$. Consider further that the stiffness of these restrainers is $K = 300\ kips/in$. These parameters yield an influence factor $q = u_y p^2/g = 6.0 \times 10^{-4}$ and $\sigma = F_u/W = 0.4$. Under a horizontal excitation only, Figure 15 indicates that a level of 78% of the Rinaldi station record is capable of overturning the block.

Figure 37 plots the response of the block with restrainer ductility, $\mu = 1$, at the verge of overturning. A 88% level of the Rinaldi station record is capable of overturning the block. Assuming that the Rinaldi station record can be approximated with a one-sine pulse with $T_p = 0.8\ sec$, the corresponding frequency ratio is $\omega_p/p = 3.64$. For this value of the frequency ratio, Figure 27 (that has been generated by considering a slightly different block) indicates an approximate acceleration amplitude, $a_{p0} = 1.87\alpha g = 0.65\ g$, which is close to the acceleration level $0.88 \times (PGA \approx 0.8g) \approx 0.7\ g$.

Figure 35 indicates that when the ductility of the restrainers is increased from $\mu = 1$ to $\mu = 5$, a slight increase is expected in the acceleration needed to overturn the same $0.5\ m \times 1.5\ m$ block. Indeed Figure 38 shows that when the restrainers have ductility, $\mu = 5$, a 93% level of the Rinaldi station record is capable of overturning the block. For this level restrainers with ductility, $\mu = 10$, are capable of preventing overturning. Figure 39 shows that a 99% level of the Rinaldi station record is capable of overturning the block that is anchored with restrainers that have $F_u = 16\ kips$, $K = 300\ kips/in$ and $\mu = 10$. Comparing this level with the 78% one that was needed to overturn the free-standing block, one concludes that restrainers have a limited effect in preventing toppling.

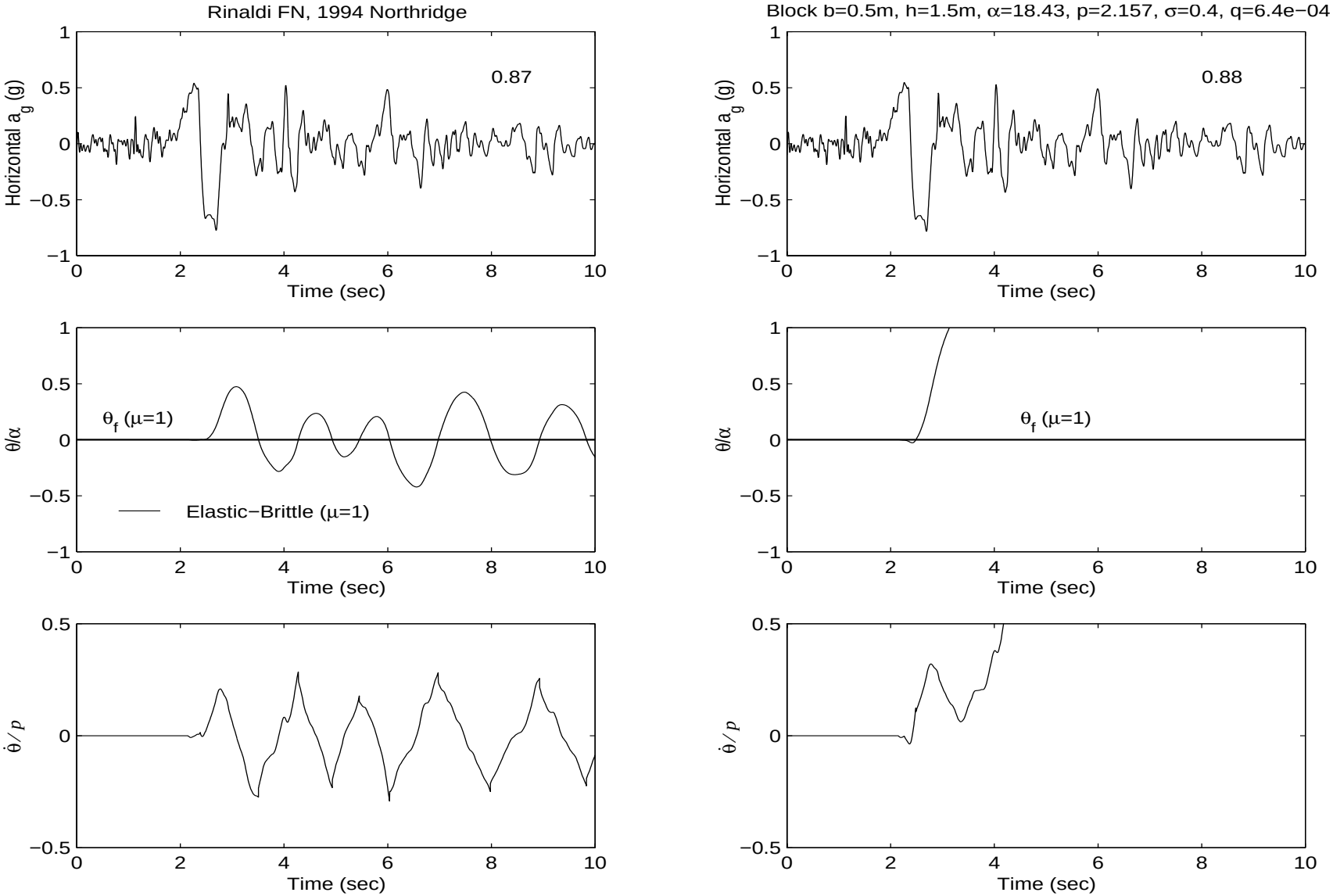

Figure 37. Rotation and angular velocity time histories of an anchored block ($b = 0.5\ m$, $h = 1.5\ m$, $F_u/W = 0.4$) subjected to the fault-normal Rinaldi station motion. An 88% acceleration level is capable of overturning the block with restrainers exhibiting ductility $\mu = 1$.

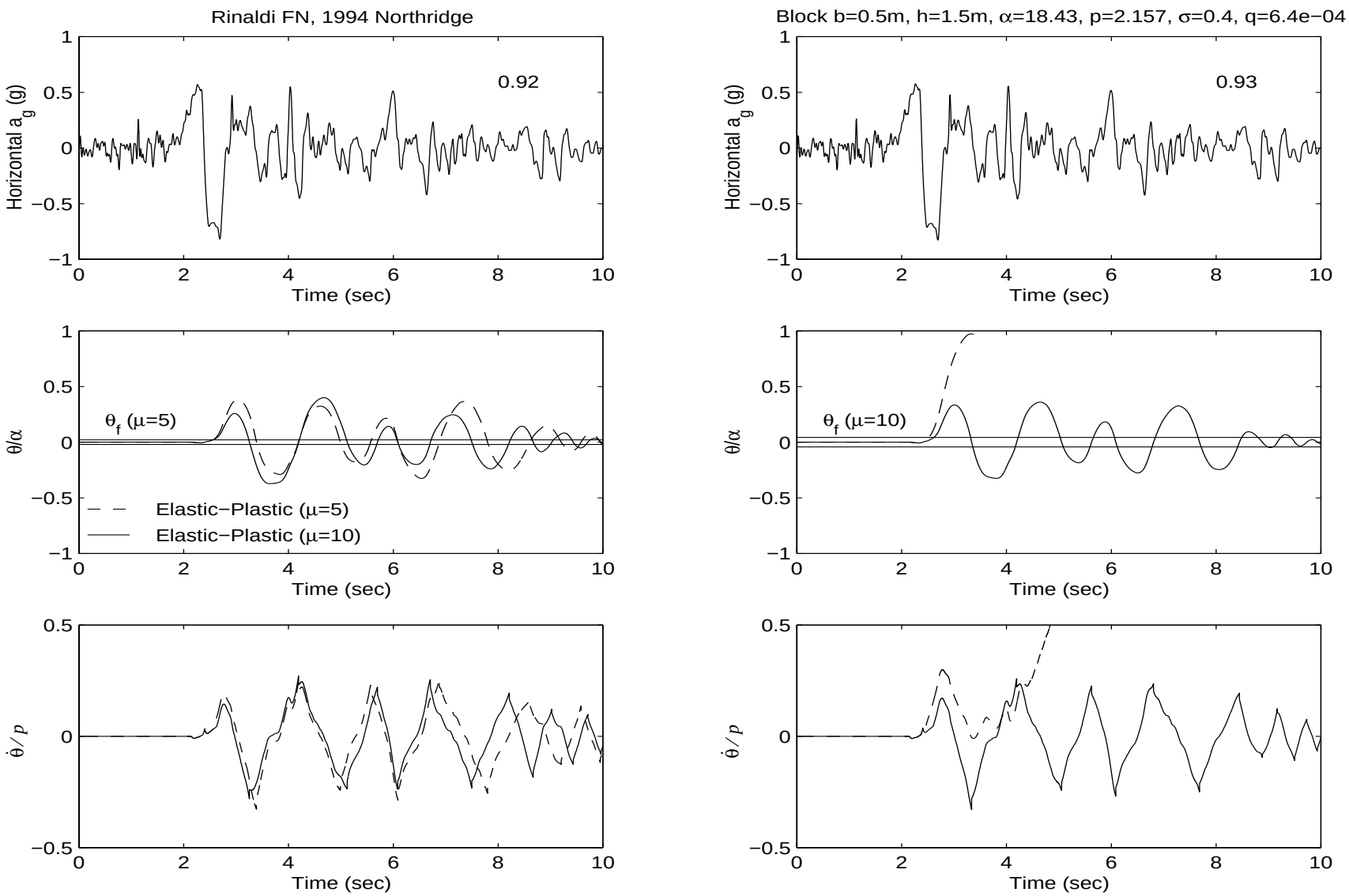

Figure 38. Rotation and angular velocity time histories of an anchored block ($b = 0.5\ m$, $h = 1.5\ m$, $F_u/W = 0.4$) subjected to the fault-normal Rinaldi station motion. A 93% acceleration level is capable of overturning the block with restrainers exhibiting ductility $\mu = 5$; whereas when $\mu = 10$ the block survives.

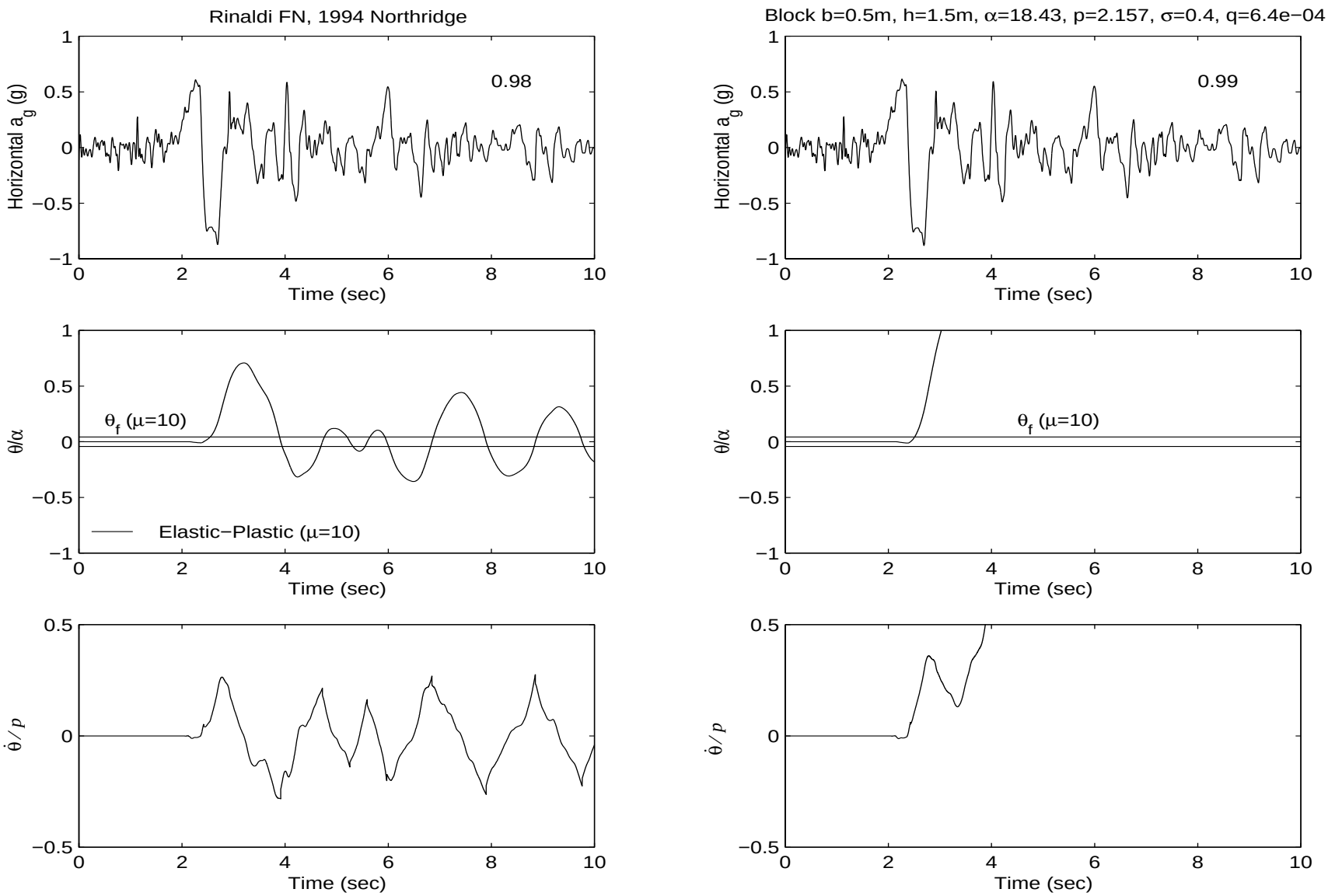

Figure 39. Rotation and angular velocity time histories of an anchored block ($b = 0.5\ m$, $h = 1.5\ m$, $F_u/W = 0.4$, $\mu = 10$) subjected to the fault-normal Rinaldi station motion. Left: no overturning (98% acceleration level). Right: overturning (99% acceleration level).

To proceed with the analysis the rocking response is computed for a larger block ($1.0\ m \times 3.0\ m$) that has a frequency parameter, $p = 1.525\ rad/sec$, and the same slenderness, $\alpha = 18.43°$. Under the same assumption that the Rinaldi station record can be approximated with a one-sine pulse with $T_p = 0.8\ sec$, the corresponding frequency ratio is $\omega_p/p = 5.15$. For this value of the frequency ratio, Figure 33 (that has been generated for a smaller, less slender block, $\alpha = 20°$, $p = 2\ rad/sec$ and $\eta = 0.825$) indicates that a free-standing block might survive a stronger acceleration level than an anchored block. Indeed Figure 40 indicates that the $1.0\ m \times 3.0\ m$ free-standing block overturns at a 127% level of the Rinaldi record, whereas the same block anchored with restrainers having strength $F_u = 0.4W = 16\ kips$ and ductility $\mu = 5$ overturns under only a 119% level of the Rinaldi acceleration record, as shown in Figure 41. This study was partly motivated by this puzzling result, and sought to address the problem in a systematic and lucid manner.

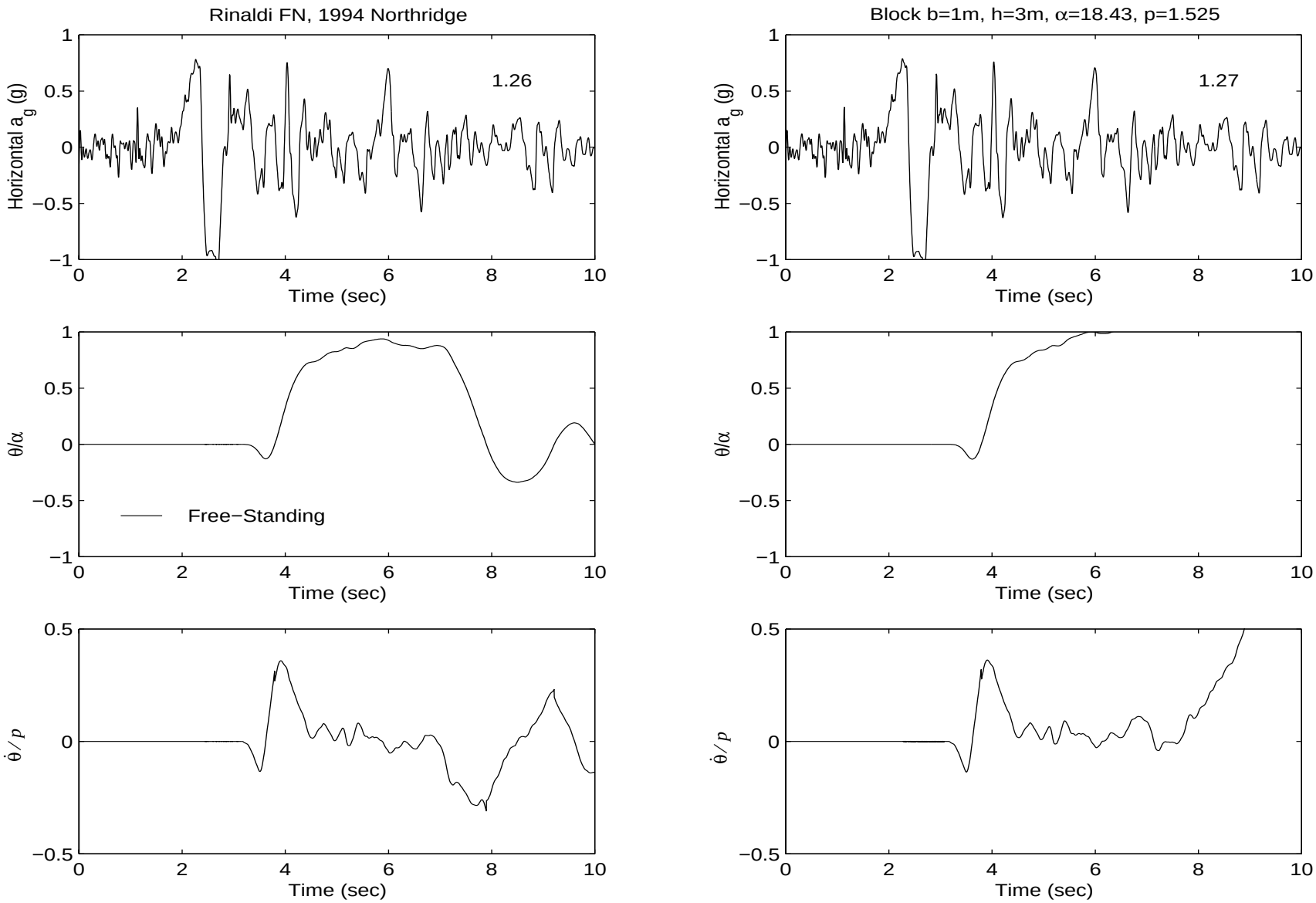

Figure 40. Rotation and angular velocity time histories of the free-standing block (*b = 1.0 m, h = 3.0 m*) subjected to the fault-normal Rinaldi station motion. Left: no overturning (126% acceleration level). Right: overturning (127% acceleration level).

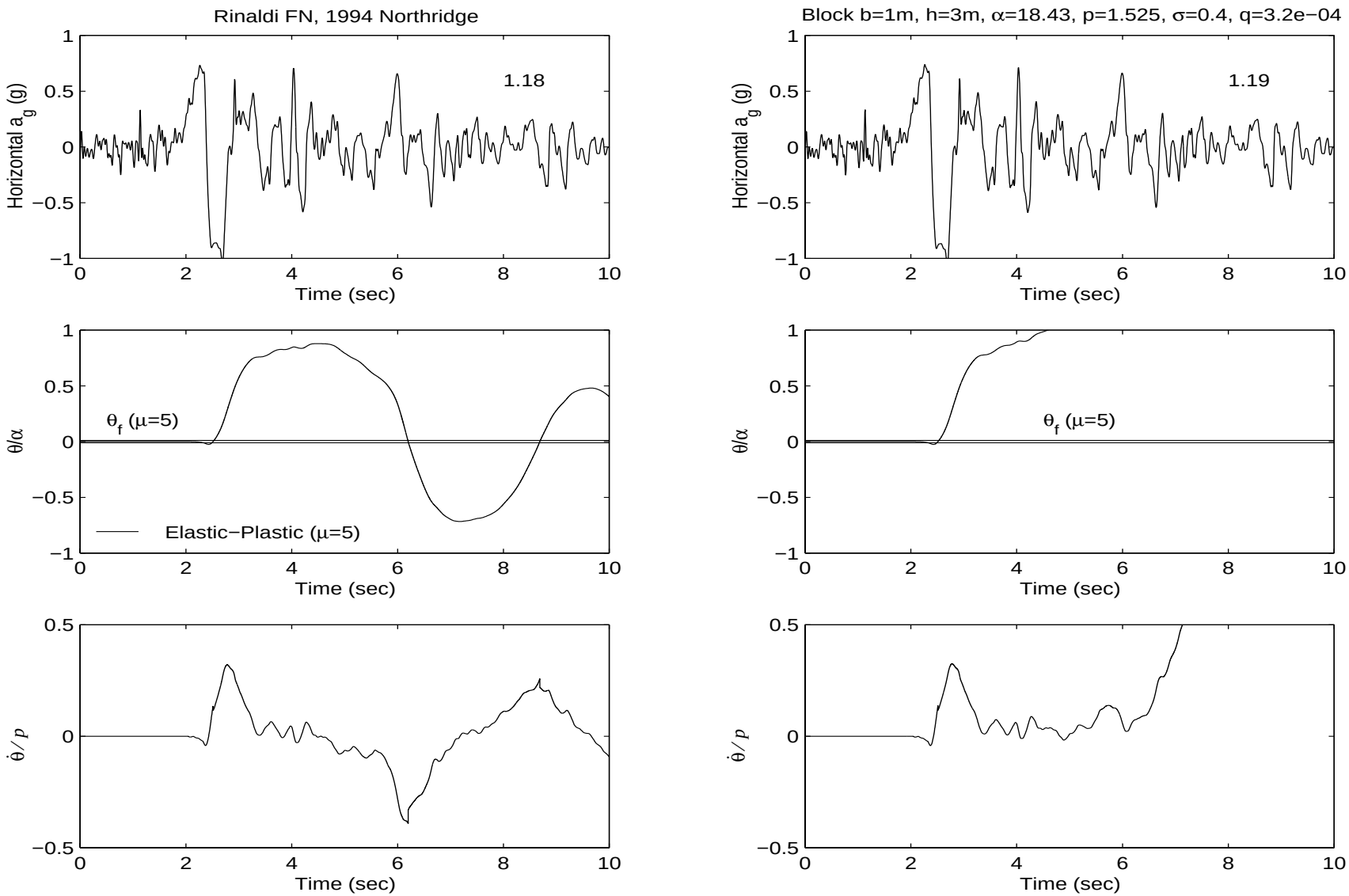

Figure 41. Rotation and angular velocity time histories of a larger anchored block ($b = 1.0\ m$, $h = 3.0\ m$, $F_u/W = 0.4$ and $\mu = 5$) subjected to the fault-normal Rinaldi station motion. Left: no overturning (118% acceleration level). Right: overturning (119% acceleration level). The free-standing block can survive a stronger acceleration level than the anchored block (see Figure 40).

CHAPTER 6
CONCLUSIONS

This report investigates the transient rocking response of anchored electrical equipment and other tall structures that can be approximated as rigid blocks. In addition, various practical issues that control overturning, such as the effect of the vertical component of ground acceleration and the effect of the coefficient of restitution during impact, are also addressed.

An in-depth study of the rocking response of a free-standing equipment subjected to a one-sine (Type-A) pulse is first presented. It is shown that under a one-sine pulse (forward displacement) rigid blocks can overturn with two distinct modes: (a) with one impact; (b) without impact. The second mode (no impact) is responsible for the existence of a safe region that is located over the minimum overturning acceleration spectrum. It is found that the shape of this region depends on the coefficient of restitution and is very sensitive to the nonlinear nature of the problem. The study uncovers a frequency range where the linear formulation can give erroneous results even for slender blocks. Under a one-cosine (Type-B) pulse, a similar safe region located over the minimum overturning acceleration spectrum exists. In this case the differences in the response obtained with the linear and nonlinear formulations are less drastic to those observed under a one-sine pulse.

Restrainers with elastic-brittle and elastic-plastic behavior are considered. It is found that restrainers are more efficient in preventing overturning of small slender blocks subjected to a low-frequency ground excitation. Again, under one-sine pulse anchored blocks can overturn with the two aforementioned modes of overturning. Before the transition from mode 1 to mode 2, the presence of restrainers has a destructive effect. The stronger the restrainer, the smaller is the acceleration amplitude needed to overturn a rigid block; whereas a free-standing block can withstand the higher acceleration amplitude. This counterintuitive response extends when the restrainers exhibit finite ductility, since the study shows that there is a frequency range where blocks with the most ductile restrainers will withstand the smaller acceleration level. Larger blocks can overturn only without experiencing any impact, and in this case the effect of restrainers is marginal even when their strength equals the weight of the equipment. The limited effect of restrainers in preventing toppling is also found under earthquake excitations. The study shows that under the Rinaldi station record restrainers with strength $F_u/W = 0.4$ and ductility $\mu = 5$ have a mild constructive effect in preventing toppling of a $0.5\ m \times 1.5\ m$ block; they have a destructive effect in prevent-

ing toppling of a $1.0\ m \times 3.0\ m$ block. The $1.0\ m \times 3.0\ m$ free-standing block survives the motion that overturns it when it is anchored.

Furthermore, the report concludes that the effect of the vertical component of recorded ground motions is marginal and virtually does not affect the level of the horizontal acceleration needed to overturn an electrical equipment. An increasingly inelastic impact (smaller coefficient of restitution) results in smaller angles of rotation; however the values of the impact velocities might occasionally be larger.

REFERENCES

Anderson, J. C., and V. V. Bertero. 1986. Uncertainties in establishing design earthquakes. *J. of Struct. Engrg.* **113**: 1709-24. ASCE.

Anooshehpoor, A., T. H. Heaton, B. Shi and J. N. Brune. 1999. Estimates of the ground acceleration at Point Reyes station during the 1906 San Francisco earthquake. *Bull. Seismological Soc. of America* 89(4): 843-53.

Aslam, M., W. G. Godden, and D. T. Scalise. 1980. Earthquake rocking response of rigid bodies. *J. of Engrg. Mech. Div.* **106**: 377-92. ASCE.

Bertero, V. V., S. A. Mahin, and R. A. Herrera. 1978. Aseismic design implications of near-fault San Fernando earthquake records. *Earthquake Engrg. and Struc. Dynamics* 6: 31-42.

Bouc, R. 1971. Modele mathematique d'hysteresis. *Acustica* **24**: 16-25.

Fujisaki, E. 1999. Personal communication.

Hall, J. F., T. H. Heaton, M. W. Halling, and D. J. Wald. 1995. Near-source ground motions and its effects on flexible buildings. *Earthquake Spectra* **11**: 569-605.

Hogan S. J. 1989. On the dynamics of rigid-block motion under harmonic forcing. *Proc. R. Soc. London* **A425**: 441-76.

Housner, G. W. 1963. The behaviour of inverted pendulum structures during earthquakes. *Bull. Seismological Soc. of America* **53**: 404-17.

Jacobsen, L. S., and R. S. Ayre. 1958. *Engineering Vibrations*. New York: McGraw-Hill.

Makris, N., and S. P. Chang. 1998. *Effect of damping mechanisms on the response of seismically isolated structures.* PEER-98/06. Pacific Earthquake Engineering Research Center, University of California, Berkeley.

Makris, N., and Y. Roussos. 1998. *Rocking response and overturning of equipment under horizontal pulse-type motions*. PEER-98/05. Pacific Earthquake Engineering Research Center, University of California, Berkeley.

Makris, N. 1997. Rigidity-plasticity-viscosity: Can electrorheological dampers protect base-isolated structures from near-source ground motions? *Earthq. Engrg. and Struc. Dynamics* **26**: 571-91.

MATLAB. 1992. *High-Performance numeric computation and visualization software*. Natick, Mass: The MathWorks.

Milne, J. 1885. Seismic experiments. *Trans. Seism. Soc. Japan* **8**: 1-82.

Scalia, A., and M. A. Sumbatyan. 1996. Slide rotation of rigid bodies subjected to a horizontal ground motion. *Earthq. Engrg. and Struc. Dynamics* **25**: 1139-49.

Shenton, H. W. III. 1996. Criteria for initiation of slide, rock, and slide-rock rigid-body modes. *J. of Engrg. Mech. Div.* **122**: 690-93. ASCE.

Shi, B., A. Anooshehpoor, Y. Zeng, and J. N. Brune. 1996. Rocking and overturning of precariously balanced rocks by earthquake. *Bull. Seismological Soc. of America* **86**(5): 1364-71.

Spanos, P. D., and A. S. Koh. 1984. Rocking of rigid blocks due to harmonic shaking. *J. of Engrg. Mech. Div.* **110**: 1627-42. ASCE.

Yim, C. K., A. K. Chopra, and J. Penzien. 1980. Rocking response of rigid blocks to earthquakes. *Earthq. Engrg. and Struc. Dynamics* **8**: 565-87.

Wen, Y-K. 1975. Approximate method for nonlinear random vibration. *J. of Engrg. Mech.* **101**(EM4): 389-401. ASCE.

Wen, Y-K. 1976. Method for random vibration of hysteretic systems. *J. of Engrg. Mech.* **102**(EM2): 249-63. ASCE.

Zhang, J., and N. Makris. 1999. Discussion on “Estimates of the ground acceleration at Point Reyes station during the 1906 San Francisco earthquake” by A. Anooshehpoor et al. *Bull. Seismological Soc. of America* (forthcoming).